TRABAJO ESPECIAL DE GRADO

DISEÑO TERMICO Y OPTIMIZACIÓN DE NÚCLEO DE UN INTERCAMBIADOR DE CALOR AUTOMOTRIZ.

THERMAL DESIGN AND OPTIMIZATION OF AUTOMOTIVE HEAT EXCHANGER CORE

Presentado ante la Ilustre
Universidad Central de Venezuela
Por la Br. Alvarez.V. Helyann. C
Para optar al Título de
Ingeniero Mecánico

Caracas, Octubre 2015

TRABAJO ESPECIAL DE GRADO

DISEÑO TERMICO Y OPTIMIZACIÓN DE NÚCLEO DE UN INTERCAMBIADOR DE CALOR AUTOMOTRIZ.

THERMAL DESIGN AND OPTIMIZATION OF AUTOMOTIVE HEAT EXCHANGER CORE

TUTOR ACADÉMICO: Prof. Pietro Asinari.

Presentado ante la Ilustre
Universidad Central de Venezuela
Por la Br. Alvarez.V Helyann. C
Para optar al Título de
Ingeniero Mecánico

Caracas, Octubre 2015

DISEÑO TERMICO Y OPTIMIZACIÓN DE NÚCLEO DE UN INTERCAMBIADOR DE CALOR AUTOMOTRIZ.

Helyann C. Alvarez V.

helycarol@gmail.com

INTRODUCCIÓN

La presente tesis se concentra en el análisis de las características de la transferencia de calor del lado del aire en los intercambiadores de calores compactos con aletas tipo persianas, utilizadas en campo automovilístico. El objetivo principal es el de encontrar una correlación de la literatura capaz de predecir el coeficiente de transferencia de calor de la geometría de aletas tipo persianas y permite entender como el coeficiente global de transferencia de calor (UA) depende de dos parámetros fundamentales de diseño que son: la profundidad del núcleo (Ld) y el paso de los tubos (Tp), con el fin de optimizar el desempeño de los intercambiadores de calor con aletas persianadas.

Las correlaciones de la literatura son convalidadas en contra de los resultados experimentales revelados de las pruebas de banco experimentales de La DENSO Thermal Systems, para las diferentes geometrías de intercambiadores de calores, sea radiadores que condensadores.

El estudio demuestra que la correlación de Chang y Wang es la que mejor aproxima las simulaciones de prueba DENSO en los intercambiadores de calor, radiadores y condensadores.

METODOLOGÍA

1) Correlaciones de la literatura.

Diversas correlaciones que modelan la transferencia de calor en el lado aire han sido encontradas, que dependen de numerosos parámetros geométricos de la aleta tipo persiana. Estas correlaciones han sido analizadas para diferentes geometrías de aletas, para luego compararlos con los datos experimentales medidos en el banco de pruebas de las instalaciones de DENSO.

La forma básica de las correlaciones es la siguiente:

$$j = C_1 Re_{Lp}^{C2} \qquad [1]$$

Donde:

- C1 es dependiente de dimensiones geométricas del intercambiador de calor.
- C2 es una constante.

Las correlaciones dan como resultado el Factor de Colburn que es un número adimensional definido de la siguiente forma:

$$j = \frac{Nu}{RePr^{\frac{1}{3}}} = \frac{hPr^{\frac{2}{3}}}{\rho u c_p} \qquad [2]$$

2) Datos Experimentales.

Existen dos software que calculan el coeficiente de transferencia de calor uno para los radiadores, y otro para los condensadores.
Los dos softwares calculan el coeficiente de transferencia de calor lado aire por diferencia, lo calculan a través del coeficiente global de transferencia de calor UA que es medido de pruebas experimentales, el coeficiente de transferencia de calor lado refrigerante es obtenido mediante una correlación, la eficiencia de la aleta calculada por la definición teórica, y las áreas calculadas con las geometrías del intercambiador.

$$UA = \frac{1}{\frac{1}{h_c . A_c} + \frac{1}{\eta_f A_f h_o} + \frac{b_w}{k_w A_w}} \qquad [3]$$

- El software HEX de los radiadores, calcula el coeficiente de transferencia de calor h_o en cada velocidad del aire, y se obtiene una función polinómica que depende de la velocidad, a continuación los resultados de desempeño se expresan con el factor de Colburn que depende de la temperatura debido a los parámetros termo-físicos del aire.
- Al contrario el MFCondenser, software de los condensadores obtiene el coeficiente de transferencia de calor lado aire con una ecuación exponencial de la velocidad, y los coeficientes a y b de la ecuación son obtenidos calibrando experimentalmente.

$$HTC_{air} = \boldsymbol{a}.\left[1 - e^{(-\boldsymbol{b}.v_{air})}\right] \qquad [4]$$

La incertidumbre de ambos software han sido calculados en cada uno de manera diversa:

- Para el HEX, las incertidumbres han sido calculadas por medio de un enfoque estadístico que es el de la propagación de las incertidumbres, considerando cada contribución de incertidumbre en el cálculo del HTC (heat transfer coefficient).

$$\Delta h_o = \sqrt{\Delta h_c^2 . \left|\frac{\partial h_o}{\partial h_c}\right|^2 + \Delta \eta_f^2 . \left|\frac{\partial h_o}{\partial \eta_f}\right|^2 + \Delta A_f^2 . \left|\frac{\partial h_o}{\partial A_f}\right|^2} \qquad [5]$$

- Para el MFCondenser, el análisis de incertidumbre ha sido estudiado con un cálculo de sensibilidad debido a que el algoritmo de cálculo discretiza el intercambiador de calor en unidades elementares de transferencia de calor. De esta forma se estudia la incertidumbre aplicando la sensibilidad en el cálculo del coeficiente de transferencia de calor lado refrigerante, por lo cual se introduce un coeficiente multiplicativo k, en la correlación de cálculo, que es 2 o 0.5.

Por lo cual ambos cálculos de incertidumbre son efectuados para obtener una banda de incertidumbre para hacer la comparación con las correlaciones.

3) Comparación entre Correlaciones y Datos Experimentales.

En la comparación entre las 8 correlaciones y los datos experimentales, sea para los radiadores que para los condensadores se estudia cuál de las correlaciones es la que mejor se ajusta a los datos experimentales, como resulta ser la correlación de Chang y Wang (Correlación 1) la que mejor se ajusta en ambos intercambiadores de calor.

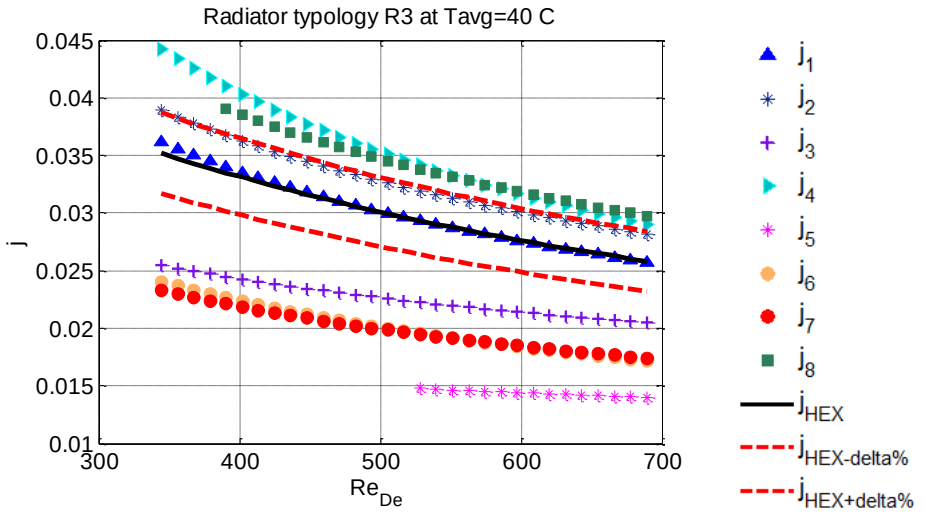

Figura 1. Comparación entre correlaciones y datos experimentales (Radiador R3).

Correlación seleccionada para el estudio: Correlación 1 de los autores Chang y Wang.

$$j = Re_{Lp}^{-0.49}\left(\frac{\theta}{90}\right)^{0.27}\left(\frac{F_p}{Lp}\right)^{-0.14}\left(\frac{F_h}{L_p}\right)^{-0.29}\left(\frac{L_d}{L_p}\right)^{-0.23}\left(\frac{L_h}{L_p}\right)^{0.68}\left(\frac{T_p}{L_p}\right)^{-0.28}\left(\frac{b}{L_p}\right)^{-0.05} \quad [6]$$

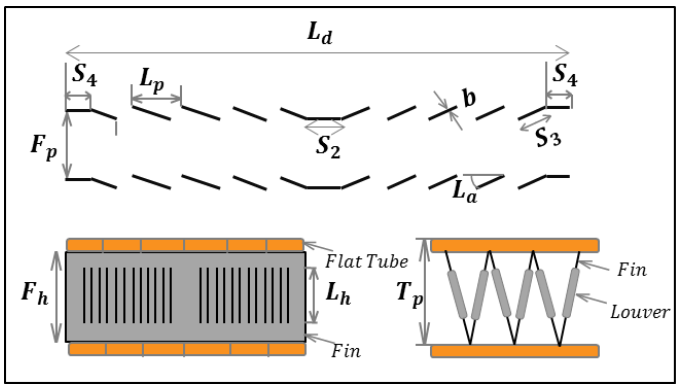

Figura 2. Parámetros geométricos de aleta tipo persiana.

4) Estudio de Función y Optimización.

4.1) Radiadores:

El estudio de función en los radiadores ha sido focalizado con el objetivo de dar a conocer nuevas configuraciones de geometrías de radiadores que obtengan igual o incluso mejores desempeños que las actuales geometrías.

Con un espesor del núcleo Ld=12.5mm y variando las geometrías del tubo (altura del tubo y paso de los tubos) se analizan los parámetros de desempeño que son: Potencia térmica, caída de presión lado aire, caída de presión lado coolant y Qv (índice de desempeño que es la relación entre potencia térmica y caída de presión aire). Los siguientes gráficos describen el comportamiento con estos parámetros de diseño en cada diferente configuración de radiadores nuevos respecto al actual R3.

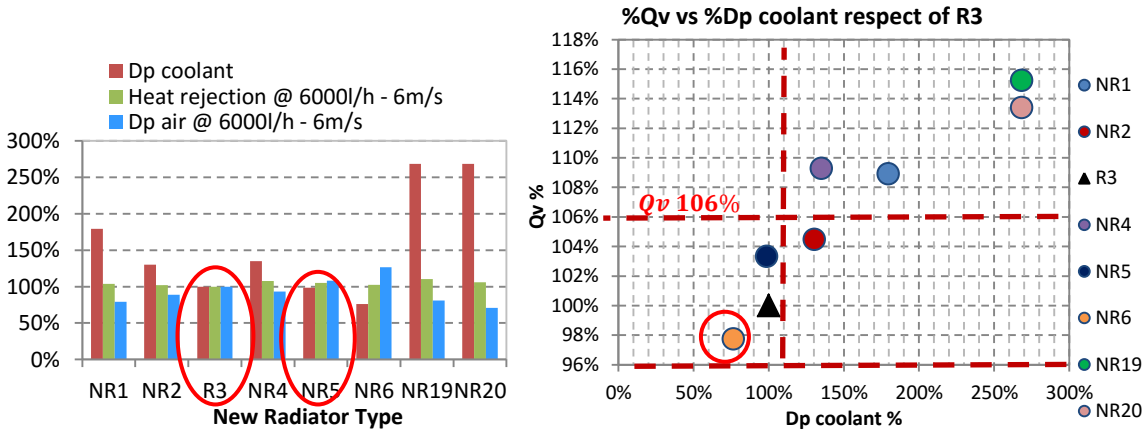

Figura.3 Radiadores-Estudio de función -Parámetros de diseño.

Se observa que considerando independientemente los tres parámetros de diseño, los óptimos radiadores son el NR5 con Th=1.6mm y Tp=6.4 y el actual R3(Th=1.8mm Tp=7.8), y en el segundo grafico considerando el Qv versus la caída de presión lado coolant y considerando una banda de ±6% del Qv, una nueva optima selección es el radiador NR6 (Th=1.8mm) teniendo una baja caída de presión del coolant y un aceptable Qv.

4.2) Condensadores:

El estudio de función en los condensadores se analiza con nuevas configuraciones de condensadores en modo de reducir la geometría del núcleo del condensador, como lo son el espesor del núcleo (Ld) y el paso de los tubos (Tp), con diferentes espesores del núcleo (Ld=10, 11.5 y 16mm) y variando la altura del tubo de 1 a 2mm se analiza la potencia térmica:

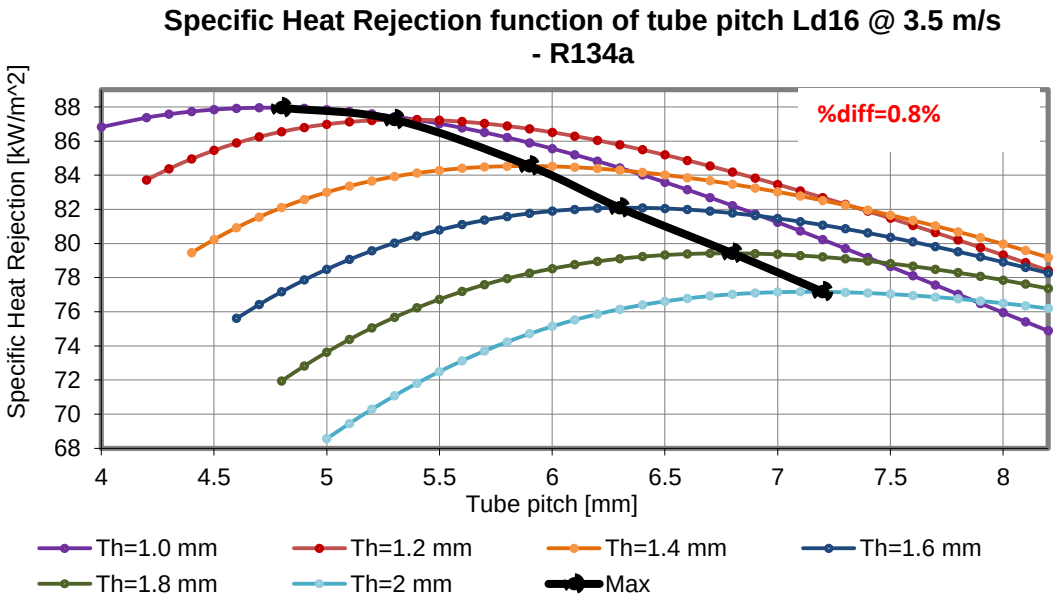

Figura 4. Condensadores-Potencia térmica en función del paso de los tubos.

A partir del grafico se observa que: hay un punto óptimo de paso de tubos con altura del tubo, la potencia térmica aumenta al disminuir de la altura del tubo, el paso de tubos que optimiza el rendimiento disminuye con la altura del tubo, y por último el paso de tubos óptimo para cada altura del tubo, no depende del espesor del núcleo ni de la velocidad del aire.

Para realizar la optimización se reducen la altura del tubo de 1.2mm (Th) y el espesor del núcleo de 10 mm (Ld) respecto al condensador de referencia C1. Se realizan las optimizaciones variando diversos parámetros geométricos de la aleta.

Tabla1. Optimización Condensadores.

	C1(Ref)	NREC133	NREC134	NREC135	NREC132	NREC129	NREC131	NREC130
$Ld[mm]$	11.5	10	10	10	10	10	10	10
$Tp[mm]$	6.4	5.3	5.3	5.3	5.4	6	6	6
$Th[mm]$	1.4	1.2	1.2	1.2	1.2	1.2	1.2	1.2
$La[^{\circ}]$	28	30	30	30	30	30	30	30
$Lp[mm]$	0.7	0.64	0.64	0.64	0.64	0.64	0.64	0.64
$Fp[mm]$	2.3	2.3	2.2	2.1	2.2	2.3	2.2	2.1

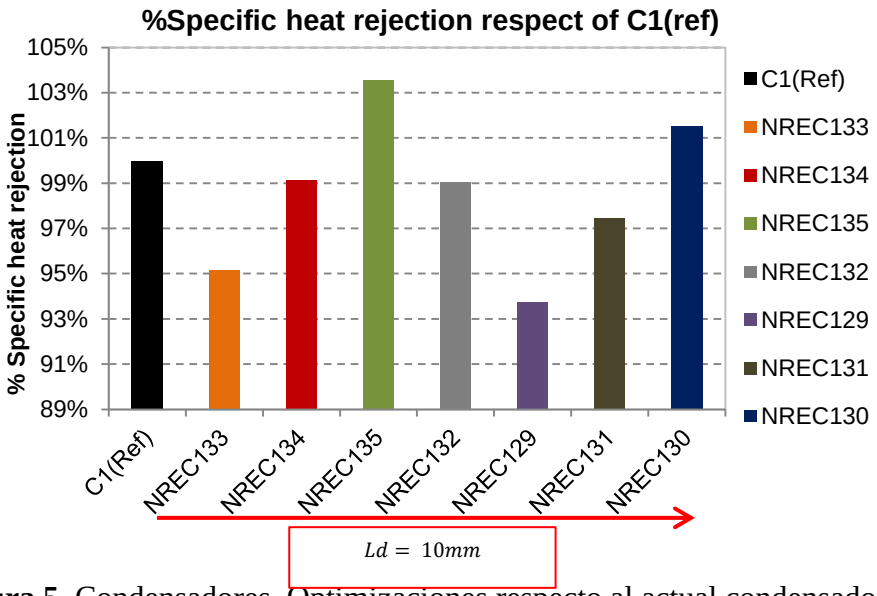

Figura 5. Condensadores. Optimizaciones respecto al actual condensador C1.

Las selecciones óptimas para condensadores son:

- El condensador **NREC134**, $Tp = 5.3mm$, y $Fp = 2.2\ mm$.
- El condensador **NREC130** $Tp = 6mm$ es mas factible de producir con la actual tecnología de proceso pero con $Fp = 2.1\ mm$.
- El condensador **NREC132** es otra opción optima con $Tp = 5.4mm$.

RESULTADOS Y DISCUSIÓN

- La correlación 1 (Chang y Wang) seleccionada para estudio del HTC tanto de condensadores como radiadores.
- Estudio de función de los Radiadores ➔ Considerando separadamente los parámetros de diseño (Dp coolant, Dp aire, potencia térmica, Qv), las configuraciones optimas de radiadores son:
  - ✓ Actual radiador R3
  - ✓ NR5 y NR6 que son posibles configuraciones de radiadores (altura de tubo y paso de tubos diferente respecto al actual radiador R3).
- Estudio de función de los Condensadores.➔ Considerando el análisis de la potencia térmica, las configuraciones de condensadores óptimos son:
  - ✓ Seleccionando la altura del tubo Th=1.2 mm y espesor del núcleo de Ld=10mm, los condensadores NREC134, NREC130 yNREC132 obtienen óptimos resultados.

CONCLUSIONES

El estudio de optimización obtenido con los radiadores y condensadores muestra resultados diferentes, debido al hecho que en los condensadores hay presencia de un fluido bi-fase en el lado refrigerante, las caídas de presión inducen el cambio de las propiedades del fluido y afectan directamente al coeficiente global de transferencia de calor, por el contrario el impacto de las caídas de presión lado coolant en los radiadores no es significativo debido a que es un fluido mono-fase.

La optimización realizada para los condensadores que se ha realizado reduciendo las dimensiones del núcleo (espesor del núcleo y paso de los tubos) de forma de obtener resultados de potencia entorno al condensador de referencia C1, ha sido posible variando otros parámetros de las aletas tipo persianas. Finalmente se han conseguido tres posibles optimizaciones a diferentes paso de tubos (Tp = 5.3; 5.4 y 6mm).

En el caso de los radiadores la optimización se ha efectuado de forma de obtener diferentes configuraciones de radiadores posibles, que obtengan un buen desempeño en términos de los tres parámetros de diseño que son Dp coolant, Dp aire y potencia térmica, que han sido estudiados separadamente. De esta forma se han obtenido dos geometrías posibles para el caso de un radiador con espesor de Ld=12.5mm que tienen diferentes paso de los tubos y altura de tubos respecto al actual radiador R3.

La optimización de los radiadores y condensadores tienen como objetivo en común de obtener un mejor rendimiento respecto a las geometrías actuales, e incluso posibilidades de reducción del material, peso y todas ellas se resumen en la reducción de costos de producción.

POLITECNICO DI TORINO

I School of Engineering

Master of Science Degree in Mechanical Engineering

Thesis

THERMAL DESIGN AND OPTIMIZATION OF AUTOMOTIVE HEAT EXCHANGER CORE

Supervisors:

Ph.D. Pietro Asinari

Ph.D. Grazia Monni

Eng. Marta Roberti

Eng. Davide Perocchio

Eng. Fabio Sandri

Candidate:

Helyann. C. Alvarez.V

October 2015

ABSTRACT

Questa tesi si concentra sull'analisi delle caratteristiche di scambio termico lato aria degli scambiatori di calore compatti con alette louvered, utilizzati in campo automobilistico.

L'obiettivo principale di questa tesi è quello di trovare una correlazione da letteratura che prevede il coefficiente di scambio termico delle geometrie di alette louvered e permette di capire come il coefficiente di scambio termico globale (UA) dipende da due parametri fondamentali di progettazione: la profondità del pacco (Ld) e passo dei tubi (Tp), al fine di ottimizzare le prestazioni degli scambiatori di calore con alette louvered.

Le correlazioni della letteratura sono state convalidate contro i risultati sperimentali rilevati alla prova al banco sperimentale DENSO, per le diverse geometrie scambiatori di calore, sia i radiatori ed i condensatori.

Lo studio ha mostrato che la correlazione di Chang e Wang è quella che meglio approssima le simulazioni di prova DENSO negli scambiatori di calore, radiatori e condensatori.

Una volta ottenuta la correlazione che meglio approssima i dati sperimentali, lo studio ottimizzazione del nucleo è stato eseguito per verificare se vi è vantaggio ulteriore riduzione del passo del tubo, profondità del pacco o variazione di qualsiasi altro parametro geometrico.

ABSTRACT

This thesis focuses on the analysis of the air-side heat transfer characteristics of compact heat exchangers louvered fins, used in the automotive field.

The main goal of this thesis is to find a literature correlation that predict the heat transfer coefficient of the louver fin geometry and allows to understand how the global heat transfer coefficient (UA) depends from two fundamental design parameters: core depth (Ld) and tube pitch(Tp) , In order to optimize the performance of the louvered fin heat exchanger.

The literature correlation has been validated against the experimental results measured at the DENSO experimental bench test, for different heat exchanger geometries, both radiators and condensers.

The study showed that the correlation of Chang and Wang is the one that better approximates the DENSO test simulations in the Radiators and Condensers heat exchangers.

Once obtained the correlation that better approximates the experimental data, the core optimization study has been performed in order to verify if there is benefit in further reduction of tube pitch, core depth or variation of any other geometric parameter.

AKNOWLEDGEMENTS

The contributions of this project would not be possible without God, who guided me and gave me the strength to keep forward in every moment.

I wish to thank and dedicate this work to my parents, who with much love and dedication they raised me, and thanks to them I am who I am, I owe them everything and they are my reason for living, likewise I would like to thank my two brothers and my grandmother, because they have always supported me and loved me, I would not be here without them.

I would like to thank to my home university, the Central University of Venezuela for giving me the opportunities for my personal growth, in the same way I would like to thank to the Polytechnic University of Turin for welcomed me to encourage this opportunity in this country who received me with their arms open.

I would like to express my gratitude to my relator Dr. Pietro Asinari, whose expertise and advices had great importance.

I am indebted to the company of DENSO Thermal Systems for giving me the opportunity to do an internship within the organization. I will forever be thankful to my company tutors Dr. Grazia Monni, Eng. Marta Roberti, Eng. Davide Perocchio and Eng. Fabio Sandri, for their infinite patience, advices and the many hours they have spent for my training, the success of this project would not be possible without them.

Last but not least, I would like to thank my fiancé and best friend Jose Quintero, who has been encouraged me and has been an unconditional help in every moment of this work.

TABLE OF CONTENTS

LIST OF FIGURES

INTRODUCTION

Finned tube heat exchangers are widely used in a variety of applications such as-air conditioning, refrigeration and in the process industry. Generally, the heat exchangers consists of a plurality of spaced parallel tubes through which a heat transfer medium, such as water-glycol, oil or refrigerant, is forced to flow while a second heat transfer fluids, like air, is directed across the tubes. For most practical applications, airside thermal resistance is roughly 5 to 10 times that of the refrigerant side.

Consequently, enhanced surfaces are often employed to effectively improve the overall performance of the fin and tube heat exchanger. One of the very popular enhanced surfaces is the interrupted surface, because can provide higher average heat transfer coefficients due to the periodical renewal of the development of boundary layer. The most common interrupted surfaces are offset strip and louvered fin.

For automotive application, such as radiators and condensers, the louvered fins are generally brazed (or soldered, mechanically expanded) to a flat, extruded tube, with a cross section of several independent passages, and formed into a serpentine or parallel flow geometry.

The first aim of this work is therefore to find a literature correlation able to model the air-side heat transfer of the heat exchanger, that has been validated by means of the experimental data from the tests performed on the DENSO heat exchangers (radiators and condensers), and highlight the dependences on fin geometrical parameters in order to perform an optimization analysis

Hence a preliminary analysis of these louvered fin correlations has been carried on in order to summarize the real performance and application ranges. Then the comparison between the correlations and the experimental data has been performed, verifying which is the one that fits better the experimental tests.

Once the more suitable correlation has been chosen, for each compact heat exchangers (radiators and condenser), it has been possible to begin to the second aim of this work, that is the study of a possible core optimization.

Optimizing radiators and condensers will be possible to have better performances or even reduce material, weight, space and all of these are summarized in cost reductions.

1. Theoretical Framework

1.1.-COMPACT HEAT EXCHANGERS

A heat exchanger is a device that is used to provide internal thermal energy (enthalpy) between two or more fluids; between a solid surface and a fluid, or between solid particulates and a fluid, in thermal contact without external heat and work interactions. The fluids may be single compounds or mixtures.

It is possible to classify the heat exchangers according to the following characteristics as shown in Figure 1:

- Transfer process
- Construction
- Flow arrangement
- Surface compactness
- Number of fluids
- Heat transfer mechanisms

The Compact heat exchangers are a class of heat exchangers that provide a large amount of heat transfer surface area per unit volume. Most automotive heat exchangers belong to the compact heat exchanger category since space is an extreme constraint for automotive applications.

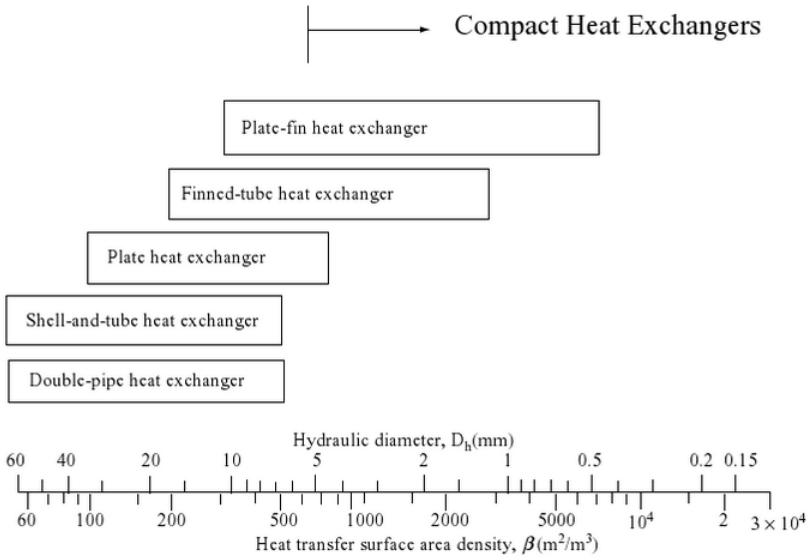

Figure 1-Compact heat exchangers

Usually the automotive compact heat exchanger use an indirect contact transfer process (single phase or multiphase), they work with two fluids which could be gas to fluid, liquid to liquid and phase change types exchangers.

In the exchanger core of the automotive heat exchanger usually are used the extended surfaces which are in direct contact with fluids and through which heat is transferred by conduction. The portion of surface which also separates the fluids is referred to as primary or direct surface. To increase heat transfer area, appendages known as fins may be intimately connected to the primary surface to provide an extended, secondary, or indirect surface. Thus, the addition of fins reduces the thermal resistance on that side and thereby increases the net heat transfer from the surface for the same temperature difference.

1.1.1.- Flow Arrangements

The flow arrangements of the fluids in a heat exchanger are:

- Counterflow: The two fluids flow parallel to each other in opposite directions.
- Parallel flow: The two fluids flow parallel to each other in the same direction.
- Crossflow: The two fluids flow normal to each other.

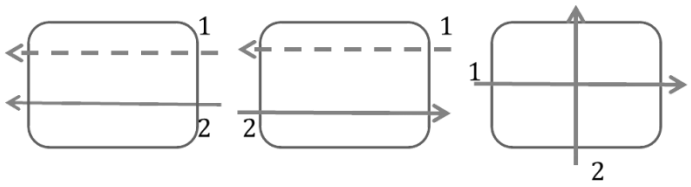

Figure 2- Parallel flow – Counterflow - Crossflow

Counterflow

Consider two counterflow channels across a wall, as shown in Figure 6a. The subscripts 1 and 2 denote the hot and cold fluids, respectively and the subscripts i and o indicate inlet and outlet, respectively. The mass flow rate is denoted as $\dot{m}$. The temperature distributions for the hot and cold fluids are shown in Figure 6b, where the dotted line indicates the approximate wall temperatures.

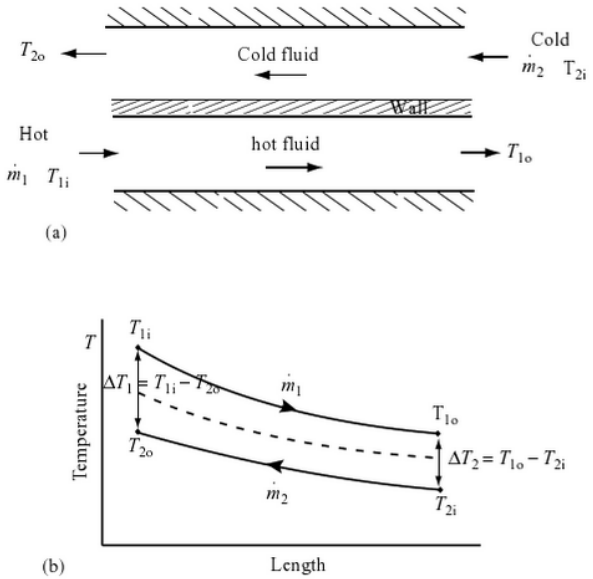

Figure 3- The counterflow arrangement: Schematic for counterflow channels and temperature distributions.

Parallel Flows

The Figure 7c. shows parallel-flow channels across a wall. The hot fluid T_{1i} enters the lower channel and leaves at the decreased temperature T_{1o} , while the cold temperature T_{2i} enters the upper channel and leaves at the increased temperature T_{2o}. The temperature distributions are presented in Figure 7d, where the dotted line indicates the wall temperatures along the length of the channel. Note that the wall temperatures in parallel flow are nearly constant compared to those changing in counterflow. Therefore, the counterflow heat exchanger is usually preferable. However, the nearly constant wall temperature is a characteristic of the parallel-flow heat exchanger, which is sometimes necessary (e.g., exhaust-gas heat exchangers usually require a constant wall temperature to avoid corrosion).

The total heat transfer rate between the two fluids can be expressed considering an enthalpy flow that is the product of the mass flow rate and the specific heat and the temperature difference. For the hot fluid, the heat transfer rate is:

$$q = \dot{m}_1 \, c_{p1} \, (T_{1i} - T_{1o})$$

Where $\dot{m}$ is the mass flow rate for the hot fluid and c_{p1} is the specific heat for the hot fluid.

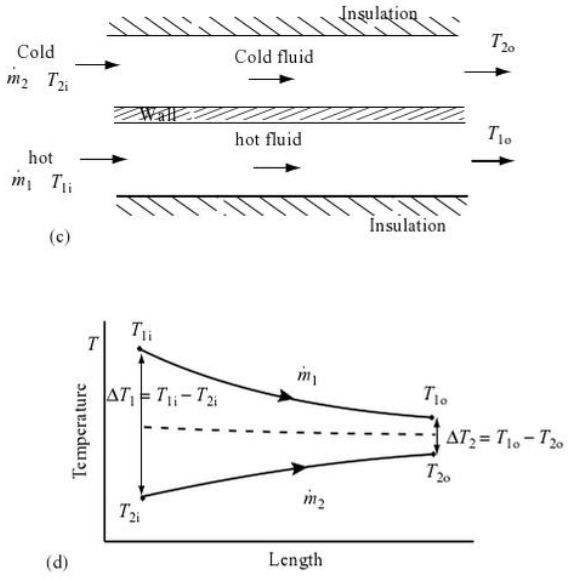

Figure 4- Parallel-flow arrangement: Schematic for parallel-flow channels and temperature distributions

For the cold fluid, the same heat transfer is expressed as :

$$q = \dot{m}_2 \, c_{p2} \, (T_{2o} - T_{2i})$$

where $\dot{m}_2$ is the mass flow rate for the cold fluid and c_{p2} is the specific heat for the cold fluid. The same heat transfer rate can be expressed in terms of the overall heat transfer coefficient,

$$q = UAF\Delta T_{lm}$$

where U is the overall heat transfer coefficient and A is the heat transfer surface area at the hot or cold side. F is the correction factor, depending on the flow arrangements. For example, $F = 1$ for counterflow or parallel flow such as the double-pipe heat exchangers, and usually $F \leq 1$ for other types of flow arrangements. Note that

$$UA = U_1A_1 = U_2A_2$$

ΔT_{lm} is the log mean temperature difference that is defined as:

$$\Delta T_{lm} = \frac{\Delta T_1 - \Delta T_2}{\ln\left(\frac{\Delta T_1}{\Delta T_2}\right)}$$

Where;

$$\Delta T_1 = T_{1i} - T_{2i} \; and \; \Delta T_2 = T_{1o} - T_{2o}$$

1.1.2.- Overall Heat Transfer Coefficient

The thermal circuit across a wall between hot and cold fluids, is shown in Figure 5. The temperature difference ($T_{1i-1o} - T_{2i-2o}$) seems complex, varying along the length, which

can be represented by the log mean temperature difference ΔT_{lm} .The heat transfer rate across the wall is:

$$q = \frac{T_{1i-1o} - T_{2i-2o}}{\frac{1}{UA}} = \frac{F\Delta T_{lm}}{\frac{1}{h_1 A_1} + R_w + \frac{1}{h_2 A_2}}$$

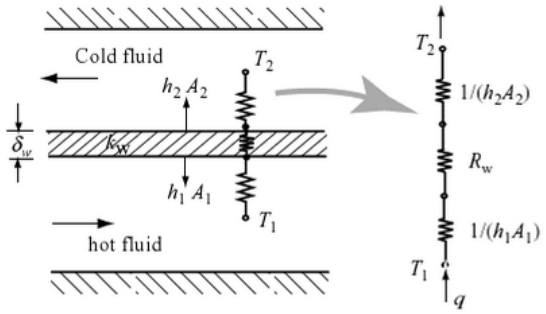

Figure 5 Thermal Resistances.

where h_1 and h_2 are the heat transfer coefficients for the hot and cold fluids, respectively, and A_1 and A_2 are the heat transfer surface areas for the hot and cold fluids, respectively, and R_w is the wall thermal resistance. For flat walls, the wall thermal resistance is:

$$R_w = \frac{\delta_w}{k_w A_w}$$

where δ_w is the thickness of the flat wall, k_w the thermal conductivity of the wall, and A_w is the heat transfer area of the wall.

The overall heat transfer coefficient for the cold fluid with the heat transfer area A_2 is:

$$U_2 = \frac{\frac{1}{A_2}}{\frac{1}{h_1 A_1} + R_w + \frac{1}{h_2 A_2}}$$

The UA value is defined as follows:

$$UA = \frac{1}{\frac{1}{h_1 A_1} + \frac{\delta_w}{k_w A_w} + \frac{1}{h_2 A_2}}$$

1.2.-AUTOMOTIVE COMPACT HEAT EXCHANGERS

Most automotive heat exchangers are similar to shell and tube cross flow design, with multiple tube passes. But instead of having a defined shell around the tubes, with another controlled fluid forced across the tubes by means of a pump, there is no limited control volume for the shell. The tubes are open to the air and are dependent upon outside conditions.

$$Q = h.A.\Delta T$$
$$Q = UA.LMTD$$

The cold flow "inlet" temperature varies dramatically and the mass flow rate is limited by the speed of the vehicle. In the previous two equations used to calculate heat transfer, this means that both "h" and "ΔT" values are subject to external conditions. To aid in more constant heat transfer rates, however, many automotive heat exchangers use fans to deliver constant cold fluid supply (longitudinal-mounted engines) or engage when working fluid temperatures reach the maximum of their operational range (transverse-mounted engines). The tubes on these heat exchangers are also aided by fins, further increasing the surface area "A" in the equations.

While the purpose of heat automotive heat exchangers is to remove heat from the mechanical systems, the goal is not merely maximum heat transfer from the system. There are other secondary purposes as well. If only maximum heat transfer were the objective, then efforts would be to only concentrate on designing the cooling system heat exchangers around the working fluid with the highest thermal conductivity, which would be water

(water & ethylene glycol mixture) which has a k value of around $0.6\,W/mK$ instead of motor oil or transmission oil which has a k value of around $0.2\,W/mK$. The reason that heavy-duty automobiles and racecars use oil or transmission coolers is for not only local heat dissipation and more uniform temperatures across multiple systems, but also to inhibit thermal breakdown of the working fluid itself. If temperatures are too high in oil, this leads to chemical breakdown and degradation of the oil and additives in the oil. This changes its viscosity and other physical properties.

After years of experience and testing over the years, automobiles have developed into very complex and functional machines. The materials of each part and the working fluids are chosen for very specific reasons. Most heat exchangers in today's automobiles are made from aluminum for its light weight, relatively high availability and its very high thermal conductivity. Radiators are filled with water because of its high heat capacity and thermal conductivity. Although ethylene glycol is added to aid the cooling system, it actually lowers the k value of the water mix. Its purpose is to increase the boiling temperature and lower the freezing temperature of water.

1.2.1.- Types of Automotive heat exchangers

Some types of automotive heat exchangers are the following:

- Heater Core
- Intercoolers
- Evaporators
- Oil Coolers (engine transmission, power steering, hydraulic oil)
- Coolant heat exchangers (Radiator)
- Condensers

The main features that an automotive heat exchanger should be satisfied are:

- Compactness: Small face and short flow depth for packaging.

- Low pressure drop: Reduced pumping power for coolants, better charge air density for charge air coolers, and increase temperature difference for refrigerants.
- Low cost and high manufacturing volume.
- Low weight: Reduced material cost and improved payload and or fuel economy.
- Durability.

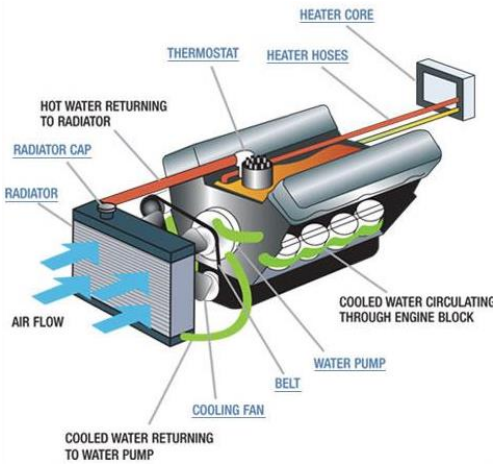

Figure 6-Engine cooling system

1.2.1.1.- Radiator

Radiators are required for the cooling of internal combustion engines. They operate by passing a liquid coolant through the engine block, where it is heated, then through the radiator where it loses the heat to the atmosphere. The coolant is generally water (with some additives, e.g. antifreezing agents, corrosion inhibitors, etc.). Usually the coolant is circulated by means of a pump and a fan is used to blow air through the radiator.

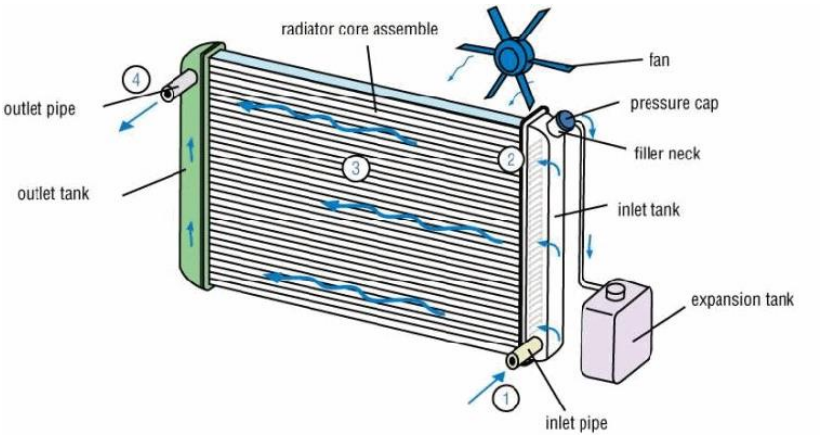

Figure 7-Radiator

In general, the radiator consists of the aluminum radiator core and two header tanks that cover the ends of the radiator and all of the required connections and fastening elements. The header tanks allow for the appropriate coolant volume to be circulated through the tubes. The radiator core is usually made of flattened aluminum tubes (although multiport extrusions can also be used) and aluminum fins that zigzag between the tubes. These fins transfer the heat in the tubes into the air stream to be carried away from the vehicle. On most modern radiators, the tubes run horizontally with the header tanks on either side. But the tubes may also run vertically with the tanks on top and bottom. There are gaskets between the aluminum core and the header tanks to seal the system and to keep the coolant from leaking out. The header tanks are generally made of plastic (e.g. fiber glass-reinforced polyamide), but there are also all-aluminum radiators. All aluminum radiators are lighter than the versions with plastic tanks, have a much smaller packaging depth, and are fully recyclable.

1.2.1.2.- Condenser

If the car has air conditioning, there is an additional heat exchanger called the air conditioner condenser, which also needs to be cooled by the air flow entering the engine compartment. Its location is usually in front of the radiator, but in some cases, due to aerodynamic improvements to the body of a vehicle, its location may differ. Condensers must have good air flow anytime the system is in operation. By exchanging heat with air, the condenser cools

the high-temperature, high-pressure gas refrigerant sent from the compressor and condenses it into liquid refrigerant. This heat exchange allows the air conditioning system to emit the heat absorbed by the evaporator from inside the vehicle to the outside.

As for all heat exchangers, in terms of performance, condensers must ensure maximum heat transfer while keeping size to a minimum. Furthermore, condensers must be of an extremely high quality, providing trouble-free performance throughout its service life at low manufacturing costs. Typically air conditioning condensers are of either of the parallel flow or of the serpentine type design. A very small fraction of condenser designs are based on mechanically assembled solutions. Practically all condensers are produced by brazing (in general using the controlled atmosphere brazing method). Serpentine condensers consist of a refrigerant tube bent in the form of a “serpentine”. The refrigerant tube is normally an extruded or precision drawn tube. Clad fins are brazed to the tube. This design is quite robust, but characterized by a high refrigerant pressure drop. Consequently, this type of design is very rarely encountered today. In the parallel flow design, a pair of parallel vertical header tanks distributes the refrigerant to horizontally aligned tubes which in turn are connected to fins. Extruded multi-port tubes are mostly used for the refrigerant tubes. Aluminum multi-port extrusions offer favorable heat transfer area to volume ratio, which makes these extrusions ideal for heat exchangers with high performance requirements. The headers, end caps, baffles, brackets and side supports are produced from rolled aluminum alloy stocks. Depending on the specific design, the header stock can be clad on one or two sides with a braze liner.

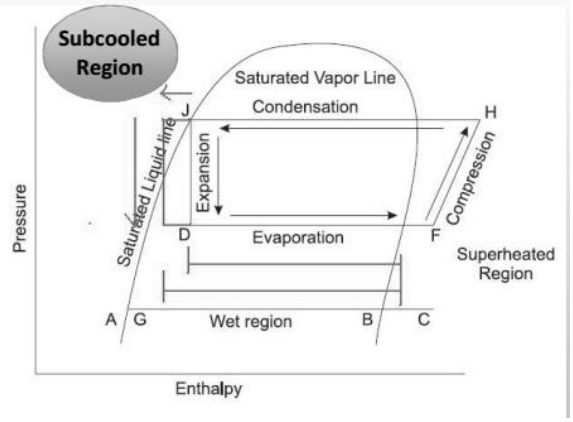

Figure 8- Diagram pressure vs enthalpy

1.2.2.- Tubes Types

The different tube types used in compact heat exchangers are the following:

- Flat tube.
- Circular tube.
- Oval tube.

In the past the circular and oval tubes have been used, but nowadays the most common is the flat tube type. There are new technologies for the tubes such as:

- Multiport tubes
- Tubes with turbulator such as dimples or helically inserts.

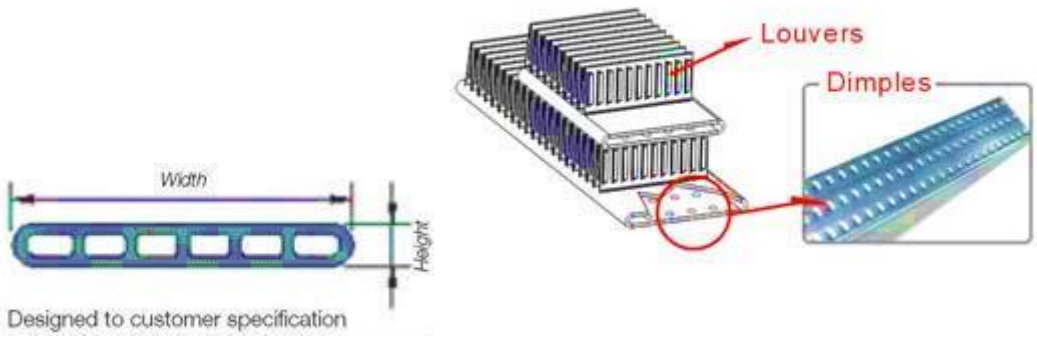

Figure 9-Tube types

In the Radiators configurations the tubes with dimples is commonly adopted, and for the Condensers the multiport tubes.

1.2.3.- Fin Types

The fins or extended surfaces in heat exchangers are primarily used to increase the surface area and, consequently, to enhance the heat transfer rate. The Compact heat exchangers are dependent on enhanced air side heat transfer surfaces, because a high percentage of total thermal resistance in a typical air cooled heat exchanger occurs on the air side.

The different types of fins are reported below:

- Rectangular fin
- Triangular fin
- Pin fin
- Offset strip fin
- Wavy fin
- Louvered fin
- Perforated fin

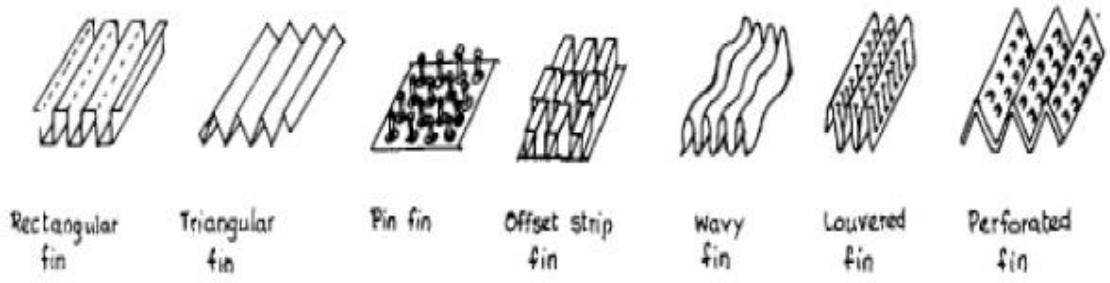

Figure 10-Fin types

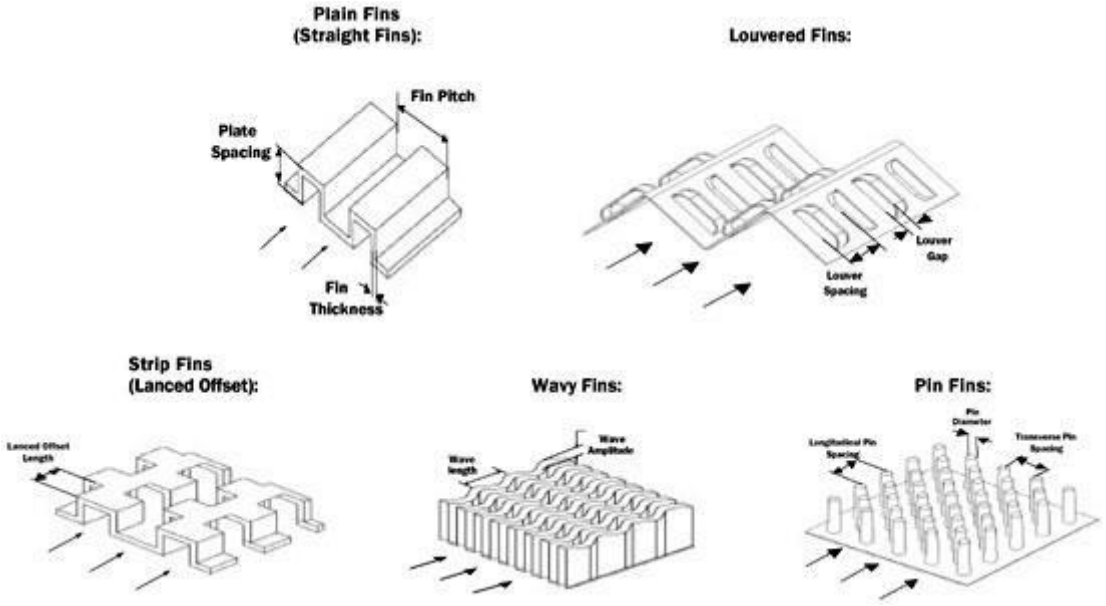

Figure 11-Fin types (Plain, Louvered, Strip, Wavy, Pin).

For compact heat exchangers as Radiators and Condensers the louvered fins are used, this kind of fins are specially indicated where the tubes are flats and it is necessary a good balance, in terms of heat transfer, pressure drop, space reduction, and costs. The louvered fins has the highest heat transfer enhancement relative to pressure drop in comprarison with most other fin types.

Figure 12-Louvered fin

Definition of the Fin Efficiency.

The Definition of the fin efficiency is the ratio of the actual heat dissipated through the fin base divided by the heat that would be dissipated if the fin possessed an infinite thermal conductivity (if the entire fin were at the base temperature).

$$\eta_f = \frac{Q_f}{Q_{fmax}} = \frac{h_f A_f (\overline{T}_f - T_a)}{h_f A_f (T_w - T_a)}$$

First of applying the conservation of energy is necessary to consider the following assumptions:

- The temperature is uniform across the fin thickness (only function of x, which means 1-Dimensional).
- Steady-state conditions.
- Thermal conductivity constant.
- The radiation from the surface is negligible.
- Heat generation effects are absent.
- Heat transfer coefficient h is uniform over the surface.

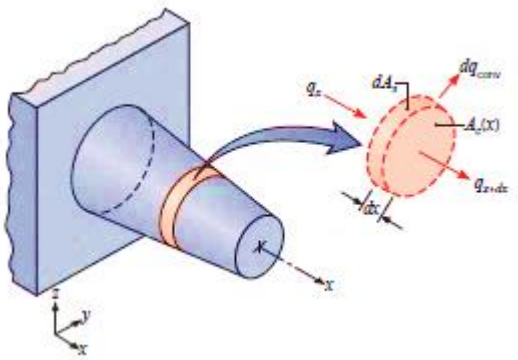

Figure 13 Energy balance for and extended surface

Applying the conservation of energy to the differential element of the Figure 13, can be obtained:

$$q_x = q_{x+dx} + dq_{conv}$$

From the Fourier's law:

$$q_x = -kA_c \frac{dT}{dx}$$

And consequently:

$$q_{x+dx} = q_x + \frac{dq_x}{dx}dx \;\; ; \;\; q_{x+dx} = -kA_c\frac{dT}{dx} - k\frac{d}{dx}\left(A_c\frac{dT}{dx}\right)dx \; ; \; dq_{conv} = hdA_s(T - T_\infty)$$

Where $A_c$is the cross-sectional area, which may vary with x, and $dA_s$is the surface area of the differential eleent. Substituting the foregoing rate equations into the energy balance, can be obtain the general form of the energy equation for an extended surface that with the appropriate boundary conditions provides the temperature distribution.

$$\frac{d}{dx}\left(A_c\frac{dT}{dx}\right) - \frac{h}{k}\frac{dA_s}{dx}(T - T_\infty) = 0 \qquad \text{or} \qquad \frac{d^2T}{dx^2} + \left(\frac{1}{A_c}\frac{dA_c}{dx}\right)\frac{dT}{dx} - \left(\frac{1}{A_c}\frac{h}{k}\frac{dA_s}{dx}\right)(T - T_\infty) = 0$$

To solve this equation it is necessary to be more specific about geometry.

Assuming:

- Straight rectangular fin geometry.
- Base surface of temperature $T(0) = T_b$.
- Cross sectional area is constant A_c.
- Surface area $A_s = Px$, where P is the fin perimeter.

Therefore, the equation in one dimension reduces to:

$$\frac{d^2T}{dx^2} - \left(\frac{h}{k}\frac{P}{A_c}\right)(T - T_\infty) = 0 \quad with \quad \theta(x) = T(x) - T_\infty$$

$$\frac{d^2\theta}{dx^2} - m^2\theta = 0 \qquad \text{Where} \qquad m^2 = \frac{h}{k}\frac{P}{A_c}$$

The second order differential equation has the following solution:

$$\theta(x) = C_1e^{mx} + C_2e^{-mx}$$

And the boundaries conditions to adopt for the cases in study are:

- Temperature at the base of the fin defined (x=0) $\rightarrow$ $\theta(0) = \theta_b$

- Insulated tip in $x = \frac{Fh}{2} \quad \rightarrow \quad \left.\frac{d\theta}{dx}\right|_{x=\frac{F_h}{2}} = 0$

It is possible to calculate the values of the constants C1 and C2 using the boundary conditions in order to finally obtain the expression of temperature distribution as follows:

$$\frac{\theta}{\theta_w} = \frac{\cosh m\left(\frac{Fh}{2} - x\right)}{coshm\frac{F_h}{2}}$$

Using this temperature distribution, the fin heat transfer rate is then:

$$q_f = \sqrt{hPkA_c}\theta_w \tanh m\frac{F_h}{2}$$

The definition of the plane fin efficiency (1-D) with a constant cross section, is given by the follow expression:

$$\eta_f = \frac{\tanh\left(m\left(\frac{F_h}{2}\right)\right)}{m\left(\frac{F_h}{2}\right)} \qquad m = \sqrt{\frac{2h_f}{kf.b}}$$

TABLE 4.5.5 Fin Efficiency Expressions for Plate-Fin and Tube-Fin Geometries of Uniform Fin Thickness

Geometry	Fin Efficiency Formula $m_i = \left[\frac{2h}{k_f \delta_i}\left(1+\frac{\delta_i}{l_f}\right)\right]^{1/2}$ $E_1 = \frac{\tanh(m_i l_1)}{m_i l_1}$ $i = 1, 2$
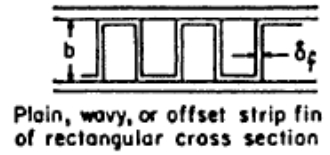 Plain, wavy, or offset strip fin of rectangular cross section	$\eta_f = E_1$ $l_1 = \frac{b}{2} - \delta_1 \quad \delta_1 = \delta_f$
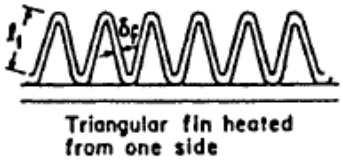 Triangular fin heated from one side	$\eta_f = \frac{hA_1(T_0 - T_a)\frac{\sinh(m_1 l_1)}{m_1 l_1} + q_e}{\cosh(m_1 l_1)\left[hA_1(T_0 - T_a) + q_e \frac{T_0 - T_a}{T_1 - T_a}\right]}$
 Plain, wavy, or louver fin of triangular cross section	$\eta_f = E_1$ $l_1 = \frac{l}{2} \quad \delta_1 = \delta_f$
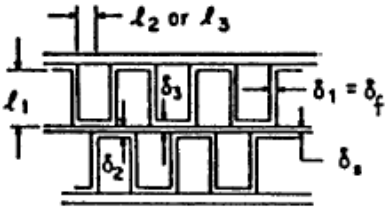 Double sandwich fin	$\eta_f = \frac{E_1 l_1 + E_2 l_2}{l_1 + l_2}\frac{1}{1 + m_1^2 E_1 E_2 l_1 l_2}$ $\delta_1 = \delta_f \quad \delta_2 = \delta_3 = \delta_f + \delta_s$ $l_1 = b - \delta_f + \frac{\delta_s}{2} \quad l_2 = l_3 = \frac{p_f}{2}$

Figure 14-Fin efficiencies

1.3.- DIAMENSIONLESS QUANTITIES

A dimensionless quantity is a quantity to which no physical dimension is applicable, and is therefore of dimension one. Dimensionless quantities are widely used in many fields, such as mathematics, physics, engineering and economics.

They are often obtained as products or ratios of quantities that are not dimensionless, but whose dimensions cancel in the mathematical operation.

The value of the dimensionless numbers often determine the behavior of the solution. For example, a flow problem with a low Reynolds Number will be laminar, while a larger value will imply turbulent behavior.

The number of dimensionless numbers determines the dimensionality of the space of solutions. For example, if a problem has two dimensionless numbers, then by varying both numbers, all the different behaviors in the problem can be accounted for.

Using the dimensionless numbers, one can gain insight about the behavior of different variables in different problems. This is because variables with different dimensions have to be constructed by dismantling the different dimensionless numbers.

Here is a list of different dimensionless numbers:

- Nusselt Number: it is the ratio of convective (advection and diffusion) and conductive heat transfer across the boundary. A Nusselt number close to one, namely convection and conduction of similar magnitude, is characteristic of laminar flow. A larger Nusselt number corresponds to more active convection, with turbulent flow typically in the 100-1000 range.

$$Nu_L = \frac{Convective\ heat\ transfer}{Conductive\ heat\ transfer} = \frac{hL}{k}$$

Where, h is the convective heat transfer coefficient of the flow, L is the characteristic length, k is the thermal conductivity of the fluid.

- Reynolds Number: it is a dimensionless quantity that helps predict similar flow patterns in different fluid flow patterns in different fluid flow situations. The Reynolds number is defined as the ratio of momentum forces to viscous forces and consequently quantifies the relative importance of these two types of forces for given flow conditions.

$$Re = \frac{inertial\ forces}{viscous\ forces} = \frac{\rho uL}{\mu} = \frac{uL}{\upsilon}$$

Where, u is the maximum velocity of the object relative to the fluid, L is the characteristic linear dimension, μ is the dynamic viscosity of the fluid, v is the kinematic viscosity and ρ is the density of the fluid.

- Prandtl Number: it is defined as the ratio of momentum diffusivity to thermal diffusivity. That is, the Prandtl number given as:

$$Pr = \frac{v}{\alpha} = \frac{viscous\ diffusion\ rate}{thermal\ diffusion\ rate} = \frac{c_p \mu}{k}$$

Where v is momentum diffusivity, α is the thermal diffusivity, k is the thermal conductivity, c_p is the specific heat and ρ is the density.

- Colburn Factor: it is a successful and widely used analogy between heat, momentum and mass transfer. Among many analogies (like Reynolds analogy, Prandtl-Taylor analogy) developed to directly relate heat transfer coefficients, mass transfer coefficients and Colburn factor analogy proved to be most accurate. The dimensionless heat transfer coefficient is the following:

$$j = \frac{Nu}{RePr^{\frac{1}{3}}} = \frac{hPr^{\frac{2}{3}}}{\rho u c_p}$$

2. Heat Transfer analysis of Louver Finned Heat Exchangers for Automotive Sector.

2.1. LOUVERED FIN HEAT EXCHANGERS

Flat plate heat exchangers with louvered fins are widely used in a variety of applications such as refrigerators, automotive industry and chemical engineering. The louvered fins and flat tube heat exchangers have a higher degree of surface compactness.

The dominant thermal resistance is usually on the airside, and therefore the use of finned surfaces on the airside is very common to effectively improve the overall performance of the fin and tube heat exchanger, and the interrupted surfaces can provide higher average heat transfer coefficients owing to periodical renewal of the development of boundary layer. The louvered pattern is more beneficial than the offset strip surface because is produced in large quantities since it can be manufactured by high speed production techniques, also are less expensive compared to other interrupted flow geometries when produced in large quantities.

The louvered fin designs have been adopted since the 1950's; it has only been after the next twenty years that serious attempts to understand the flow phenomena and performance characteristic of the louvered fin were made. Because of the good characteristics of thermal hydraulic performances, the louvered fins have been studied by a number of researchers ever since their appearance, not only experimental studies but also numerical simulations.

2.1.1. Main Geometrical parameters of Louvered Fins.

The geometrical parameters of a louvered fin are listed below:

- L_p: Louver pitch.
- L_h: Louver height.
- L_a: Louver angle.
- H_{fin}: Vertical projection of the Fin height.
- F_p: Fin pitch.
- L_d: Core depth.
- F_h: Fin height.
- b: Fin thickness
- T_h: Tube height.
- T_p: Tube pitch➔ $T_p = F_h + T_h$
- S_2: Central unlouvered section.
- S_4: Unlouvered inlet and outlet sections.
- S_3: Inclined portion on the louvers.
- D_{eq}: Equivalent diameter

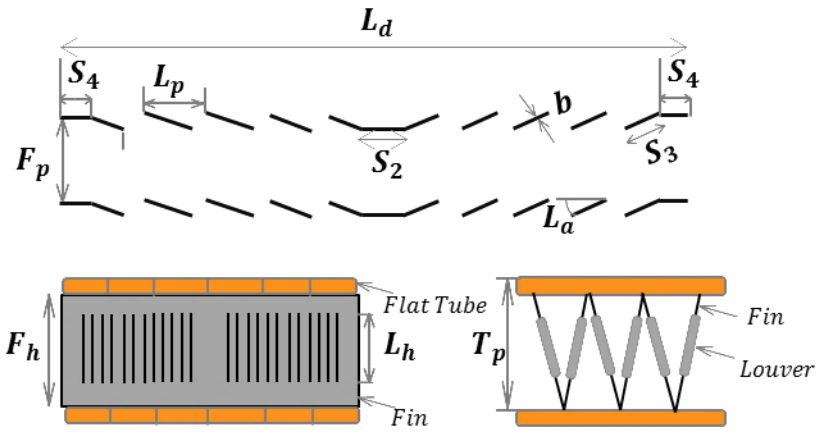

Figure 15-Fin geometrical parameters

2.1.2. Past Studies.

Some investigators contend that louvers serve as flow turbulators, disturbing the airflow path and thereby increasing fluid mixing. Others investigators believe louvers align the airflow in the louver direction creating a series of miniature flat plates with heat transfer typical of flat plate boundary layers. The complexity of the flow and the difficulty in constructing a large array of test samples has limited louvered fin flow modeling efforts.

Davenport [7] performed an important study of louvered fin performance, conducted smoke filament visualization and velocity profile measurements on scale models of triangular louvered fins. He also tested thirty-two full scale heat exchangers where the louver and fin geometries were systematically varied, and using this data he developed an empirical correlation for heat transfer and pressure drop based on these parameters. He noted that the mean flow angle increased with flow velocity, particularly on the model with the largest fin pitch. He also noted the flow angle was greater for the smaller fin pitches, and the mean angle for the upstream louver bank was greater than for the downstream bank. Finally he

theorized that the flow angle dependency on Re_{Lp} and fin geometry was a result of boundary layer growth on the louvers.

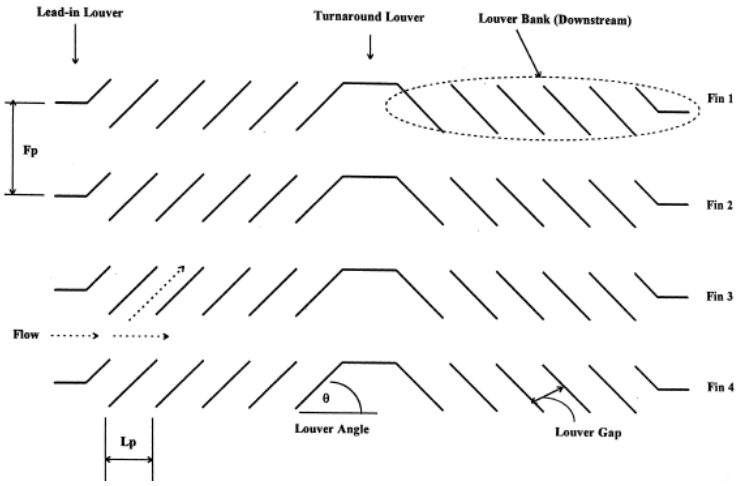

Figure 16 – Section through typical louvered-fin showing key geometrical parameters.

At low flow rates, the boundary layer on each louver is thick, severely restricting flow within the gap between louvers. Flow then prefers the more open duct path between louver banks and the majority of the flow bypasses the louvers altogether. The boundary layer thins as the flow velocity increases and the flow begins to follow the louvers.

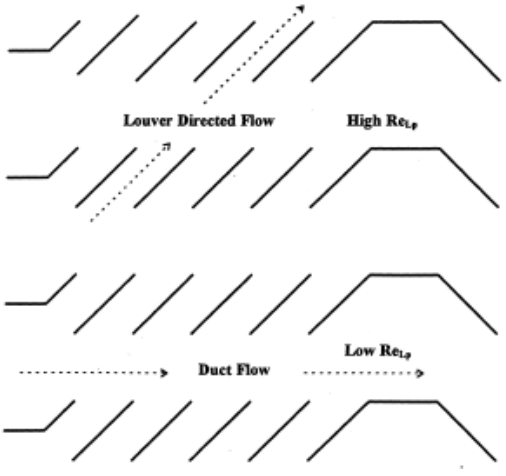

Figure 17 – Duct vs louver-directed flow behavior.

Tura studied the effect of louver angle and flow reversal length on louvered fin performance. He used an innovative phase change paint technique on 4:1 model triangular fins to determine heat transfer coefficient of each individual louver. The results showed a high heat transfer coefficient at the leading edge of each individual louver, typical to flat-plate boundary layer flow, as shown in the figure [18].

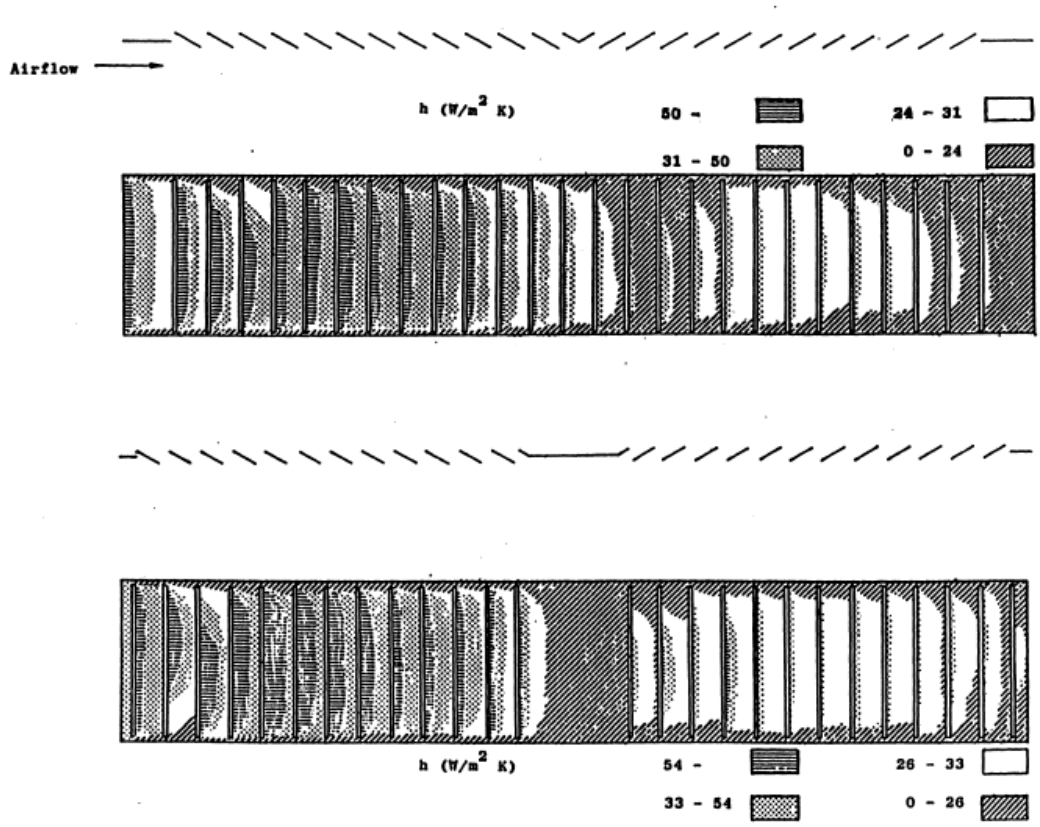

Figure 18 – Heat transfer coefficient measured on louvered-fins using phase change spray paint. Note the high heat transfer at louver leading edge and developing flow at first few louvers in each bank.

The testing also clearly showed developing flow at the first few louvers and degraded performance in the region of the flow reversal. Tura also conducted his studies in rectangular fins, and he concluded that the flow behavior in triangular and rectangular fins was similar.

Tura also conducted full scale heat exchangers testing which showed a strong dependence on louver angle but no significant impact of flow reversal length. In agreement with Davenport, he noted a distinct fall off in louvered fin performance for $Re_{Lp} < 270$. Tura attributed the louvered fin performance degradation to a transition from forced to free convection at the lower flow velocities. He recommended the optimal louver design should maximize the number of louvers and minimize both the length and number of flow reversals.

Achaichia and Cowell [12] used numerical methods to predict the mean flow angle of louvered fins. Their model is based on steady, two-dimensional flow into and out of a louver in the fully developed periodic region. The technique predicts an asymptotic mean flow angle (less than the louver angle) at a large Re_{Lp} and a rapid fall off in the flow angle for $Re_{Lp} < 100$ see the following figure 19.

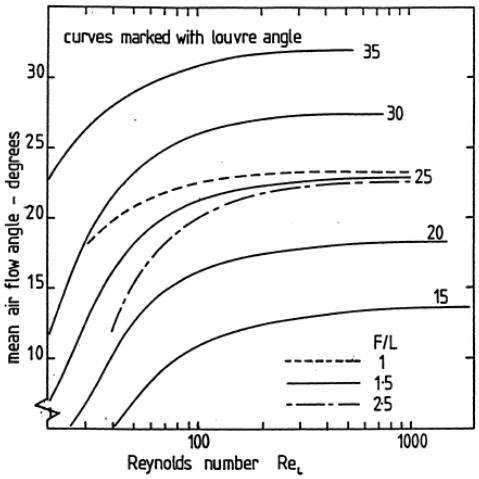

Figure 19 – Flow efficiency, predicted by Achaichia and Cowell's numerical correlation.

Flow angle drop off is more rapid as F_p/L_p increases. Since it ignores the developing flow region at the entry to each louver bank, Achaichia and Cowell's model probably over predicts the flow angle measured across the entire fin array.

Webb and Trauger [9] performed louvered fin flow visualization studies using scale models in an open water channel. They characterized each model in terms of its flow efficiency,

defined as the actual transverse distance the flow travels (N) divided by the ideal travel (D) if the flow followed the louver perfectly. They noted laminar flow for $Re_{Lp} < 500$ for all thest sections. At small fin pitches, they observed laminar boundary layers and wakes; the wakes appeared to fully dissipate before reaching the downstream louver. They noted a flow efficiency dependence on Re_{Lp}.

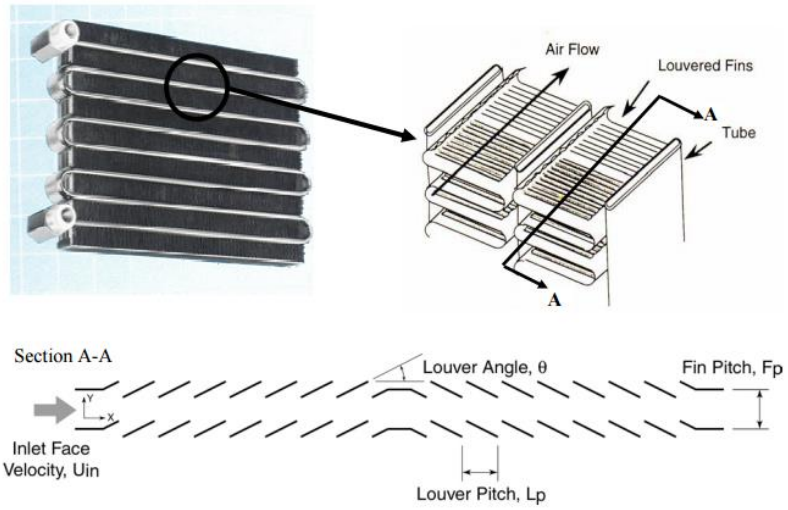

Figure 20-Louvered fins.

Effect of Geometrical Parameters on Heat Transfer Characteristics of Compact Heat Exchanger with Louvered Fins.

Experimental studies aimed at optimizing due to the large number of geometrical parameters involved such as louver pitch, louver angle, louver length and fin pitch. Thus, Webb and Trauger [9] and Sahnoun and Webb [10] in their further research used visualization techniques to investigate the relationship between the flow alignment and the geometrical parameters of the louver angle, louver pitch, and fin pitch. They found that the degree of flow alignment at a given Reynolds number is increased as the fin to louver pitch ratio is reduced. Kim Bullard [13] analyzed experimentally the air-side thermal and hydraulic performance of multi-louvered fin aluminum heat exchangers, and according to them, a

multilouvered fin and flat tube CHE is one of the other alternatives that can replace conventional finned tube heat exchangers. The air side thermal and hydraulic performance of multilouvered fin and flat tube CHE depends on louver geometry such as fin and louver pitches, louver angle, and flow depth. They concluded that the heat transfer coefficient increases exponentially with face air velocity and decreases with flow depth. Also, pressure drop increases with the increase of louver angle and flow depth and decreases with the increase of fin pitch.

Malapure et al. [11] performed numerical investigations on the fluid flow and heat transfer characteristics over louvered fins and flat tube in CHEs. Each case is performed for different geometries with change of louver angle, fin pitch, louver pitch and tube pitch and also for different Reynolds number study cases. They found that at low Reynolds number, the flow is fin directed; while at high Reynolds number, the flow is louver-directed. They concluded that the Nusselt number is substantially high at the fin tip and at the leading and trailing edges of the louver.

2.1.3. Flow Efficiency

The Flow efficiency is used to describe the percentage of the fluid flowing along the louver direction. A 100% efficiency represents ideal louver directed flow, while 0% represents complete duct directed flow. In the past, two kinds of definitions of flow efficiency have been used.

- In experimental dye injection studies, flow efficiency is defined as the ratio of actual transverse distance (N) traveled by the dye to the ideal distance (D) if the flow were aligned with the louver.

$$F_{e_{exp}} = \frac{N}{D}$$

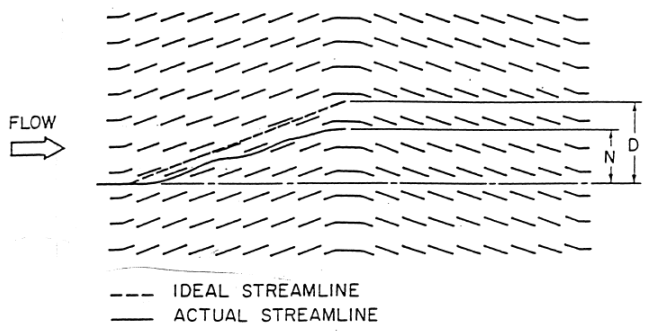

Figure 21 – Flow efficiency Fe

- In numerical simulations, because the flow angle can be easily obtained for each individual louver, flow efficiency is defined to be the ratio of mean flow angle(α_{mean}), which is obtained by averaging flow angles through out the louver bank (inlet, redirection and exit louvers are not included), to louver angle (L_a) as follows:

$$F_e = \frac{\alpha_{mean}}{L_a}$$

The average velocity ratio v (the average normal velocity across top boundary to that across the left boundary) is used to define flow angle in an individual block surrounding a louver is:

$$\alpha = \tan^{-1} \frac{\int vdx/Lp}{\int udy/Fp}$$

For a small louver angle($\theta < 30$), the difference between $F_{e_{exp}}$ and F_e is small.

Webb and Trauger experimentally studied the flow structure in multilouvered fin geometries for six fin pitch ratios (0.7 to 1.5), one thickness ratio (0.0423) and two louver angles (20 and 30 degrees). Reynolds number (based on louver pitch) ranged from 400 to 4000. Their results showed that flow efficiency increased with increasing Reynolds number until a critical Reynolds number was reached,

$$Re_{W,c} = 828 \left(\frac{L_a}{90}\right)^{-0.34} \qquad [1]$$

Before the critical value, flow efficiency depends on Reynolds number, louver angle increasing, and decreases with fin pitch ratio.

$$F_{e_w} = 0.091Re^{0.39}\left(\frac{L_p}{F_p}\right)^{0.44}\left(\frac{L_a}{90}\right)^{0.3} \qquad [2]$$

Beyond the critical value of Reynolds number, flow efficiency is only affected by fin pitch ratio, the expression is the following:

$$F_{e_{max,W}} = 0.95\left(\frac{L_p}{F_p}\right)^{0.23} \qquad [3]$$

The above flow efficiency is not continuous at the critical Reynolds number, To remedy this deficiency, Shahnoun and Webb [10] modified the equation [2] to keep the flow efficiency continuous at the critical Reynolds number:

$$Fe_{SW} = 0.95\left(\frac{L_p}{F_p}\right)^{0.23} - 0.00003717x\left[828\left(\frac{2L_a}{\pi}\right)^{-0.34} - Re\right]^{1.1}\left(\frac{Lp}{Fp}\right)^{-1.35}\left(\frac{2L_a}{\pi}\right)^{-0.61} \qquad [4]$$

Achaichia and Cowell [12] used numerical calculations to model the flow through a simplified two-dimensional louver array. The louver were assumed to be infinitely thin, and the flow to be fully developed. From their numerical simulations, the following for flow efficiency was given:

$$Fe_A = \left(0.936 - \frac{243}{Re} - 1.76.\frac{Fp}{Lp} + 0.995L_a\right)/L_a \qquad [5]$$

As Reynolds number tends to infinity, flow efficiency in equation [5] approaches an asymptotic value depending on fin pitch ratio and louver angle:

$$Fe_{max,A} = \left(0.936 - 1.76\frac{Fp}{Lp} + 0.995L_a\right)/L_a \qquad [6]$$

The critical Reynolds number is:

$$Re_{A,c} = \frac{4860}{\left(0.936 - 1.76\left(\frac{Fp}{Lp}\right) + 0.995L_a\right)} \qquad [7]$$

Bellows in 1996 conducted flow visualization experiments and investigated the effects of fin pitch ratio and louver angle on flow efficiency. Using Achaichia and Cowell correlation as a starting point, and taking into consideration developing flow effects, a general correlation was developed:

$$Fe_B = (-5 - \frac{300}{Re} - 10\frac{Fp}{Lp} + 1.34La)/La \qquad [8]$$

The asymptotic flow efficiency as Reynolds number tends to infinity is:

$$Fe_{max,B} = \left(-5 - 10\frac{Fp}{Lp} + 1.34L_a\right)L_a \qquad [9]$$

The critical Reynolds number is :

$$Re_{B,c} = \frac{6000}{\left(-5-10\frac{Fp}{Lp}+1.34L_a\right)} \qquad [10]$$

To conclude, the flow efficiency is a function of:

- Reynolds number
- Fin pitch ratio
- Louver angle

Flow efficiency increases with increases of Reynolds number and louver angle, and decreases with fin pitch ratio. As Reynolds number increases, flow undergoes a transition from duct directed flow (low efficiency) to louver directed flow (high efficiency). There exists a critical Reynolds number beyond which the flow efficiency is independent of Reynolds number.

All previous correlations agree in predicting the general trends. However, substantial quantitative differences exist.

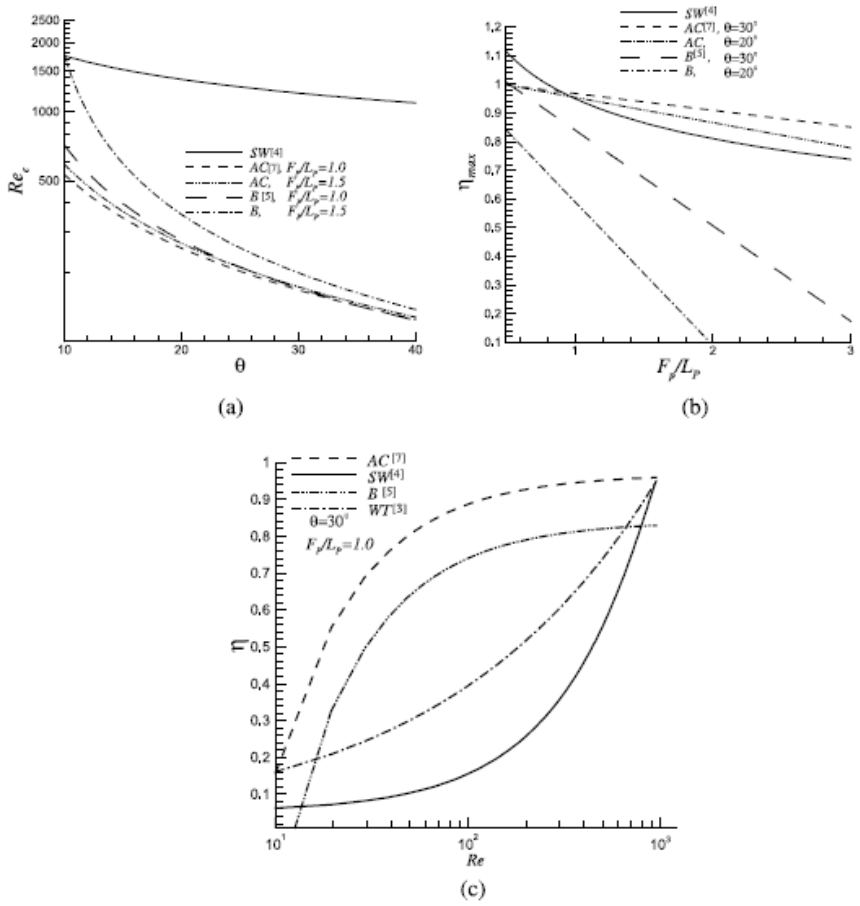

Figure 22 – (a) Critical Reynolds number versus louver angle; (b) asymptotic value of flow efficiency versus fin pitch ratio; (c) flow efficiency versus Reynolds number. Note the large qualitative as well as quantitative discrepancies between the correlations.

2.2. Heat transfer Correlations for corrugated louvered fin geometries.

Louver fins are used extensively in the automotive industry due to their mass production manufacturability and, hence, lower cost. They have generally higher Colburn factors j than the other discontinuous fin geometries, but the increase in the friction factors is in general higher than the increase in j factors.

The aim of this chapter is find a fin thermal model that depends on geometrical parameters of the heat exchanger core. Therefore several correlations that model the heat exchange on

the air side have been found, that depend on a numerous fin geometrical parameters. These correlations have been analyzed for different fin geometries.

The results have been compared with the experimental data measured at the DENSO test bench facility.

The following table 1 shows the fin geometrical parameters that have been studied.

	RADIATORS					**CONDENSERS**							
FIN	**R1**	**R2**	**R3**	**R4**	**R5**	**C1**	**C2**	**C3**	**C4**	**C5**	**C6**	**C7**	**C8**
$\boldsymbol{Ld}$	12 – 27					12-16							
$\boldsymbol{Lp}$	0.68-1					0.68-1							
$\boldsymbol{La}$	26 - 28					23 - 28							
$\boldsymbol{Fh}$	5 - 6					5-8							
$\boldsymbol{Fp}$	2.25 – 2.5					2.0-3.0							

Table 1-Fin geometrical parameters studied.

Correlation 1

Title: **A generalized heat transfer correlation for louver fin geometry**

Authors: **Chang and Wang [1997]**

A generalized heat transfer correlation for louver fin geometry is developed with a large data bank; this data bank consists in 91 samples of louvered fin heat exchangers with different geometrical parameters.

The data bank includes those from Davenport [7] (30 samples, Fig 23,Type A), Tanaka[18] (one sample, Fig 23 TypeC), Achaichia and Cowell [12] (15 samples, Fig 23, Type B), Webb [9](5 samples,Fig 23, Type C),Sunden and Svantesson [14](6 samples, Fig 23, Type C), Webb

and Jung[19](6 samples, Fig 23, Type C and Type E), Rugh [15] (1 sample, Fig 23, Type D) and Chang and Wang (27 samples, Fig 23, Type C).

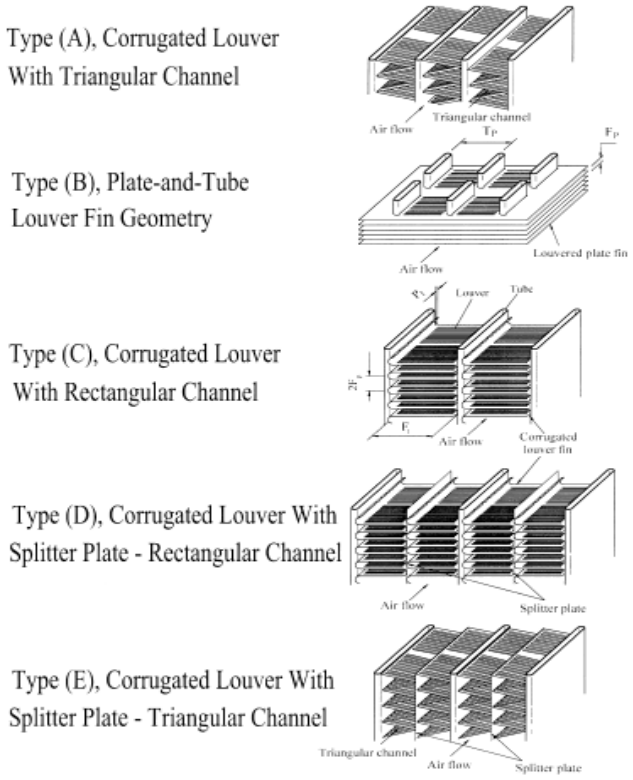

Figure 23- Louver fin types considered in correlation 1

Uncertainty

For the corrugated louver fin geometry, it is shown that 89.3% of the corrugated louver fin data are correlated within $\pm$15% with mean deviation of 7.55%. With the inclusion of the plate and tube louver fin data in the heat transfer correlation results in a mean deviation of 8.21%.

Reynolds range

$100 < Re_{Lp} < 3000$

The Colburn j factor:

$$j = Re_{Lp}^{-0.49}\left(\frac{L_a}{90}\right)^{0.27}\left(\frac{F_p}{Lp}\right)^{-0.14}\left(\frac{F_h}{L_p}\right)^{-0.29}\left(\frac{L_d}{L_p}\right)^{-0.23}\left(\frac{L_h}{L_p}\right)^{0.68}\left(\frac{T_p}{L_p}\right)^{-0.28}\left(\frac{b}{L_p}\right)^{-0.05}$$

Dependence on fin geometrical parameters

For the parametric analysis of this correlation have been considered the geometric parameters from the R5 radiator typology, a mean temperature of 40 °C and a fixed velocity of 6 m/s.

- **Effect of Louver Angle**

The Figure 24 shows the Correlation 1 behavior with the louver angle variation.

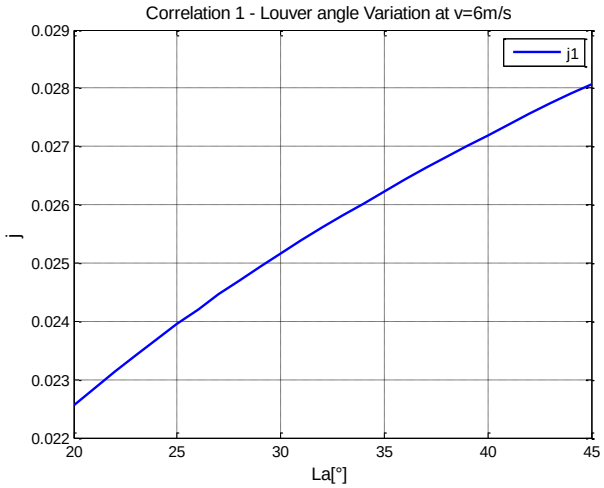

Figure 24- Correlation 1 Louver angle variation.

It is possible to note that increasing the louver angle the colburn factor j raises, but there is no presence of a critical angle.

- **Effect of Fin height, Fin pitch and Core depth.**

The effect due to the fin height variation as a function of the core depth and fin pitch has been plotted in two surfaces and analyzed for the present correlation.

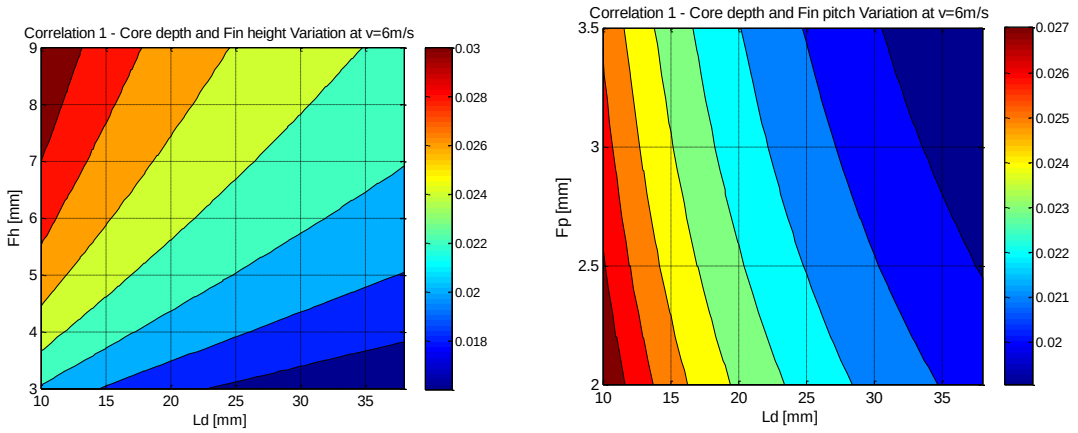

Figure 25 Correlation 1 a)Core depth and fin height variation; b) Core depth and fin pitch variation

The Figure 25.a shows that the Colburn factor j raises with increasing the fin height and decreasing the core depth, therefore the Correlation 1 provides a suitable performance as found in the reality. On the other hand the Figure 25.b shows that the Colburn factor j raises with lower values of fin pitch and core depth.

- **Effect of Louver pitch and Louver angle**

The effect due to louver pitch and louver angle variation has been plotted in a surface and analyzed for the present correlation.

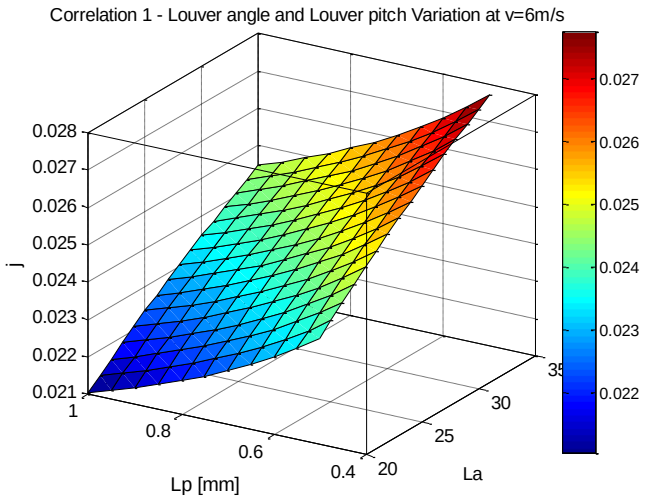

Figure 26 Correlation 1 Louver angle and louver pitch variation.

The Figure 26 shows that increasing the louver angle and decreasing the louver pitch the Colburn factor j raises.

Correlation 2

Title: *Air-side Heat Transfer and Friction Correlations for Flat-tube, Louver-fin Heat Exchangers, J.Heat Transfer.*

Authors: **Park and Jacobi [2009a]**

A heat transfer correlation for louver fin geometry is developed with a large data bank, this data bank consists in 126 samples of louvered fin heat exchangers with different geometrical parameters.

The experimental data sources include those from Achaichia and Cowell [12], Davenport [7], Chang and Wang [1], Kim and Bullard [13], Sunden and Svantesson [14], Rugh Pearson and Ramadhyani [15], Jacobi, Park, Zhong and Xia [16], Kim, Yun and Lee [17], Webb and Jung [19]

- Uncertainty

There is *j-RMS* uncertainty of 11.5%.

- Reynolds range

$27 < Re_{Lp} < 4132$

- The Colburn j factor:

$$j_{cor} = C_1 j_{Re} j_{low} j_{louver} L_a{}^{C_2} N_{LB}^{C_3} \left(\frac{F_h}{L_p}\right)^{C_4} \left(\frac{L_d}{F_p}\right)^{C_5} \left(\frac{L_h}{F_h}\right)^{C_6} \left(\frac{F_h}{T_p}\right)^{C_7} \left(1 - \frac{b}{L_p}\right)^{C_8} \left(\frac{L_p}{F_p}\right)^{C_9}$$

Where,

$$j_{Re} = Re_{Lp}^{\left[C_{10} + C_{11}\cosh\left(\frac{F_p}{L_p} - 1\right)\right]}$$

$$j_{low} = 1 - \sin\left(\frac{L_p}{F_p}.L_a\right)\left[\cosh\left(C_{12}Re_{Lp} - C_{13}\frac{L_d}{N_{LB}F_p}\right)\right]^{-1}$$

$$j_{louver} = 1 - C_{14}\tan(L_a)\left(\frac{L_d}{N_{LB}F_p}\right)\cos\left[2\pi\left(\frac{F_p}{L_p\, tan(L_a)} - 1.8\right)\right]$$

C_1	0,8723	C_8	2,624
C_2	0,2190	C_9	0,3005
C_3	-0,0881	C_{10}	-0,4578
C_4	0,1491	C_{11}	-0,008737
C_5	-0,2585	C_{12}	0,04897
C_6	0,54	C_{13}	0,1417
C_7	-0,9023	C_{14}	-0,0065

Table 2- Constants for correlation 2

Dependence on fin geometrical parameters

For the parametric analysis of this correlation, the R5 fin geometry have been considered with a mean air temperature of 40 °C and a fixed velocity of 6 m/s.

- **Effect of Louver Angle**

The Figure 27 shows the Correlation 2 behavior with the louver angle variation.

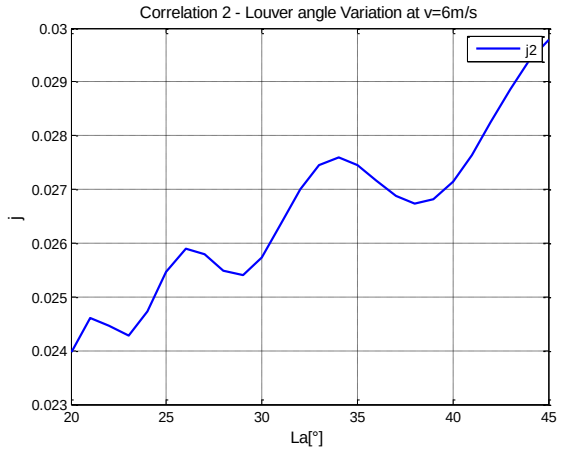

Figure 27- Correlation 2 Louver angle variation.

It is possible to note that increasing the louver angle the Colburn factor j shows a periodic behavior due to the presence of trigonometric functions in the components in which the j factor is divided, and there is no presence of a critic angle.

- **Effect of Fin height, Fin pitch and Core depth.**

The effect due to fin height as a function of core depth, fin pitch and core depth variations have been plotted in two surfaces and analyzed for the present correlation.

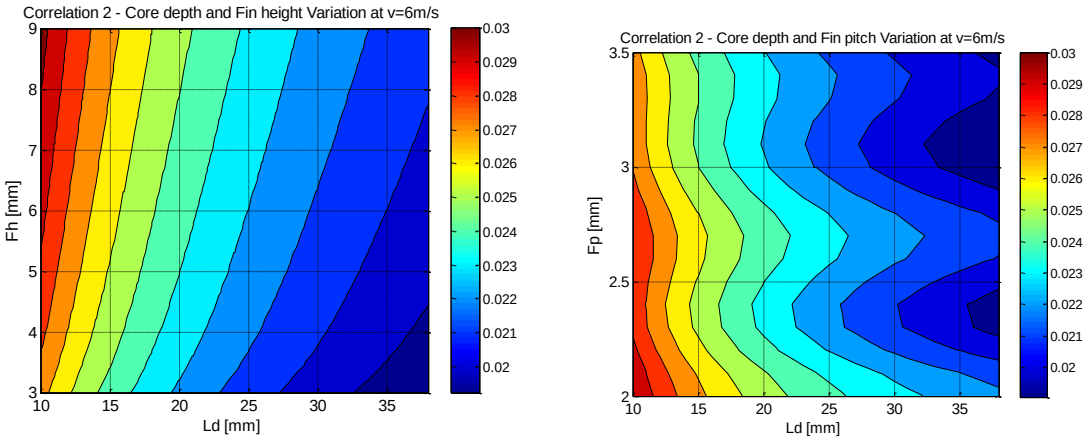

Figure 28 Correlation 2 a)Core depth and fin height variation; b) Core depth and fin pitch variation

The Figure 28.a shows that the Colburn factor j raises with increasing the fin height and decreasing the core depth, therefore the Correlation 2 provides a suitable performance. On the other hand the Figure 28.b shows that the Colburn factor j raises with lower values of fin pitch and core depth, but there is a periodicity, which is not a normal result.

- **Effect of Louver pitch and Louver angle**

The effect due to louver pitch and louver angle variation has been plotted in a surface and analyzed for the present correlation.

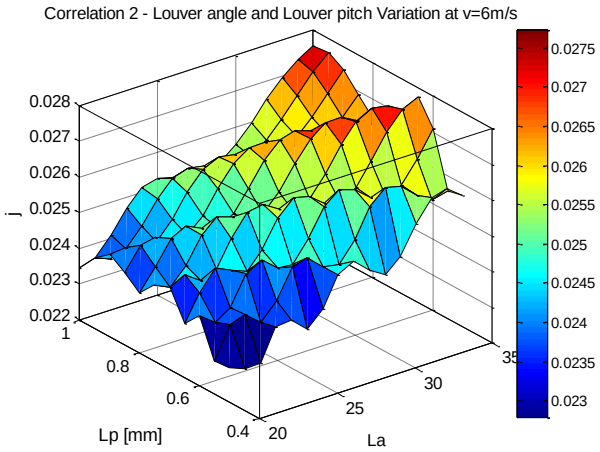

Figure 29-Correlation 2 Louver angle and louver pitch variation.

The Figure 29 shows that, with the variation of these parameters, the result is a periodic behavior, therefore the Correlation 2 does not provides a normal result based on the real behavior.

Correlation 3

Title: *The Air-side Thermal-hydraulic Performance of Flat-tube Heat Exchangers with Louvered, Wavy and Plain Fins Under Dry and Wet Conditions, J.Heat Transfer.*

Authors: **Park and Jacobi [2009b]**

A heat transfer correlation for louver fin geometry is developed with a large data bank, this data bank consists in 47 samples of louvered fin heat exchangers with different geometrical parameters.

Uncertainty

There is *j-RMS* uncertainty of 22.7%.

Reynolds range

$50 < Re_{Lp} < 1400$

The Colburn j factor:

$$j_{cor} = a_1 {Re_{Lp}}^{a_2} \left(\frac{L_p}{F_p}\right)^{a_3} (\sin(L_a))^{a_4} \left(\frac{L_h}{F_h}\right)^{a_5} \left(\frac{L_d}{F_p}\right)^{a_6} \left(\frac{F_h}{T_p}\right)^{a_7}$$

a_1	0.4260
a_2	-0.3149
a_3	0.6705
a_4	0.3489
a_5	0.5123
a_6	-0.2698
a_7	-0.2845

Table 3-Constants for correlation 3

Dependence on fin geometrical parameters

For the parametric analysis of this correlation have been considered the geometric parameters from the R5 fin typology, a mean temperature of 40 °C and a fixed velocity of 6 m/s.

- **Effect of Louver Angle**

The Figure 30 shows the Correlation 3 behavior with the louver angle variation.

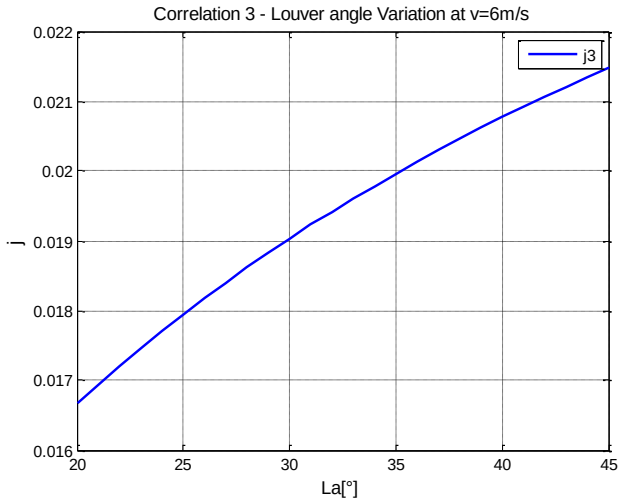

Figure 30- Correlation 3 Louver angle variation.

It is possible to note that increasing the louver angle the Colburn factor j raises, but there is no presence of a critical angle.

- **Effect of Fin height, Fin pitch and Core depth.**

The effect due to fin height as function of core depth, fin pitch and core depth variations have been plotted in two surfaces and analyzed for the present correlation.

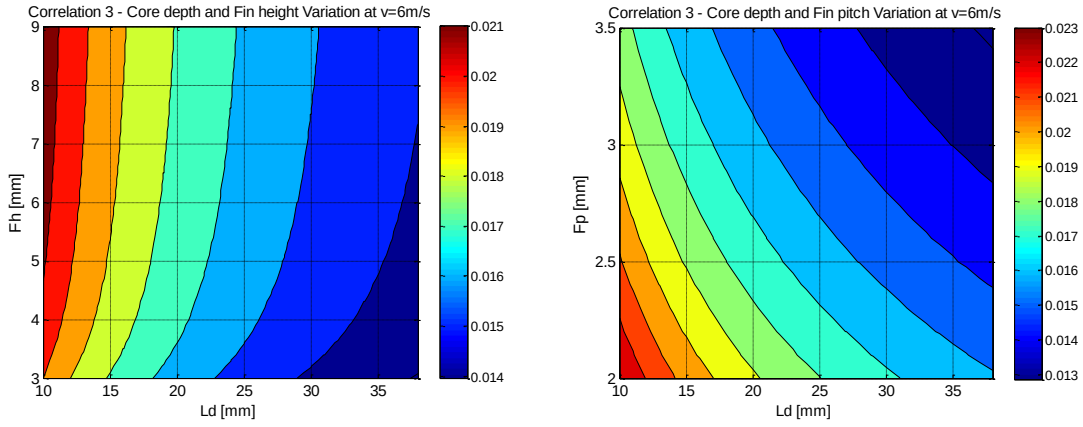

Figure 31 Correlation 3 a)Core depth and fin height variation; b) Core depth and fin pitch variation

The Figure 31.a shows that the Colburn factor j raises with increasing the fin height and decreasing the core depth, therefore the Correlation 3 provides a suitable performance. On the other hand the Figure 31.b shows that the Colburn factor j raises with lower values of fin pitch and core depth.

- **Effect of Louver pitch and Louver angle**

The effect due to louver pitch and louver angle variation has been plotted in a surface and analyzed for the present correlation.

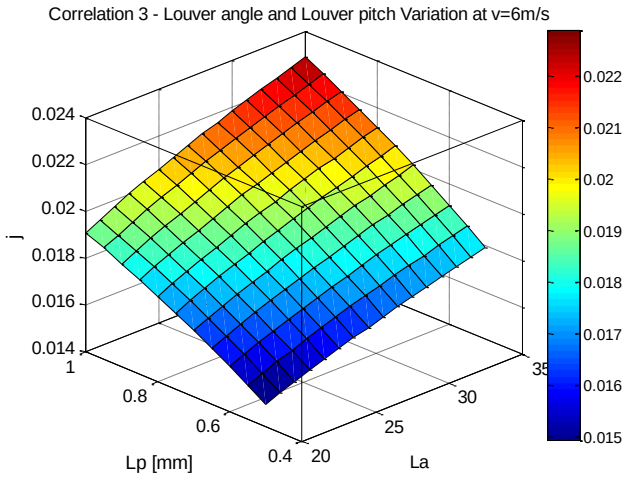

Figure 32-Correlation 3 louver angle and louver pitch variation.

The Figure 32 shows that increasing the louver angle and the louver pitch the Colburn factor j raises.

Correlation 4

Title: ***Experimental investigation of geometry effects on the performance of a compact louvered heat exchange.***

Authors: **A.Vaisi, M.Esmaeilpour,H.Taherian [2011].**

An experimental investigation is performed for the determination of the heat transfer and the pressure drop characteristics of flow over louvered fins in compact heat exchangers. Two different configurations are studied: the symmetrical and the asymmetrical arrangement. A series of tests were conducted to examine the effect of the geometrical parameters (louver pitch, louver arrangement and number of louver regions). The simulations results are compared with $\varepsilon - NTU$ data.

The calculated results indicate that a symmetrical arrangement of the louvered fins provides a 9.3% increase in heat transfer performance and a 18.2% decrease in pressure drop than the asymmetrical arrangement of louvered fin.

Reynolds range

$$100 < Re_{Lp} < 3000$$

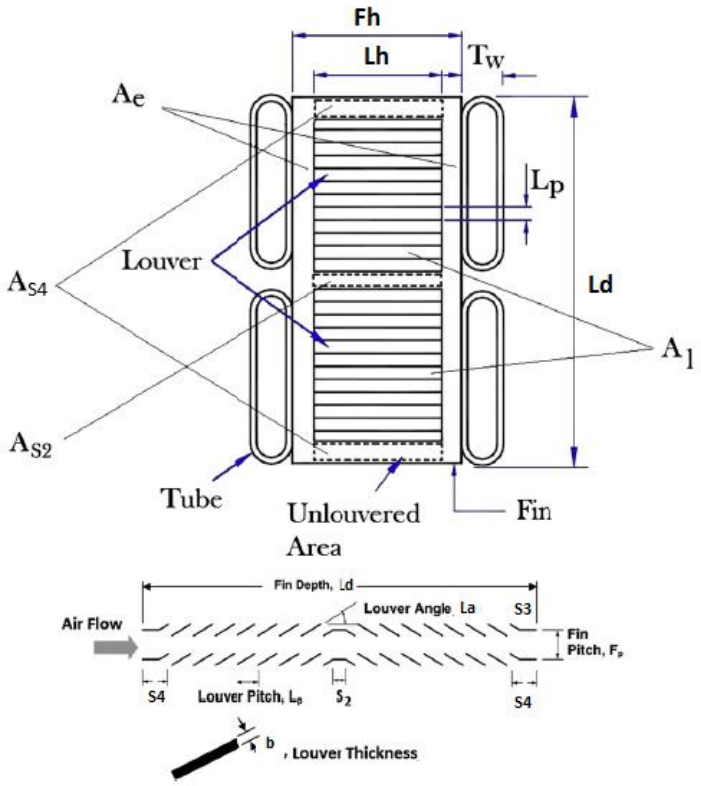

Figure 33-Louvered fin geometrical parameters. A.Vaisi, M.Esmaeilpour,H.Taherian [2011]

Calculation of performance parameters:

The air will choose a path through the louvers (Boundary Layer Flow) and the axial passage between the fins (Duct Flow). Therefore, Webb and Trauger defined the Flow Efficiency, Fe, as:

$$F_e = \frac{Actual\ Transvers\ Distance}{Ideal\ Transvers\ Distance}$$

The value Fe=1 is the ideal condition, in which all the air passes through the louvers, this flow path will have the maximum heat transfer rate.

The value fe=0 corresponds to a condition in which the air passes in the duct region, and therefore the minimum heat transfer rate will be obtained.

This accurate correlation for flow efficiency as a function of non-dimensional numbers Re, Fe Lp/Fp and La is developed by Sahnoun and Webb as follows:

Flow Efficiency:

$$F_e = F_e^* - 37.17 * 10^{-6} * (Re_L^* - Re_L)^{1.1} \left(\frac{L_p}{F_p}\right)^{-1.35} \left(\frac{2L_a}{\pi}\right)^{-0.610}$$

$$F_e^* = 0.95 \left(\frac{L_p}{F_p}\right)^{0.23} \quad Re_L^* = 828 \left(\frac{2L_a}{\pi}\right)^{-0.34} \quad Re_L = \frac{u_c L_P}{\nu}$$

Air-side heat conductance consists of 4 terms, that consists for the four areas that are shown in the Figure 33 .

$$\eta_0 h_0 A_0 = \eta_{f,l}\, h_l A_l + \eta_{s.f1} h_{s4} A_{s4} + \eta_{f.s2} h_{s2} A_{s2} + h_e A_e$$

Based in Pohlhausen solution for laminar boundary layer over constant temperature flat plate, the heat transfer coefficients are calculated as follows:

$$h_l = \frac{0.664 k_0 u_l Pr_0^{\frac{1}{3}}}{v_0 Re_{Lp}^{0.5}}$$

$$h_{s_4} = \frac{0.664 k_0 u_c Pr_0^{\frac{1}{3}}}{v_0 Re_{Ls4}^{0.5}}$$

$$h_{s_2} = \frac{0.664 k_0 u_c Pr_0^{\frac{1}{3}}}{v_0 Re_{Ls2}^{0.5}}$$

Where,

Reynold Numbers on each fin region are:

1) Louver part:

$$Re_{Lp} = \frac{ul.Lp}{v}$$

2) Inlet and Outlet straight parts:

$$Res4 = \frac{u.S4}{v}$$

3) Central straight portion:

$$Res2 = \frac{u.S2}{v}$$

Where, the air velocity over the louvers is obtained from the conservation of mass:

$$u_l = u_c\left(F_e\frac{F_p - b}{F_pCos\theta - b}\right)$$

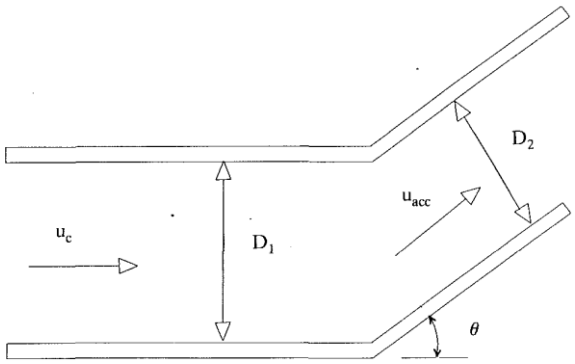

Figure 34- Air velocity through the louver

And u_c is the air velocity in the duct.

$$u_c = \frac{u_a}{\sigma}; \qquad \sigma = \frac{(T_p - T_w)(F_p - b)}{(T_p b)}$$

The heat transfer coefficient in the end region h_e is predicted by Shah and London with an analytical solution for the fully developed laminar flow in rectangular channel with constant wall temperature.

$$\frac{h_e D_{he}}{k_0} = 7.541(1 - 2.610A_r + 4.970Ar^2 - 5.119Ar^3 + 2.702A_r^4 - 0.548Ar^5)$$

Where, Ar is the aspect ratio of the end region, D_{he} is the hydraulic diameter

$Ar = \frac{T_p - T_w - L_h}{F_p - b}$; $D_{he} = \frac{2(T_p - T_w - L_h)(F_p - b)}{(T_p - T_w - L_h + F_p - b)}$

Fin efficiency by Sahnoun and Webb

The fin efficiency of plane fins is typically calculated by:

$$\eta_f = \frac{\tanh\left(\sqrt{\frac{2.h_o}{kf.b}}\left(\frac{F_h}{2}\right)\right)}{\sqrt{\frac{2.h_o}{kf.b}}\left(\frac{F_h}{2}\right)}$$

This equation is not precisely correct because there are four different heat transfer coefficients over the fin length; the end region is with a distance "$\boldsymbol{a}$" from the fin base with a heat transfer coefficient , $\boldsymbol{hl}$ in the louvered region, $\boldsymbol{hs2}$ and $\boldsymbol{hs4}$ for the central and the inlet-outlet flat regions respectively. Therefore the Author has derived the follow equation for the louvered fin geometries.

The Fin efficiency equation developed by Sahnoun and Webb is the following:

$$\eta_f * = \frac{k_f b\left[\frac{1}{\frac{1}{m_e}\tanh(m_e a)} - \frac{1}{\frac{1}{m_e}\cosh(m_e a)\sinh(m_e a) + \frac{m_*}{m_e^2}\sinh^2(m_e a)\tanh\left(m_*\left(\frac{F_h}{2} - a\right)\right)}\right]}{2\left(ah_e + \left(\frac{F_h}{2} - a\right)h_*\right)}$$

Where:

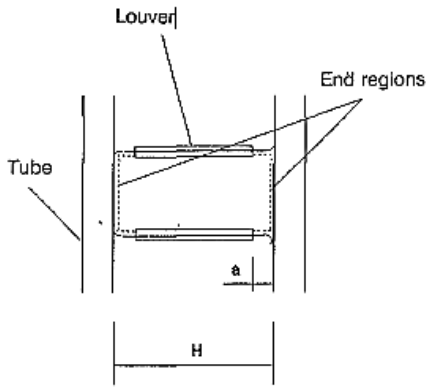

Figure 35- Correlation 4- Fin design to define "a".

$$a = (T_p - T_w - L_h)/2$$

$$m_e = \sqrt{\frac{2h_e}{k_f b}}$$

$$m* = \sqrt{\frac{2h*}{k_f b}}$$

Where * stands for$l, S2\ and\ S4$.

Modifications for correlation 4

Due to the fact that with the original louver velocity equation from the present correlation, the values decrease respect to the inlet air velocity, has been proposed to consider another approach of air velocity through the louver, an accelerated velocity due to the reduction of the area.

$$uc = u_a . \frac{Tp}{(Tp - Tw)}$$

$$u_l = u_c \left(F_e \frac{F_p - b}{F_p Cos\theta - b} \right)$$

Dependence on fin geometrical parameters

For the parametric analysis of this correlation there have been considered the geometric parameters of the R5 fin geometry and a mean temperature of 40 °C with a fixed velocity of 6 m/s.

- **Effect of Louver Angle**

The Figure 36 shows the Correlation 4 behavior with the louver angle variation.

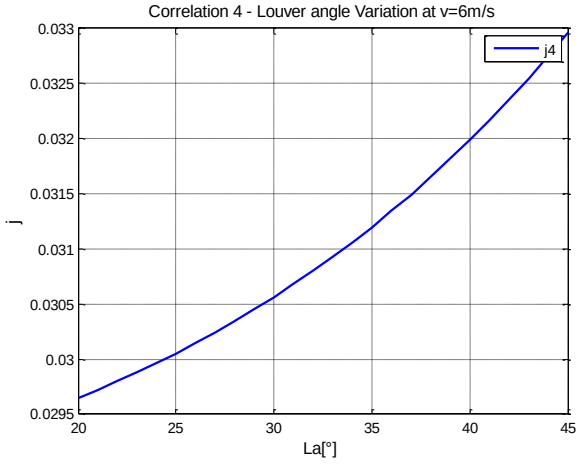

Figure 36-Correlation 4 louver angle variation.

It can be noticed that increasing the louver angle, the Colburn factor j raises but with a convex form that can't be easily explained, and consequently makes impossible to have a critical angle in which the j factor stabilizes.

- **Effect of Fin height, Fin pitch and Core depth.**

The effect due to fin height as function of core depth, fin pitch and core depth variations have been plotted in two surfaces and analyzed for the present correlation.

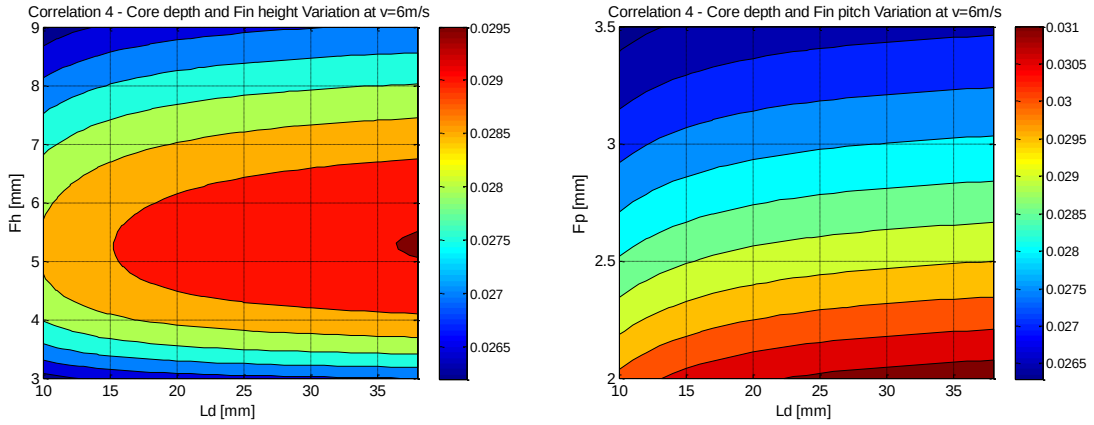

Figure 37Correlation 4 a)Core depth and fin height variation; b) Core depth and fin pitch variation

The Figure 37.a shows that the Colburn factor j raises with increasing the core depth and with the fin height variation show an anomaly behavior. The Figure 37.b shows that increasing the core depth and reducing the fin pitch can be obtained higher values of the Colburn factor j, which is not a normal behavior with the core depth variation.

- **Effect of Louver pitch and Louver angle**

The effect due to louver pitch and louver angle variation has been plotted in a surface and analyzed for the present correlation.

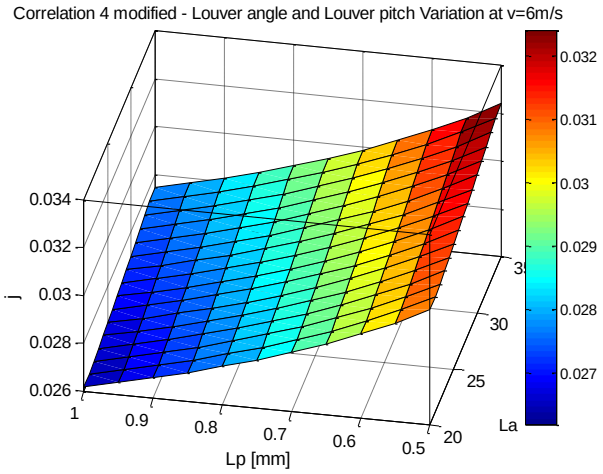

Figure 38-Correlation 4 Louver angle and louver pitch.

The Figure 38 shows that increasing the louver angle and decreasing the louver pitch the Colburn factor j raises.

- **Flow Efficiency (Fe):**

Flow efficiency varies respect of:

- ✓ Velocity
- ✓ Louver Angle
- ✓ Fin pitch ratio (Fp/Lp)

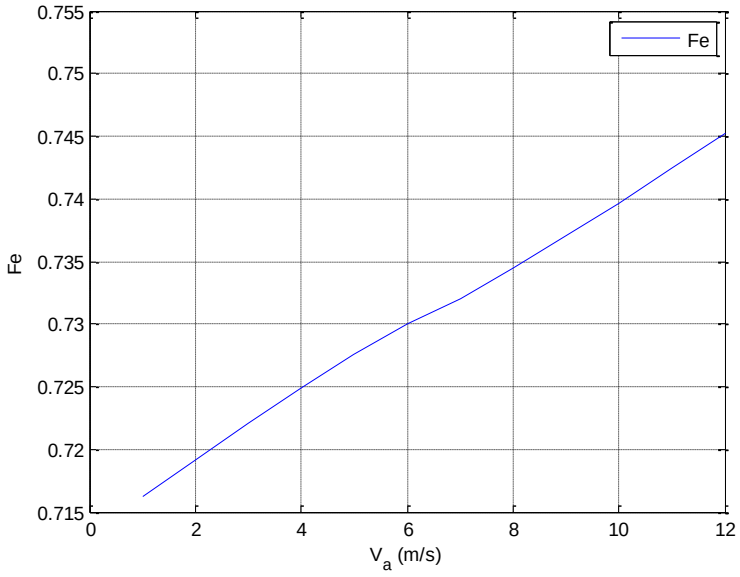

Figure 39-Correlation 4. Flow efficiency.

Correlation 5

Title: ***Heat transfer and pressure drop correlations for the multi-louvered fin compact heat exchangers.***

Authors: **Junqi.D, Jiangping Chen, Zhijiu Chen, Wenfeng Zhang, Yimin Zhou [2007]**

Heat Transfer characteristics of multilouvered fins have been investigated experimentally using 20 different multi-louvered fin and flat tube heat exchangers. The general correlation for the j factor is derived by regression analysis and F test of significance using 336 experimental data.

Uncertainty

It is shown that 95% of the experimental data for the j factor are correlated within $\pm$10% with mean deviation of 4.1%.

Reynolds range

$$200 < Relp < 2500$$

The Colburn j factor applied with F_p/L_p >1.

$$j = 0.26712 Re_{L_p}^{-0.1944} \left(\frac{L_a}{90}\right)^{0.257} \left(\frac{F_p}{L_p}\right)^{-0.5177} \left(\frac{F_h}{L_p}\right)^{-1.9045} \left(\frac{L_h}{L_p}\right)^{1.7159} \left(\frac{L_d}{L_p}\right)^{-0.2147} \left(\frac{b}{L_p}\right)^{-0.05}$$

Dependence on fin geometrical parameters

For the parametric analysis of this correlation have been considered the geometric parameters from the R5 fin typology, a mean temperature of 40 °C and a fixed velocity of 6 m/s.

- **Effect of Louver Angle**

The Figure 40 shows the Correlation 5 behavior with the louver angle variation.

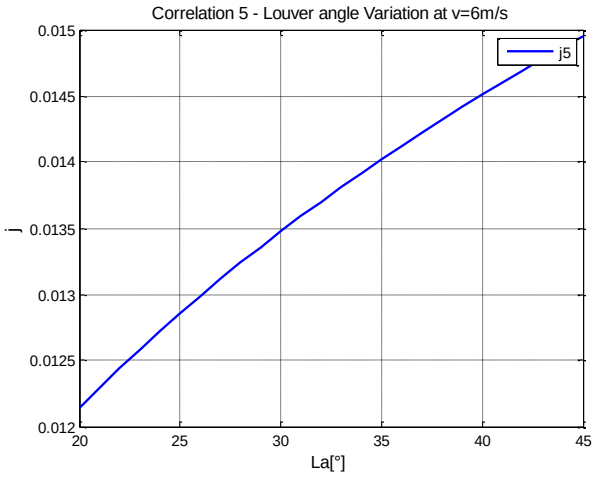

Figure 40-Correlation 5 louver angle variation.

It can be noticed that increasing the louver angle, the Colburn factor j raises but there is not a critical angle in which the j factor stabilizes.

- **Effect of Fin height, Fin pitch and Core depth.**

The effect due to fin height as function of core depth, fin pitch and core depth variations have been plotted in two surfaces and analyzed for the present correlation.

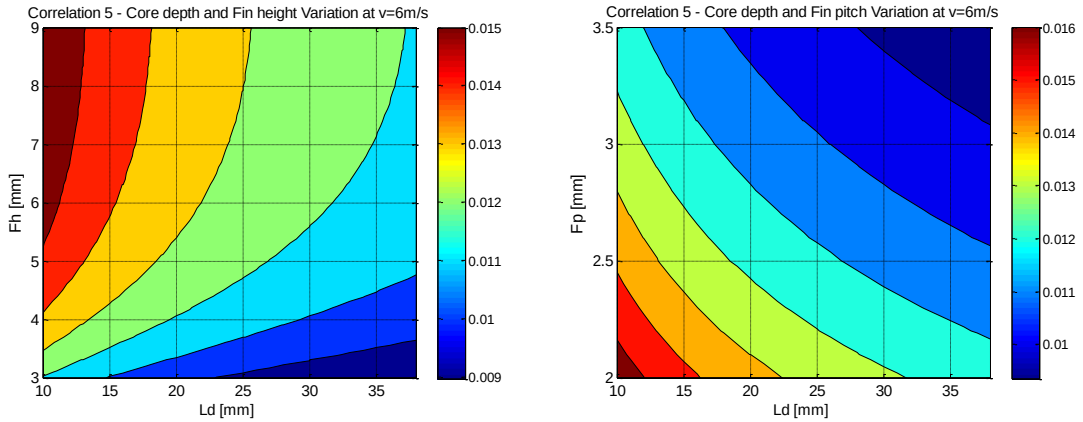

Figure 41 Correlation 5 a)Core depth and fin height variation; b) Core depth and fin pitch variation

The figure 41.a shows that the Colburn factor j raises with increasing the fin height and decreasing the core depth. On the other hand the figure41.b shows that the Colburn factor j raises with lower values of fin pitch and core depth.

- **Effect of Louver angle and Louver pitch**

The effect due to louver pitch and louver angle variation has been plotted in a surface and analyzed for the present correlation.

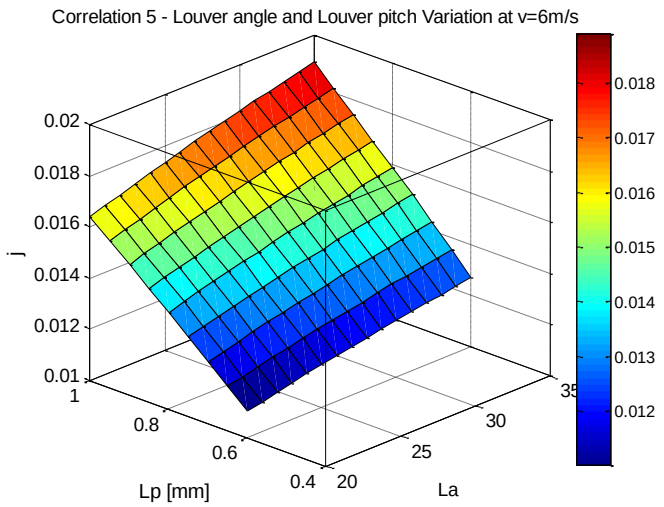

Figure 42-Correlation 5 Louver angle and louver pitch.

The figure 42 shows that increasing the louver angle and the louver pitch the Colburn factor j raises.

Correlation 6

Title: ***Generalized heat-transfer and fluid-flow correlations for corrugated louvered fins.***

Authors: **Kijung Ryu, Kwan-Soo Lee [2015].**

In the present study is reported a heat transfer correlation to describe the performance of heat exchangers that use corrugated louvered fins. The Colburn factor j was investigated with respect to the ratio of the fin pitch to the louver pitch (Fp/Lp). Whereas correlations developed in the past cannot be applied for Fp/Lp>1, the actual j correlation can be utilized in a wide range of Fp/Lp which is not only to Fp/Lp<1, but also to Fp/Lp>1 for 100< Relp <3000.

Reynolds range

$$100 < Relp < 3000$$

The Colburn j factor.

$$j = Re_{L_p}^{\left(-0.484-\frac{1.887}{lnRe_{Lp}}\right)} \left(\frac{L_d}{L_p}\right)^{0.157} \left(2.24 - 0.588 \ln\left(\frac{F_p}{L_p sin L_a}\right)\right)$$

Dependence on fin geometrical parameters

For the parametric analysis of this correlation have been considered the geometric parameters from the R5 fin typology, a mean temperature of 40 °C and a fixed velocity of 6 m/s.

- **Effect of Louver Angle**

The figure 43 shows the Correlation 6 behavior with the louver angle variation.

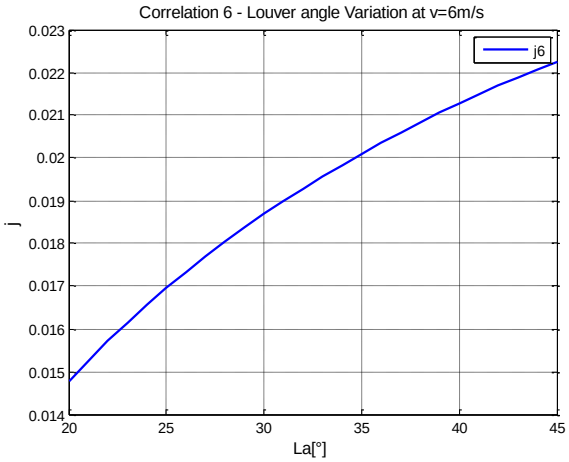

Figure 43-Correlaton 6 Louver angle variation

It can be noticed that increasing the louver angle, the Colburn factor j raises but there is not a critic angle in which the j factor stabilizes.

- **Effect of Fin height, Fin pitch and Core depth.**

The effect due to fin height as function of core depth, fin pitch and core depth variations have been plotted in two surfaces and analyzed for the present correlation.

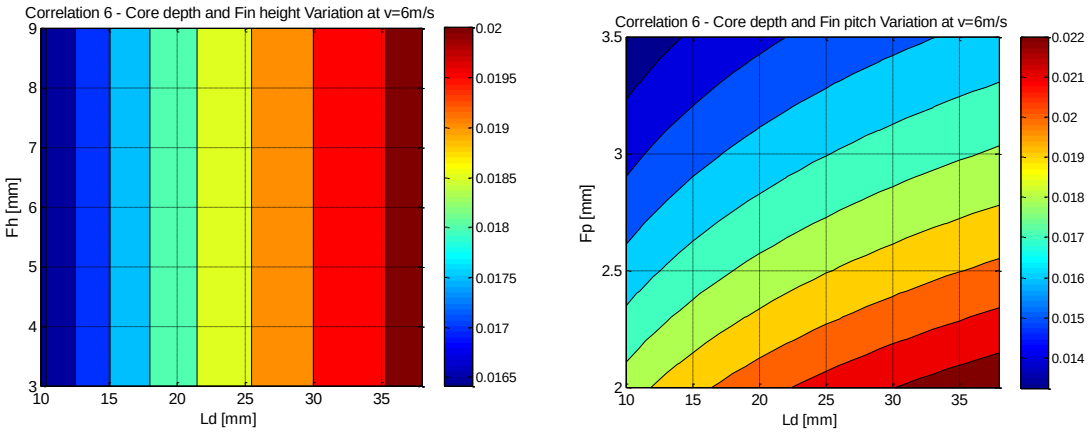

Figure 44 Correlation 6 a) Core depth and fin height variation; b) Core depth and fin pitch variation

The Figure 44.a shows that the Colburn factor j raises with increasing the core depth, and the present correlation does not depends on the fin height therefore there is not variation with this geometric parameter. The Figure 44.b shows that increasing the core depth and reducing the fin pitch can be obtained higher values of the Colburn factor j, which is not a normal behavior with the core depth variation.

- **Effect of Louver angle and Louver pitch**

The effect due to louver pitch and louver angle variation has been plotted in a surface and analyzed for the present correlation.

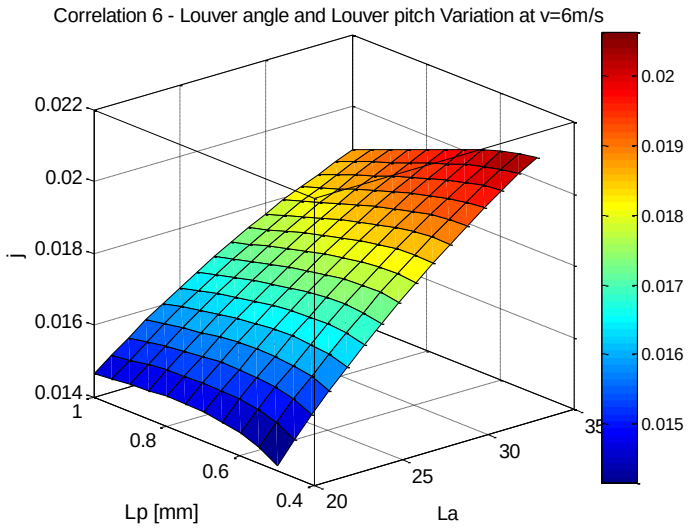

Figure 45-Correlation 6 Louver angle and louver pitch variation.

The figure 45 shows that increasing the louver angle and decreasing the louver pitch the Colburn factor j raises.

Correlation 7

Title: ***Correlations for Heat Transfer and Flow Friction Characteristics of Louvered Fin.***

Authors: **Davenport [1983b].**

Davenport tested 32 one-row louver fin geometries, and developed multiple regression correlation for the j versus Re_{De}.

Uncertainty

The author has used this correlation to predict the heat transfer performance of automotive radiators and has found agreement to within $\pm$ 15% of the test data. This correlation does not fully account for all the dimensional variables in the louver fin geometry, for example does not contain the length of the inlet louver (S4), the length of the flow re-direction louver (S2) and the number of louvers.

Reynolds range

$300 < Re_{De} < 4000$

The Colburn j factor.

$$j = 0.249 Re_{Lp}^{-0.42} (S_3 * sin(L_a))^{0.33} Fh^{0.26} \left(\frac{L_h}{F_h}\right)^{1.1}$$

Dependence on fin geometrical parameters

For the parametric analysis of this correlation have been considered the geometric parameters from the R5 fin typology, a mean temperature of 40 °C and a fixed velocity of 6 m/s.

- **Effect of Louver Angle**

In the figure 46 has been studied the Correlation 7 behavior varying the Louver angle.

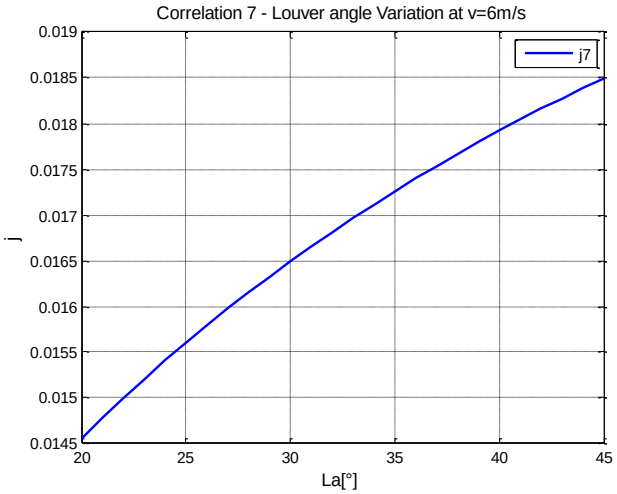

Figure 46-Correlation 7 louver angle variation.

It can be noticed that increasing the louver angle, the Colburn factor j raises but there is not a critical angle in which the j factor stabilizes.

- **Effect of Fin height and Core depth.**

The effect due to fin height as a function of core depth variations has been plotted and analyzed for the present correlation.

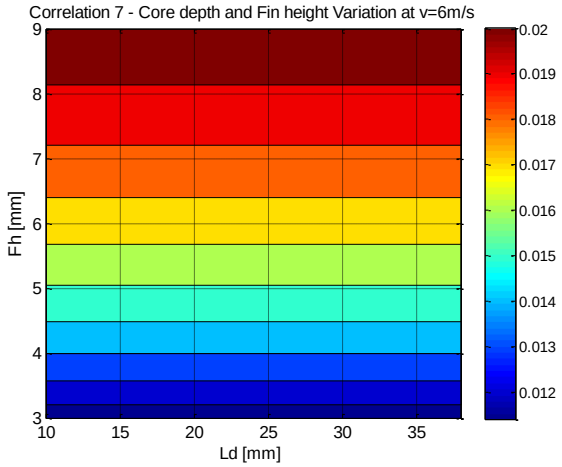

Figure 47-Correlation 7 Core depth and fin height variation.

The Figure 47 shows that the Colburn factor j rises with increasing the fin height, but the present correlation does not depend on the core depth nor the fin pitch, therefore there is not variation with this geometric parameter.

- **Effect of Louver angle and Louver pitch**

The effect due to louver pitch and louver angle variation has been plotted in a surface and analyzed for the present correlation.

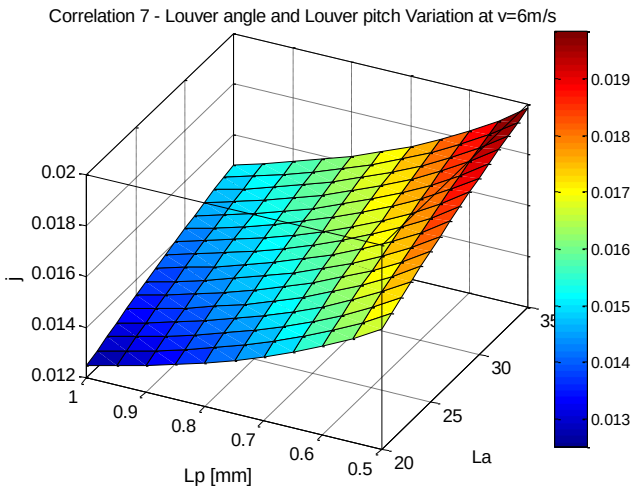

Figure 48-Correlation 7 Louver angle and louver pitch variation.

The Figure 48 shows that increasing the louver angle and decreasing the louver pitch the Colburn factor j raises.

Correlation 8

Title: ***Air-side performance of louver-finned flat aluminum heat exchangers at a low velocity region***

Authors: **Nae-Hyun Kim & Jin-Pyo Cho [2007]**

The heat transfer characteristics having louver fins were experimentally investigated. The samples had small fin pitches (1.0 – 1.4mm) and experiments were conducted up to a very low frontal air velocity (as low as 0.3 m/s) with a total of 12 heat exchangers having different dimensional variables.

Uncertainty

The correlation predicts 92% of j factors within $\pm$ 10%.

The Colburn j factors.

$$\mathrm{Re}_{\mathrm{Lp}} > 150$$

$$j = 0.705 Re_{Lp}^{-0.477} \left(\frac{L_a}{90}\right)^{0.271} \left(\frac{L_p}{F_p}\right)^{0.155}$$

$$Re_{Lp} < 150$$

$$j = 0.0311 Re_{Lp}^{0.183} \left(\frac{L_a}{90}\right)^{0.0475} \left(\frac{L_p}{F_p}\right)^{-1.25}$$

Dependence on fin geometrical parameters

For the parametric analysis of this correlation have been considered the geometric parameters from the R5 fin typology, a mean temperature of 40 °C and a fixed velocity of 6 m/s.

- **Effect of Louver Angle**

In the figure 49 has been studied the Correlation 8 behavior varying the Louver angle.

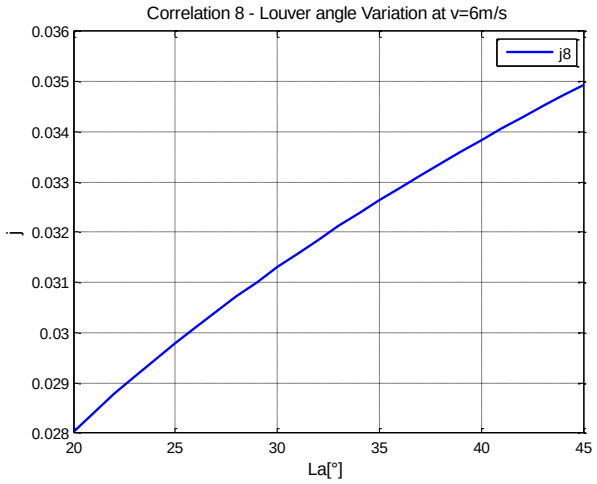

Figure 49-Correlation 8 Louver angle variation.

It can be noticed that increasing the louver angle, the Colburn factor j raises but there is not a critical angle in which the j factor stabilizes.

- **Effect of Fin height, Fin pitch and Core depth.**

The present correlation 8 does not depend on the fin height and core depth parameters.

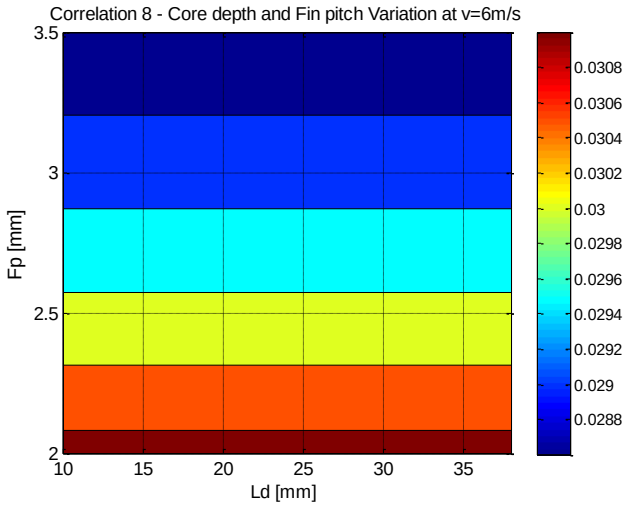

Figure 50-Correlation 8 core depth and fin pitch variation.

The figure 50 represents variation with the fin pitch only, and it is possible to observe that the Colburn factor j increases with lower values of fin pitch.

- **Effect of Louver angle and Louver pitch**

The effect due to louver pitch and louver angle variation has been plotted in a surface and analyzed for the present correlation.

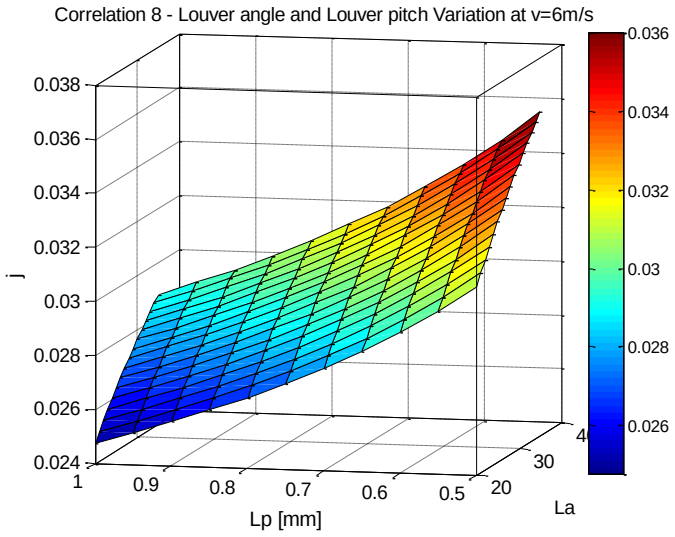

Figure 51-Correlation 8 Louver angle and louver pitch variation.

The figure 51 shows that increasing the louver angle and decreasing the louver pitch the Colburn factor j raises.

2.3. Experimental Data.

2.3.1. CONDENSERS

The thermo-fluid dynamic analysis on the air side of the DENSO Condensers has been developed by a software *MF-CONDENSER 5.3*, which has the function of simulate the condensers performance formed by flat tubes with multi channels and multi louver fins.

The program is divided in four different calculation sections:

- CALIBRATION.
- PREVISION.
- SHOWING RESULTS.
- CONVERSION RESULTS IN EXCEL FILES.

In the heat transfer coefficient analysis, the focus of this study goes to the CALIBRATION section of the code, which allows to evaluate the regression coefficients of defined functions (chosen on the basis of experimental results) that link the convective heat transfer coefficient on the air side and the air side friction factor to the air velocity entering to the condenser. These coefficients are specific to the particular matrix air side of the condenser analyzed.

The CALIBRATION section requires the knowledge of the geometrical characteristics of the condenser and the experimental results of a performance test of the Condenser that is object of study. Therefore as input parameters the CALIBRATION section requires:

- Geometrical parameters of the Condenser.
- Results of an experimental test conducted on the type of condenser considered.

From the General equation of Overall heat transfer coefficient per area:

$$UA = \frac{1}{\frac{1}{h_{cold}.A_{cold}} + \boxed{\frac{b_{wall}}{k_{wall}.A_{wall}}} + \frac{1}{h_{hot}.A_{hot}}}$$

- Where the wall thermal resistance is neglected.

The Equation used in the simulation code is the following:

$$UA_{\ elem1} = \frac{1}{\frac{10^6}{HTC_{ref,elem1}.A_{elem,1}} + \frac{10^6}{HTC_{air}.\left(A_{fin,elem}.\eta_{fin} + A_{e,elem}\right)}}$$

The function that links the heat transfer coefficient on the air side with the inlet air velocity of the condenser is the following:

$$h_{air} = a.\left[1 - e^{(-b.w_{aria})}\right]$$

The CALIBRATION section has the function to determine the coefficients $\boldsymbol{a}$ and $\boldsymbol{b}$ shown in the previous mentioned equation, based on the geometrical features of the condenser (Tube pitch, Tube height, Core depth, Fin pitch and Louver path) and the experimental results of a specific test performed according to standard procedures for performance characterization. Therefore this section requires the implementation of a calculation algorithm, based on a discretization of the condenser in elementary units of heat exchange, the number of elementary exchangers in which divide the single tube may be chosen by the user.

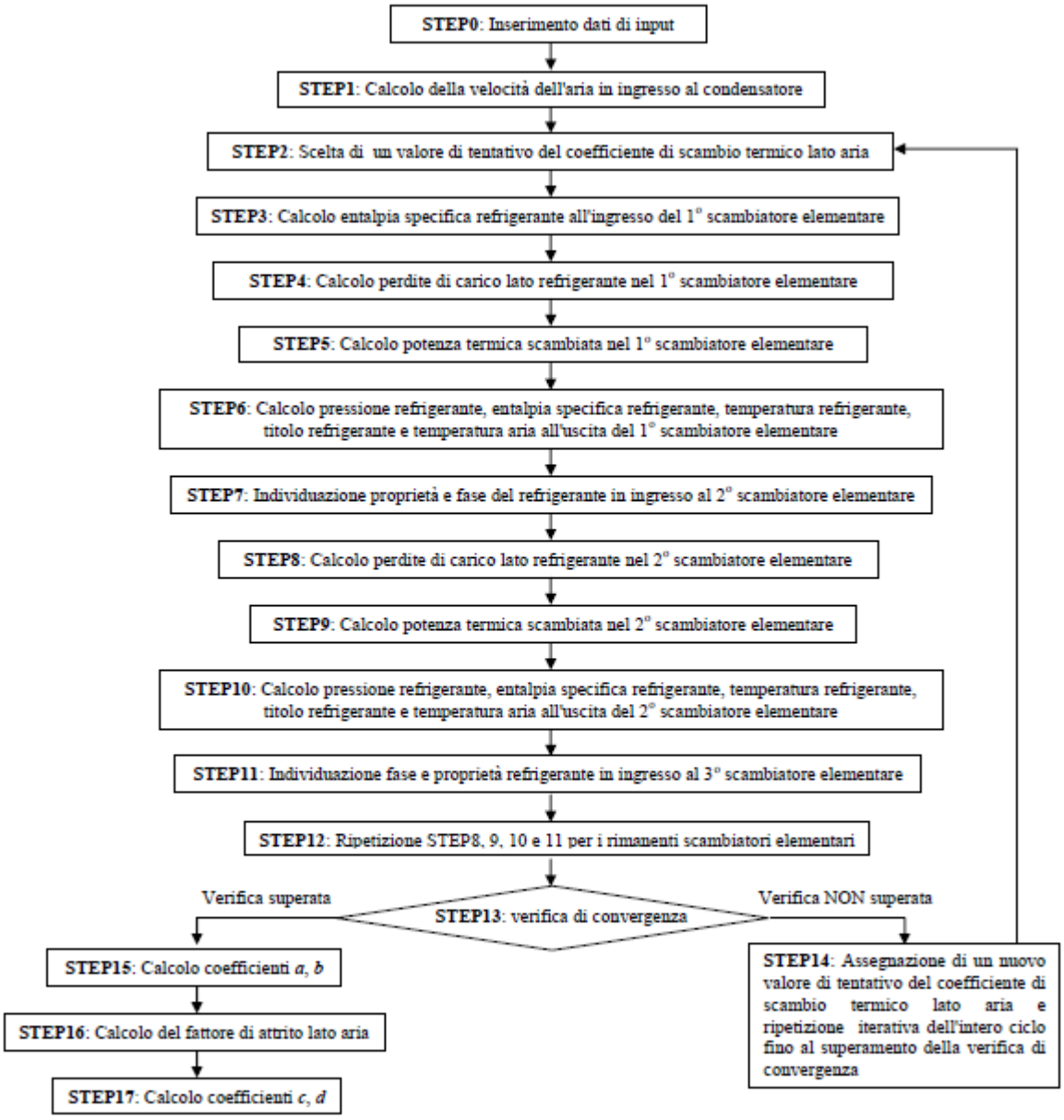

Figure 52 Calculation Algorithm of CALIBRATION section.

Finally, once the coefficients a and b have been calculated and saved for a specific condenser and test, it is possible to calculate the heat transfer coefficients on the air side for determined velocities.

Application Ranges

The bench tests are performed according to standard procedures, and is necessary to note the application ranges used for Temperature, velocity and Reynold numbers.

- ***Temperature***

The tests have been conducted by a different stardard tests, shown in the table 4 below:

Standard	P ref,in [bar G]	Tref,in [˚C]	Tair,in [˚C]	Subcooling [˚C]
Euroclim	19	100	45	5
PSA	19	100	45	10
Fiat for R1234yf	18.4	100	45	10
GM	19	97.5	40	8

Table 4 Standard tests

- ***Velocity***

The inlet air velocities of the condenser for the calculation of the air heat transfer coefficients are$2.5\ m/s \leq v_{air} \leq 6\ m/s$.

- ***Reynolds range***

The Reynolds numbers considered by the MFCondenser are in laminar flow regimes, which mean Reynolds numbers less than 2000 approximately.

2.3.1.1- MF-CONDENSER Uncertainties.

In this section is studied the uncertainties of air heat transfer coefficients calculation on the CALIBRATION section of the software, but due to the complicity of the CALIBRATION algorithm in which are discretized the heat exchangers (into elementary units) the propagation of uncertainties calculations are a complex task.

For this reason the uncertainty analysis is studied by sensitivity due to the calculation of:

- Refrigerant heat transfer coefficients.
- Inlet air temperature of the tests.

Sensitivity of Refrigerant's heat transfer coefficient calculation

Due to the fact that the refrigerant heat transfer coefficient is calculated by a correlation which has an uncertainty, has been introduced a sensitivity factor. The sensitivity analysis of the refrigerant heat transfer coefficient (HTC_{ref}), is studied multiplying by a factor k in the equation of the refrigerant heat transfer coefficient in the CALIBRATION code; therefore this factor will increase or decrease the values of the air heat transfer coefficient, and as a consequence can be obtained an uncertainty band.

$$HTC_{ls} = 0.023.\frac{(Re_{ref,ls})^{0.8}(Pr_{ref,ls})^{0.4}k_{ref,ls}}{d_{h,ref}}$$

$$HTC_{ref,elem2} = \boldsymbol{k}.HTC_{ls}\left[1 + 1.128(x_{in,ref,elem2})^{0.817}\left(\frac{\rho_{ref,ls}}{\rho_{ref,vs}}\right)^{0.3685}\left(\frac{\mu_{ref,ls}}{\mu_{ref,vs}}\right)^{0.2363}\left(1 - \frac{\mu_{ref,ls}}{\mu_{ref,vs}}\right)^{2.144}(Pr_{ref,ls})^{-0.1}\right]$$

The standard tests of all Condenser typologies have been conducted with an Inlet air temperature of 45°C, Sub cooling temperature of 10°C, and for each of them has been determined the uncertainty band due to the HTC_{ref} calculation.

- HTC refrigerant Sensitivity for the Condenser typology C1.

The following table 5 shows the values of HTC_{air} calculated with each sensitivity factor k, with its respective a and b coefficients.

$\boldsymbol{HTC_{air}}$	**COEFFICIENTS**		**Velocity [m/s]**				
k	**a**	**b**	**2.5**	**3**	**4**	**5**	**6**
0.50	**0.562222**	**0.101074**	125.537	147.058	186.969	223.044	255.650
1.00	**0.430236**	**0.127637**	117.537	136.869	172.023	202.963	230.197

2.00	**0.439407**	**0.117480**	111.829	130.517	164.755	195.198	222.267

Table 5-HTC refrigerant sensitivity for C1

It is possible to plot the HTC_{air} in velocity function, and as shown in the figure below, there is an uncertainty band.

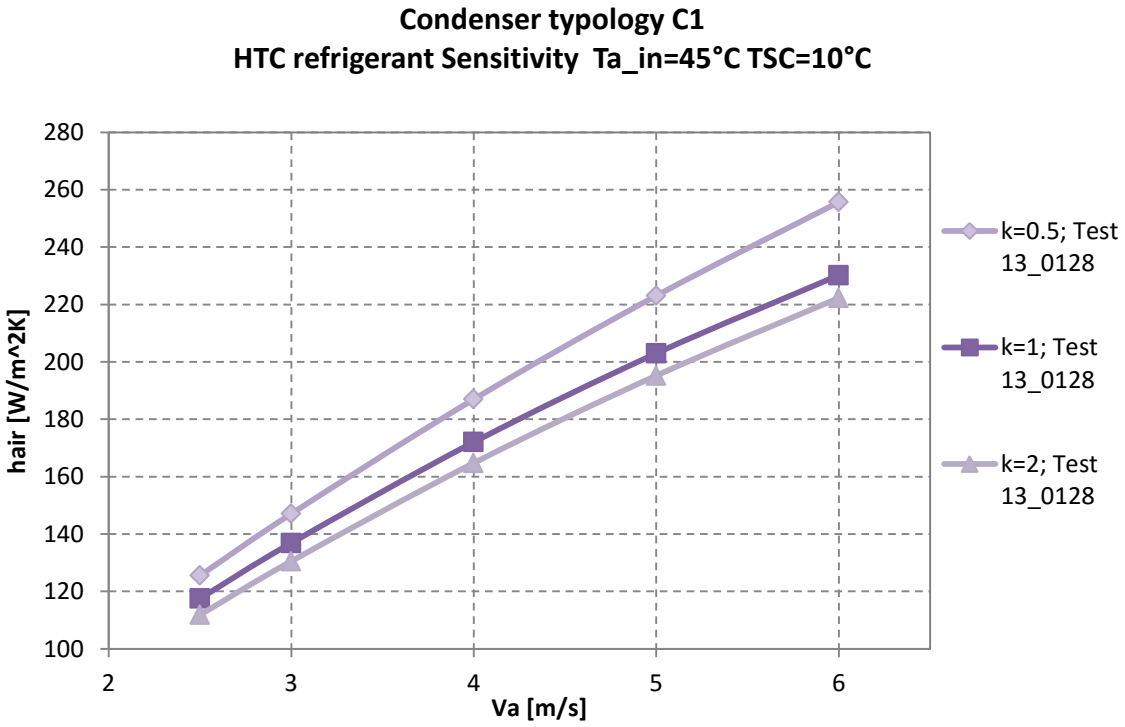

Figure 53- HTC ref sensitivity for C1

Diff % [k=2 e k=1]	-5%	-5%	-4%	-4%	-3%
Diff % [k=0.5 e k=1]	7%	7%	9%	10%	11%

Table 6-% Sensitivity Differences for C1.

- HTC refrigerant Sensitivity for the Condenser typology C2 .

The following table shows the values of HTC_{air} calculated with each sensitivity factor k, with its respective a and b coefficients.

HTC_{air}	COEFFICIENTS		Velocity [m/s]				
k	**a**	**b**	**2.5**	**3**	**4**	**5**	**6**

0.50	**0.70763**	**0.07587**	122.273	144.065	185.246	223.418	258.801
1.00	**0.49116**	**0.09502**	103.852	121.823	155.302	185.746	213.431
2.00	**0.39636**	**0.11064**	95.782	111.960	141.750	168.419	192.296

Table 7- HTC refrigerant sensitivity for C2.

It is possible to plot the HTC_{air} in velocity function, and as shown in the figure below, there is an uncertainty band.

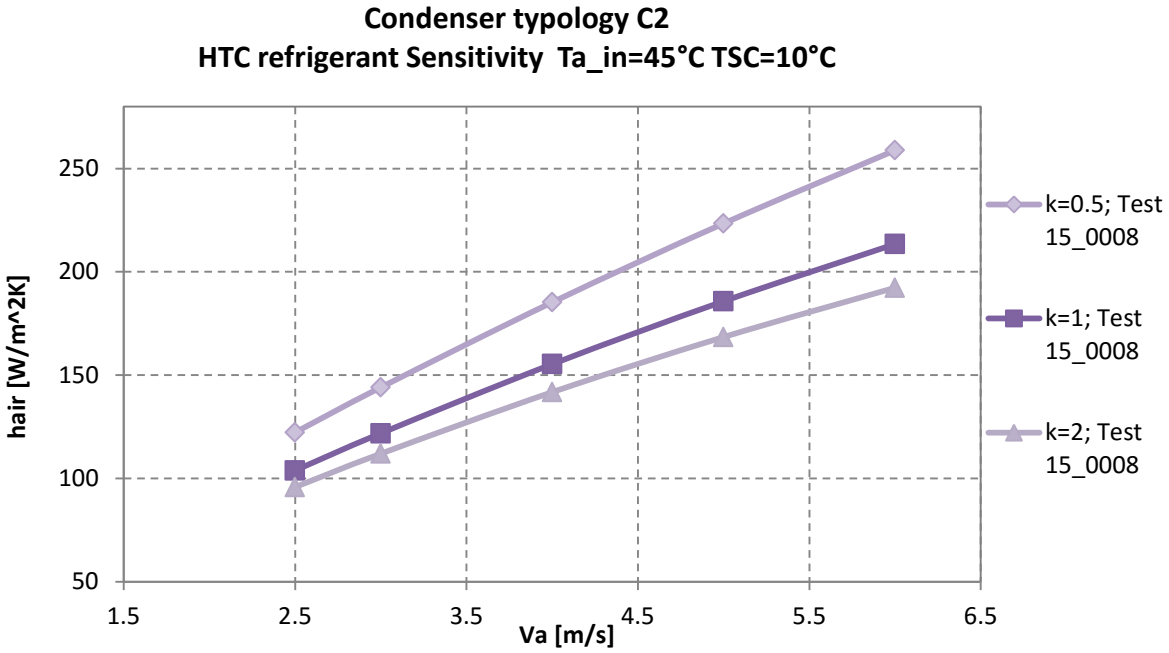

Figure 54- HTC ref sensitivity for C2

Diff % [k=2 e k=1]	-8%	-8%	-9%	-9%	-10%
Diff % [k=0.5 e k=1]	18%	18%	19%	20%	21%

Table 8-% Sensitivity Differences for C2.

- HTC refrigerant Sensitivity for the Condenser typology C3 .

The following table shows the values of HTC_{air} calculated with each sensitivity factor k, with its respective a and b coefficients.

HTC_{air}	COEFFICIENTS		Velocity [m/s]				
k	a	b	2.5	3	4	5	6
0.50	2.171525	0.022168	117.072	139.718	184.263	227.832	270.446
1.00	1.137965	0.037207	101.077	120.188	157.361	193.176	227.683
2.00	0.718244	0.056543	94.680	112.062	145.386	176.878	206.640

Table 9- HTC refrigerant sensitivity for C3.

It is possible to plot the HTC_{air} in velocity function, and as shown in the figure below, there is an uncertainty band.

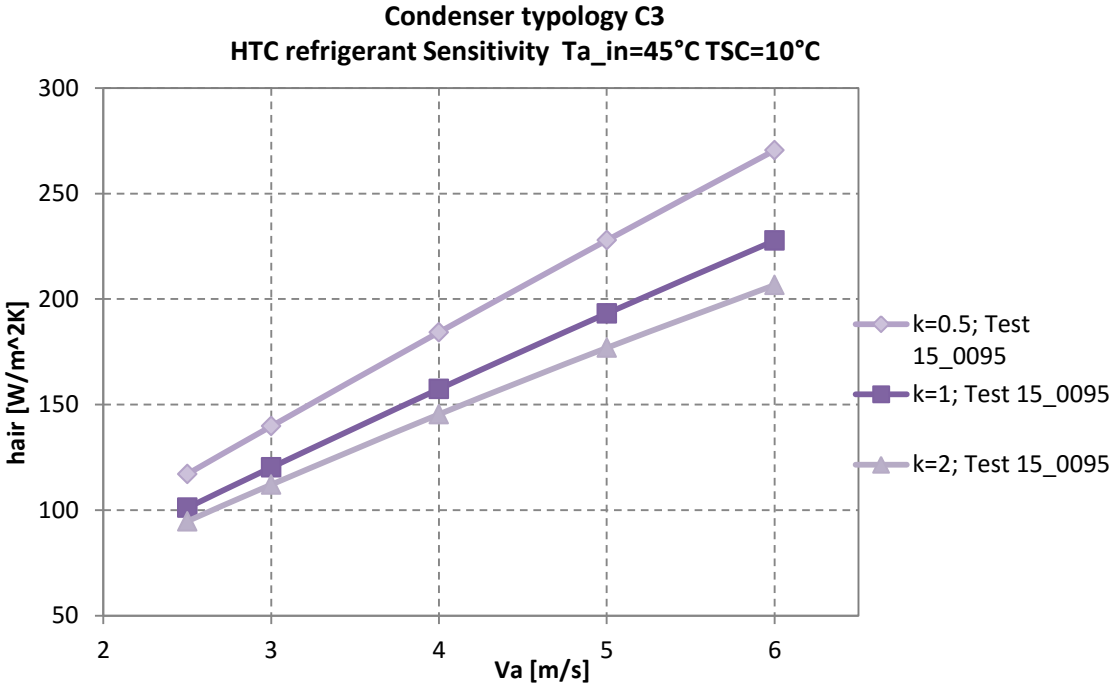

Figure 55- HTC ref sensitivity for C3

Diff % [k=2 e k=1]	-6%	-7%	-8%	-8%	-9%
Diff % [k=0.5 e k=1]	16%	16%	17%	18%	19%

Table 10-% Sensitivity Differences for C3.

- HTC refrigerant Sensitivity for the Condenser typology C4 .

The following table shows the values of HTC_{air} calculated with each sensitivity factor k, with its respective a and b coefficients.

HTC_{air}	COEFFICIENTS		Velocity [m/s]				
k	a	b	2.5	3	4	5	6
0.95	0.817654	0.058301	110.897	131.202	170.078	206.753	241.350
1.00	0.745648	0.063965	110.193	130.195	168.329	204.101	237.656
2.00	0.622812	0.069824	99.758	117.704	151.770	183.538	213.164

Table 11- HTC refrigerant sensitivity for C4

It is possible to plot the HTC_{air} in velocity function, and as shown in the figure below, there is an uncertainty band.

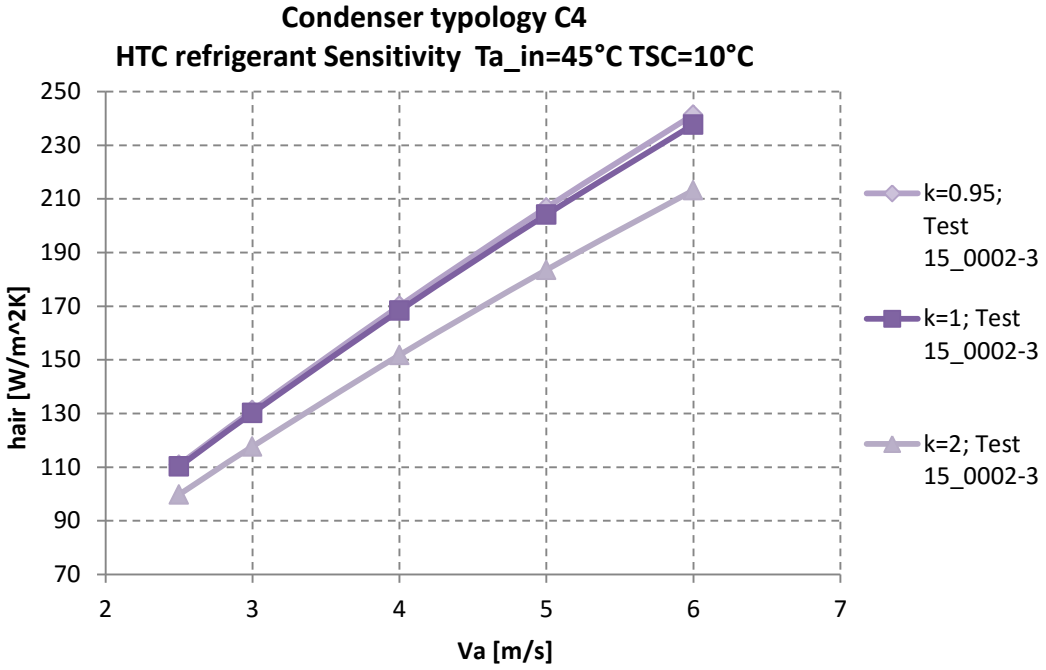

Figure 56 HTC ref sensitivity for C4

Diff % [k=2 e k=1]	-9%	-10%	-10%	-10%	-10%
Diff % [k=0.95 e k=1]	1%	1%	1%	1%	2%

Table 12-% Sensitivity Differences for C4.

- HTC refrigerant Sensitivity for the Condenser typology C5.

The following table shows the values of HTC_{air} calculated with each sensitivity factor k, with its respective a and b coefficients.

HTC_{air}	COEFFICIENTS		Velocity [m/s]				
k	a	b	2.5	3	4	5	6
0.8	0.8462	0.0606	119.040	140.758	182.268	221.334	258.102
1.00	0.6353	0.0776	112.075	131.996	169.592	204.379	236.567
2.00	0.4990	0.0870	97.545	114.634	146.661	176.020	202.931

Table 13-HTC refrigerant sensitivity for C5.

It is possible to plot the HTC_{air} in velocity function, and as shown in the figure below, there is an uncertainty band.

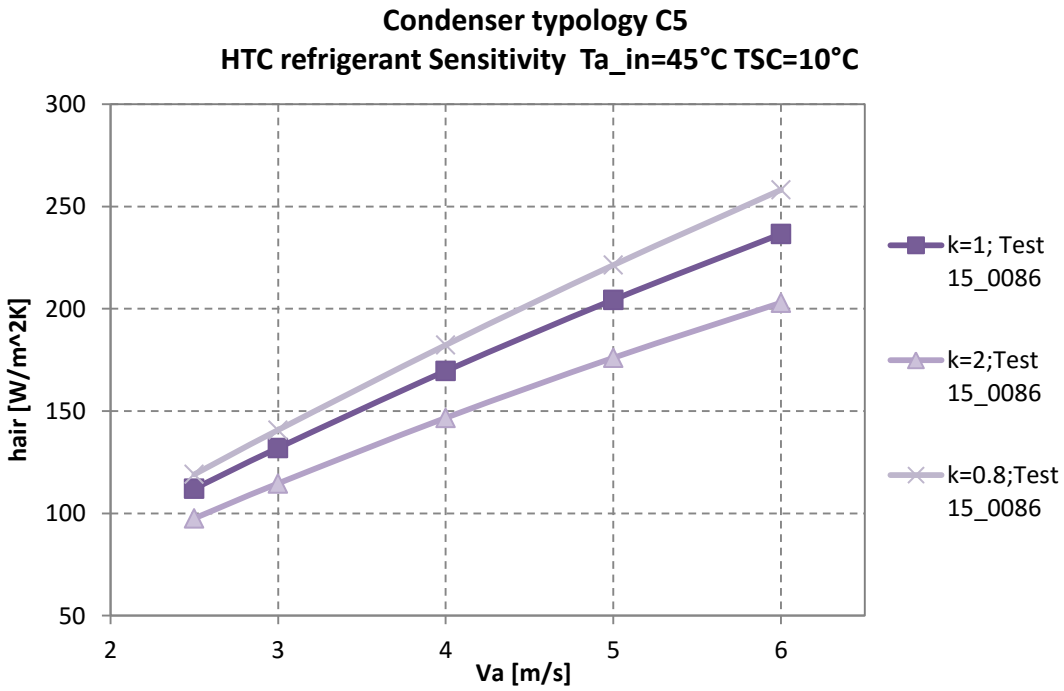

Figure 57-HTC ref sensitivity for C5

Diff % [k=2 e k=1]	-13%	-13%	-14%	-14%	-14%
Diff % [k=0.8 e k=1]	6%	7%	7%	8%	9%

Table 14-% Sensitivity Differences for C5.

- HTC refrigerant Sensitivity for the Condenser typology C6.

The following table shows the values of HTC_{air} calculated with each sensitivity factor k, with its respective a and b coefficients.

HTC_{air}	COEFFICIENTS		Velocity [m/s]				
k	a	b	2.5	3	4	5	6
0.5	0.75198	0.05869	102.623	121.402	157.346	191.242	223.205
1.00	0.56936	0.06631	86.976	102.707	132.646	160.665	186.886
2.00	0.46845	0.07607	81.132	95.588	122.901	148.213	171.671

Table 15-HTC refrigerant sensitivity for C6.

It is possible to plot the HTC_{air} in velocity function, and as shown in the figure below, there is an uncertainty band.

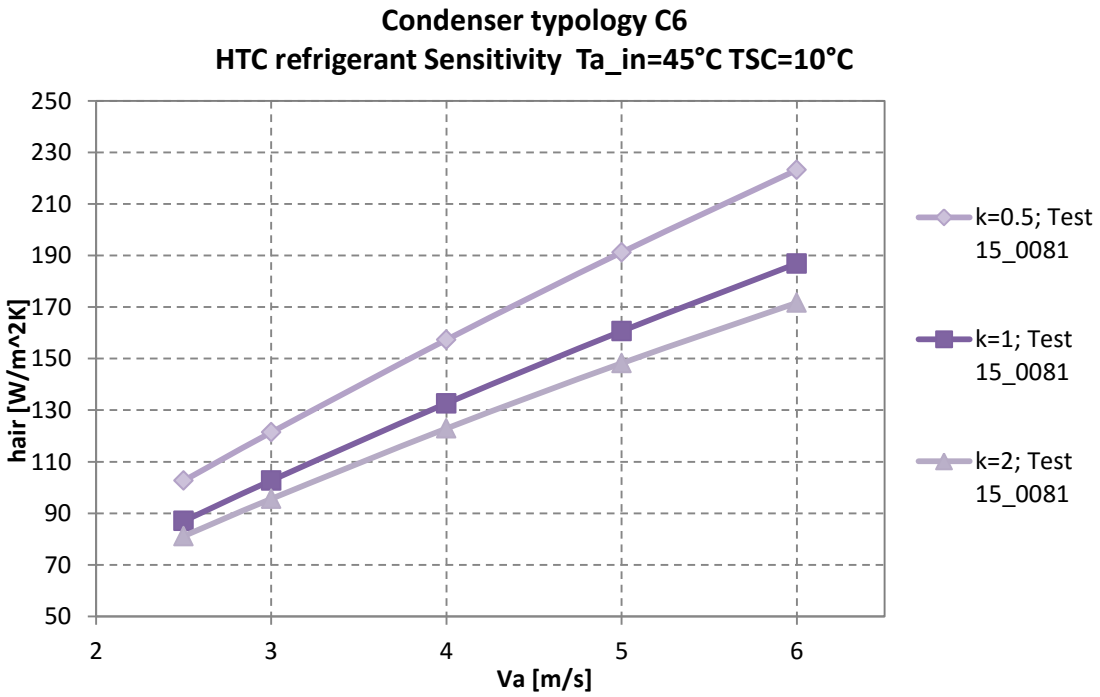

Figure 58-HTC ref sensitivity for C6

Diff % [k=2 e k=1]	-7%	-7%	-7%	-8%	-8%
Diff % [k=0.5 e k=1]	18%	18%	19%	19%	19%

Table 16-% Sensitivity Differences for C6.

- HTC refrigerant Sensitivity for the Condenser typology C7.

The following table shows the values of HTC_{air} calculated with each sensitivity factor k, with its respective a and b coefficients.

HTC_{air}	COEFFICIENTS		Velocity [m/s]				
k	**a**	**b**	**2.5**	**3**	**4**	**5**	**6**
0.5	**0.91119**	**0.04814**	103.329	122.544	159.613	194.940	228.607
1.00	**0.64057**	**0.06045**	89.846	106.242	137.585	167.090	194.863
2.00	**0.53662**	**0.06826**	84.189	99.370	128.222	155.170	180.340

Table 17-HTC refrigerant sensitivity for C7.

It is possible to plot the HTC_{air} in velocity function, and as shown in the figure below, there is an uncertainty band.

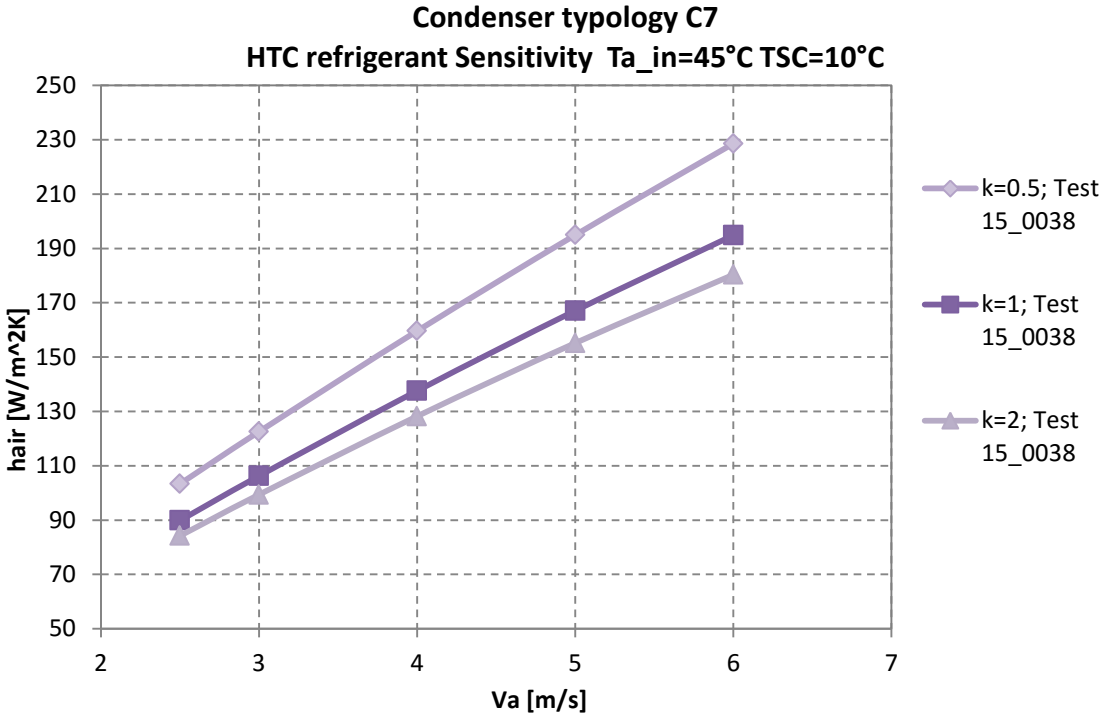

Figure 59-HTC ref sensitivity for C7

Diff % [k=2 e k=1]	-6%	-6%	-7%	-7%	-7%
Diff % [k=0.5 e k=1]	15%	15%	16%	17%	17%

Table 18-% Sensitivity Differences for C8.

- HTC refrigerant Sensitivity for the Condenser typology C8.

The following table shows the values of HTC_{air} calculated with each sensitivity factor k, with its respective a and b coefficients.

HTC_{air}	COEFFICIENTS		Velocity [m/s]				
k	a	b	2.5	3	4	5	6
0.5	0.7763	0.0667	119.228	140.780	181.785	220.145	256.029
1.00	0.5521	0.0899	111.169	130.557	166.814	199.952	230.240
2.00	0.4945	0.0983	107.787	126.342	160.826	192.080	220.406

Table 19-HTC refrigerant sensitivity for C8.

It is possible to plot the HTC_{air} in velocity function, and as shown in the figure below, there is an uncertainty band.

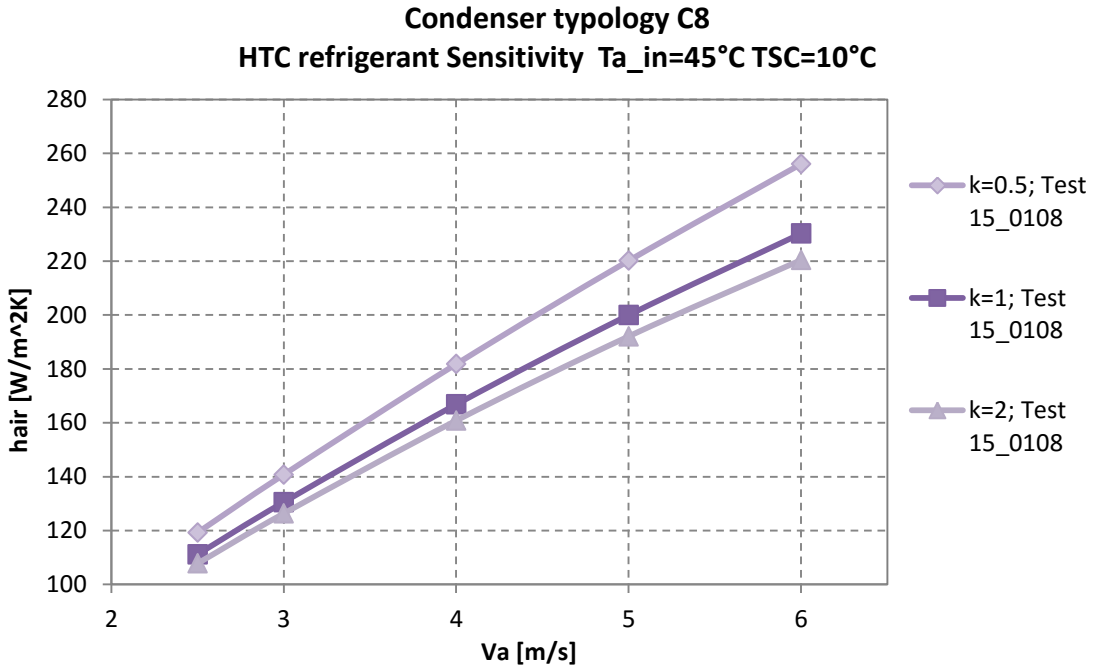

Figure 60- HTC ref sensitivity for C8.

Diff % [k=2 e k=1]	-3%	-3%	-4%	-4%	-4%
Diff % [k=0.5 e k=1]	7%	8%	9%	10%	11%

Table 20-% Sensitivity Differences for C8.

Temperature sensitivity

The previous standard test has been conducted with an inlet air temperature of 45°C with a Sub cooling temperature of 10°C, therefore has been analyzed the sensitivity due to the variation of the bench tests temperatures. Hence new tests have been conducted with the following standard conditions as seen in the following table 21.

Ta inlet	T SC	Test Number
45°C	10 °C	15_0126

45°C	15 °C	15_0128
40°C	10 °C	15_0129
50°C	10°C	15_0130
35°C	10°C	15_0134

Table 21-Standard conditions-Temperature sensitivity

The above bench tests have been conducted only for the Condenser typology C1, and with the MFCondenser can be calculated the coefficients a and b for each test.

					velocità [m/s]				
Ta inlet	**T SC**	**Test Number**	**a**	**b**	**2.5**	**3**	**4**	**5**	**6**
45°C	10 °C	15_0126	**0.4639**	**0.1188**	119.25	139.14	175.54	207.85	236.55
45°C	15 °C	15_0128	**0.3926**	**0.1454**	119.68	138.82	173.18	202.88	228.57
40°C	10 °C	15_0129	**0.5473**	**0.0993**	120.34	141.03	179.45		
50°C	10°C	15_0130	**0.4594**	**0.1184**	117.75	137.40	173.37	205.32	233.70
35°C	10°C	15_0134	**0.5534**	**0.0983**	120.63	141.39			

Table 22-Temperature sensitivity, coefficients a and b

Some of these tests have not been done until the velocity of 6 m/s like the others, because of the high pressure drops on the refrigerant side.

The following graph figure 61 shows the HTC_{air} in function of the velocity.

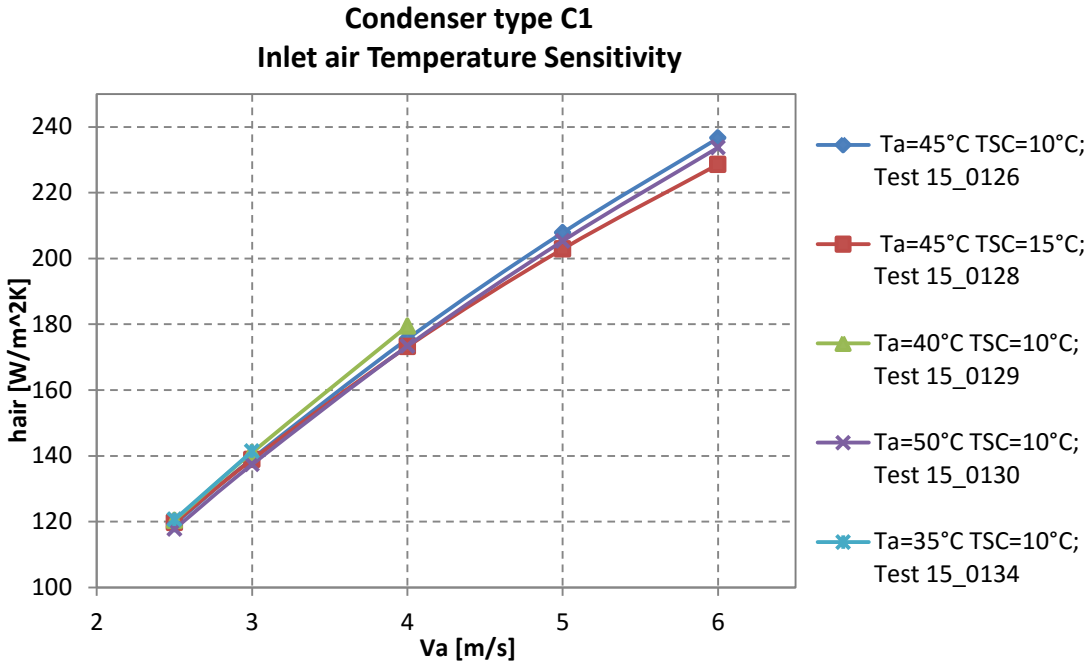

Figure 61-Temperature sensitivity on the C1 condenser.

Ta in	T SC	Test number	% Difference respect of the test Tain=45°C TSC=10°C				
45°C	15 °C	***15_0128***	0%	0%	-1%	-2%	-3%
40°C	10 °C	***15_0129***	1%	1%	2%		
50°C	10°C	***15_0130***	-1%	-1%	-1%	-1%	-1%
35°C	10°C	***15_0134***	1%	2%			

Table 23-%difference of the new tests respect original test.

The previous table 23 shows the percentage difference between the new tests and the reference test conducted at $Ta_{in} = 45°C$ and Sub Cooling temperature$= 10°C$.

At this point, for an uncertainty study on Condenser tests, has been considered only the effect of the calculation of refrigerant heat transfer coefficient; the inlet and sub cooling temperatures variation does not have a relevant impact.

2.3.2.- RADIATORS

The thermo-fluid dynamic analysis on the air side of the DENSO Radiators has been performed by means of the DENSO internal software *HEX*, which can be used for both performance simulations and experimental performance analysis.

The *HEX* software requires the knowledge of the geometrical characteristics of the radiator and the experimental performance of a radiator having the same matrix geometry that is object of study. Therefore as input parameters the software requires:

- Geometrical parameters of the radiator.
- Results of an experimental test conducted on the type of radiator considered.

These tests are performed varying the air velocity in a defined range, at different coolant mass flow rates.

The software *HEX* calculates the performance on the air side of the Radiator, by the overall heat transfer coefficient of the radiator.

$$UA = \frac{1}{\frac{1}{h_c . A_c} + \frac{1}{\eta_f A_f h_o} + \frac{b_w}{k_w A_w}}$$

- The Overall heat transfer coefficient is obtained by the experimental results of the tests.
- The coolant heat transfer coefficient is obtained by the application of a correlation chosen by the user.
- The fin efficiency is calculated with the theoretical expression, which depends on the air heat transfer coefficient.
- The tube area and the fin areas are defined for each radiator configuration.

Therefore, it is possible to obtain the air heat transfer coefficient for a specific experimental test.

Application Ranges

The bench tests are performed according to standard procedures, in the following range of Temperature, velocity and Reynold numbers.

- ***Temperature***

The tests have been conducted with the following conditions:

T mean ref,in [˚C]	T mean air,in [˚C]
80 - 95	20 - 30

Table 24-HEX Temperature ranges of the tests

- ***Velocity***

The air inlet velocity range considered in the tests are:

Air inlet velocity [m/s]
3 - 6

Table 25- air inlet velocity in the tests

- ***Reynold numbers***

The Reynold numbers considered is in laminar flow regimes, which means $Re < 2000$.

2.3.2.1.- HEX Uncertainties.

Due to the fact that the air-side heat transfer coefficient is not directly measured, but it is obtained from the overall heat transfer coefficient by means of the HEX software, the uncertainty analysis and the error propagation study is required.

Propagation of uncertainties

The propagation of uncertainties is the effect of variables on the uncertainty of a function based on them.

$$\Delta f = \sqrt{\Delta x_1^2 . \left|\frac{\partial f}{\partial x_1}\right|^2 + \Delta x_2^2 . \left|\frac{\partial f}{\partial x_2}\right|^2 + \Delta x_3^2 . \left|\frac{\partial f}{\partial x_3}\right|^2 + \Delta x_4^2 . \left|\frac{\partial f}{\partial x_4}\right|^2 + \cdots + \Delta x_n^2 . \left|\frac{\partial f}{\partial x_n}\right|^2}$$

Where,

$$x_1, x_2, x_3, .., x_n \; are \; variables \; with \; uncertainty.$$

Therefore this analysis allows us to implement this theory on the uncertainty calculation of air heat transfer coefficient due to the effect of variables with uncertainties.

$$h_o = \left[\left(\frac{1}{UA} - \frac{1}{h_c . A_c}\right) . \eta_f A_f\right]^{-1}$$

- Note that has been neglected the wall thermal resistance for this calculation.

$$\Delta h_o = \sqrt{\Delta h_c^2 . \left|\frac{\partial h_o}{\partial h_c}\right|^2 + \Delta \eta_f^2 . \left|\frac{\partial h_o}{\partial \eta_f}\right|^2 + \Delta A_f^2 . \left|\frac{\partial h_o}{\partial A_f}\right|^2}$$

Derivation respect to the variables with uncertainty:

1. $\frac{\partial h_o}{\partial h_c} = -\left[\left(\frac{1}{UA} - \frac{1}{h_c A_c}\right) \eta_f A_f\right]^{-2} . \eta_f A_f . \left(\frac{1}{h_c^2 A_c}\right)$
2. $\frac{\partial h_o}{\partial \eta_f} = -\left[\left(\frac{1}{UA} - \frac{1}{h_c A_c}\right) \eta_f A_f\right]^{-2} . \left(\frac{1}{UA} - \frac{1}{h_C A_c}\right) A_f$

   2.1. $\frac{\partial \eta_f}{\partial h_o} = -\frac{\tanh\left(\sqrt{\frac{2h}{bk}}H\right)}{\left(\frac{2h}{bk}\right)^{\frac{3}{2}} bHk} + \frac{\left(\operatorname{sech}\left(\sqrt{\frac{2h}{bk}}H\right)\right)^2}{2h}$
3. $\frac{\partial h_o}{\partial A_f} = -\left[\left(\frac{1}{UA} - \frac{1}{h_c A_c}\right) \eta_f A_f\right]^{-2} . \left(\frac{1}{UA} - \frac{1}{h_C A_c}\right) \eta_f$

- ***Fin Areas.***

The Radiator total fin areas are reported in this section, the real and the calculated by *HEX.*

The Fin Area percent error:

$$\%\boldsymbol{\Delta} = \frac{\boldsymbol{Af_{HEX} - Af}}{\boldsymbol{Af}}$$

Fin	$\boldsymbol{Af}\ [\boldsymbol{dm^2}]$	$\boldsymbol{Af_{HEX}}\ [\boldsymbol{dm^2}]$	$\%\ \boldsymbol{\Delta Af}$
$\boldsymbol{R1}$	885.98	902.22	1.8%
$\boldsymbol{R2}$	885.98	902.22	1.8%
$\boldsymbol{R3}$	554.36	558.21	0.7%
$\boldsymbol{R4}$	554.36	558.21	0.7%
$\boldsymbol{R5}$	604.87	614.28	1.6%

Table 26-Fin area percent errors

The percent error of all the fin areas is chosen as 2%.

- ***Fin Efficiencies*** $(\boldsymbol{\eta_f})$

The Radiator fin efficiencies are reported in this section, comparing the values calculated by a different approach with the one calculated by *HEX.* The equation used by the software HEX to calculate the fin efficiency is the one dimensional efficiency (defined in the first chapter), and the model used to compare is:

  - The Sahnoun and Webb correlation (defined above in the Correlation 4 description).

The Fin Efficiency percent error:

$$\%\boldsymbol{\Delta} = \frac{\boldsymbol{\eta f_{HEX} - \eta f}}{\boldsymbol{\eta f}}$$

Fin	$\boldsymbol{kf}\ \left[\frac{\boldsymbol{W}}{\boldsymbol{mK}}\right]$	$\boldsymbol{h}\ \left[\frac{\boldsymbol{W}}{\boldsymbol{m^2K}}\right]$	$\boldsymbol{md}$	$\boldsymbol{\eta f_{sahnoun}}$	$\boldsymbol{n_{2D}}$	$\boldsymbol{\eta f_{HEX}}$	$\%\boldsymbol{\Delta \eta f_{sahnoun}}$
$\boldsymbol{R1}$	207.3	642.24	297.5	57.76%	59.39%	62.15%	7.59%
$\boldsymbol{R2}$	207.3	642.24	297.5	57.99%	59.36%	62.15%	7.17%
$\boldsymbol{R3}$	207.3	422.69	241.3	59.10%	58.25%	61.82%	4.61%
$\boldsymbol{R4}$	207.3	422.69	241.3	59.10%	58.25%	61.82%	4.61%
$\boldsymbol{R5}$	207.3	338.30	215.9	71.83%	71.50%	73.46%	2.26%

Table 27-Fin efficiency percent error

- ***Coolant heat transfer coefficient*** $\left(\boldsymbol{HTC_{ref}}\right)$.

The uncertainty due to the calculation of the HTC_{ref} has been considered as a fixed value equal to 30 %.

Hence, for each radiator typology is calculated the uncertainty of the air heat transfer coefficient proposed by the propagation of uncertainty theory.

Propagation of uncertainty radiator R1.

The air heat transfer coefficient for the fin R1 has the following uncertainty that is reported in the table 28:

$Variable$	$\boldsymbol{Units}$	$\%\,\boldsymbol{Difference}$	$\boldsymbol{Nominal}$	$\boldsymbol{\Delta(var)}$	$\frac{\boldsymbol{dho}}{\boldsymbol{d(var)}}$
$\boldsymbol{\eta_f}$	-	7.6%	0.62145	0.04719	454.93
$\boldsymbol{h_c}$	$\left[\frac{W}{m^2C}\right]$	30%	3854.22	1156.266	0.014
$\boldsymbol{A_f}$	$[m^2]$	2%	9.02	0.18044	31.33
$\boldsymbol{UA}$	$\left[\frac{W}{m^2C}\right]$	-	1318.71	-	-
$\boldsymbol{A_c}$	$[m^2]$	-	2.03	-	-
$\boldsymbol{h_o}$	$\left[\frac{W}{m^2C}\right]$	**4%**	**642.24**	28.04	

Table 28-HTCair uncertainties (R1)

Propagation of uncertainty radiator R2.

The air heat transfer coefficient for the fin R2 has the following uncertainty that is reported in the table 29:

$Variable$	$\boldsymbol{Units}$	$\%\boldsymbol{Difference}$	$\boldsymbol{Nominal}$	$\boldsymbol{\Delta(var)}$	$\frac{\boldsymbol{dho}}{\boldsymbol{d(var)}}$
$\boldsymbol{\eta_f}$	-	7.2%	0.62145	0.04454	454.93
$\boldsymbol{h_c}$	$\left[\frac{W}{m^2C}\right]$	30%	3854.22	1156.26	0.0148
$\boldsymbol{A_f}$	$[m^2]$	2%	9.022	0.18	31.33
$\boldsymbol{UA}$	$\left[\frac{W}{m^2C}\right]$	-	1318.71	-	-
$\boldsymbol{A_c}$	$[m^2]$	-	2.0358	-	-
$\boldsymbol{h_o}$	$\left[\frac{W}{m^2C}\right]$	**4%**	**642.24**	27.13	

Table 29-HTCair uncertainties (R2)

Propagation of uncertainty radiator R3

The air heat transfer coefficient for the fin R3 has the following uncertainty that is reported in the table 30:

$Variable$	$\boldsymbol{Units}$	$\%\boldsymbol{Difference}$	$\boldsymbol{Nominal}$	$\boldsymbol{\Delta(var)}$	$\boldsymbol{\frac{dho}{d(var)}}$
$\boldsymbol{\eta_f}$	-	4.6%	0.61824	0.028517	785.64
$\boldsymbol{h_c}$	$\left[\frac{W}{m^2C}\right]$	30%	6914.15	2074.24	0.0175
$\boldsymbol{A_f}$	$[m^2]$	2%	5.5821	0.111	87.013
$\boldsymbol{UA}$	$\left[\frac{W}{m^2C}\right]$	-	1340.99	-	-
$\boldsymbol{A_c}$	$[m^2]$	-	0.9697	-	-
$\boldsymbol{h_o}$	$\left[\frac{W}{m^2C}\right]$	**10%**	**422.69**	43.85	

Table 30-HTCair uncertainties (R3)

Propagation of uncertainty radiator R4.

The air heat transfer coefficient for the fin R4 has the following uncertainty that is reported in the table 31:

$Variable$	$\boldsymbol{Units}$	$\%\boldsymbol{Difference}$	$\boldsymbol{Nominal}$	$\boldsymbol{\Delta(var)}$	$\boldsymbol{\frac{dho}{d(var)}}$
$\boldsymbol{\eta_f}$	-	4.6%	0.61824	0.0285	785.64
$\boldsymbol{h_c}$	$\left[\frac{W}{m^2C}\right]$	30%	6914.15	2074.24	0.017
$\boldsymbol{A_f}$	$[m^2]$	2%	5.58	0.111	87.01
$\boldsymbol{UA}$	$\left[\frac{W}{m^2C}\right]$	-	1340.99	-	-
$\boldsymbol{A_c}$	$[m^2]$	-	0.9697	-	-
$\boldsymbol{h_o}$	$\left[\frac{W}{m^2C}\right]$	**10%**	**422.69**	43.84	

Table 31-HTCair uncertainties (R4)

Propagation of uncertainty radiator R5.

The air heat transfer coefficient for the fin R5 has the following uncertainty that is reported in the table 32:

$Variable$	$\boldsymbol{Units}$	$\%\boldsymbol{Difference}$	$\boldsymbol{Nominal}$	$\boldsymbol{\Delta(var)}$	$\boldsymbol{\frac{dho}{d(var)}}$
$\boldsymbol{\eta_f}$	-	2.3%	0.73456	0.0166	391.92
$\boldsymbol{h_c}$	$\left[\frac{W}{m^2C}\right]$	30%	7357.53	2207.25	0.0056
$\boldsymbol{A_f}$	$[m^2]$	2%	6.1428	0.122	46.86
$\boldsymbol{UA}$	$\left[\frac{W}{m^2C}\right]$	-	1134.49	-	-
$\boldsymbol{A_c}$	$[m^2]$	-	1.2172	-	-
$\boldsymbol{h_o}$	$\left[\frac{W}{m^2C}\right]$	**5%**	**338.3**	15.25	

Table 32-HTCair uncertainties (R5)

Finally the uncertainty bands of the HTC_{air} obtained for each radiator typology are the following:

$\boldsymbol{Fin}$	$\%\boldsymbol{Difference}$
R1	±4%
R2	±4%
R3	±10%
R4	±10%
R5	±5%

Table 33- Uncertainty bands of the HTCair for Radiators

3. Comparison between Correlations and Experimental data.

The correlations observed in the previous chapter have been studied in the specified ranges of geometrical and physical parameters. It is possible at this point to make a comparison between the Colburn factor estimated with the correlations and the experimental data obtained at the Denso test bench.

3.1. CONDENSERS

3.1.1. Comparison between the application range of correlations and experimental data.

At this point according to the fin geometrical parameters with which has been studied the function regression to obtain the correlations, is necessary to verify if the parameters from Denso are suitable for the application range of each correlation.

The data bank of each correlation has been collected from a wide range of geometric dimensions some obtained from other articles (described in the previous chapter). In tables from 34 to 40, are reported for each correlation a complete list of geometric parameters with their descriptions, their corresponding ranges of application, and in addition the values of each condenser typology.

To identify if each parameter is inside the range, has been marked with a ✓ if is inside the range and x if it is not.

Correlation 1

Authors: Chang and Wang [1997]

Sym	Description	min	max	C1	C2	C3	C4	C5	C6	C7	C8
L_p	Louver pitch [mm]	**0.5**	**3**	✓	✓	✓	✓	✓	✓	✓	✓
L_h	Louver height [mm]	**0.94**	**18.5**	✓	✓	✓	✓	✓	✓	✓	✓
L_a	Louver angle [°]	**8.43**	**35**	✓	✓	✓	✓	✓	✓	✓	✓
F_p	Fin pitch [mm]	**0.51**	**3.33**	✓	✓	✓	✓	✓	✓	✓	✓
L_d	Core depth [mm]	**15.6**	**50**	X	✓	✓	X	✓	✓	✓	X
F_h	Fin height [mm]	**6**	**20**	X	✓	✓	✓	✓	X	X	X
b	Fin thickness [mm]	**0.04**	**0.16**	✓	✓	✓	✓	✓	✓	✓	✓
T_p	Tube pitch [mm]	**7.51**	**25**	X	✓	✓	✓	✓	X	X	X
D_h	Hydraulic Diameter[mm]	**0.824**	**4.94**	✓	✓	✓	✓	-	✓	-	✓

Table 34-Correlation 1 parametrical range-Condensers

Correlation 2

Authors:Park and Jacobi [2009a]

Sym	Description	Min	max	C1	C2	C3	C4	C5	C6	C7	C8
L_p	Louver pitch [mm]	**0.5**	**3**	✓	✓	✓	✓	✓	✓	✓	✓
L_h	Louver height [mm]	**0.94**	**18.5**	✓	✓	✓	✓	✓	✓	✓	✓
L_a	Louver angle [°]	**8.43**	**35**	✓	✓	✓	✓	✓	✓	✓	✓
F_p	Fin pitch [mm]	**0.51**	**5.08**	✓	✓	✓	✓	✓	✓	✓	✓
L_d	Core depth [mm]	**15.6**	**57.4**	X	✓	✓	X	✓	✓	✓	X
F_h	Fin height [mm]	**2.84**	**20**	✓	✓	✓	✓	✓	✓	✓	✓
b	Fin thickness [mm]	**0.0254**	**0.16**	✓	✓	✓	✓	✓	✓	✓	✓
T_p	Tube pitch [mm]	**3.76**	**25**	✓	✓	✓	✓	✓	✓	✓	✓

Table 35-Correlation 2 parametrical range pt1-Condensers

Sym	Correlation 2 - Inclusive range of heat exchangers parameters.									
	min	max	C1	C2	C3	C4	C5	C6	C7	C8
Fp/Lp	**0.45**	**4.44**	✓	✓	✓	✓	✓	✓	✓	✓
Fh/Lp	**2.6**	**16**	✓	✓	✓	✓	✓	✓	✓	✓
Lh/Fh	**0.63**	**0.96**	✓	✓	✓	✓	✓	✓	✓	✓

La	**8.4**	**35.9**	✓	✓	✓	✓	✓	✓	✓	✓
Ld/Fp	**5**	**40**	✓	✓	✓	✓	✓	✓	✓	✓
Tp/Fh	**1.12**	**1.37**	✓	✓	✓	✓	✓	✓	✓	✓
b/Lp	**0.025**	**0.155**	✓	✓	✓	✓	✓	✓	✓	✓
NLB	**1**	**4**	✓	✓	✓	✓	✓	✓	✓	✓

Table 36- Correlation 1 parametrical range pt2-Condensers

Correlation 3

Authors: Park and Jacobi [2009b]

Sym	Description	Min	max	C1	C2	C3	C4	C5	C6	C7	C8
L_p	Louver pitch [mm]	**0.95**	**2.66**	X	✓	✓	X	✓	X	X	X
L_h	Louver height [mm]	**6.15**	**11.15**	X	✓	✓	✓	X	X	X	X
L_a	Louver angle [°]	**15**	**42**	✓	✓	✓	✓	✓	✓	✓	✓
F_p	Fin pitch [mm]	**1.0**	**5.08**	✓	✓	✓	✓	✓	✓	✓	✓
L_d	Core depth [mm]	**15.6**	**57.4**	X	✓	✓	X	✓	✓	✓	X
F_h	Fin height [mm]	**7.93**	**12.43**	X	X	X	X	✓	X	X	X
b	Fin thickness [mm]	**0.08**	**0.15**	X	✓	✓	✓	✓	X	X	X
T_p	Tube pitch [mm]	**9.7**	**15.7**	X	X	X	X	✓	X	X	X

Table 37- Correlation 3 parametrical range-Condensers

Correlation 4

Authors: A.Vaisi, M.Esmaeilpour, H.Taherian

The present correlation is a theoretical model that has been developed for only one type of heat exchanger.

Correlation 5

Authors: Junqi.D,Jiangping Chen, Zhijiu Chen,Wenfeng Zhang, Yimin Zhou [2007]

Sym	Description	Min	max	C1	C2	C3	C4	C5	C6	C7	C8
L_a	Louver angle [°]	**22**	**28**	✓	✓	✓	✓	✓	✓	✓	✓
F_p	Fin pitch [mm]	**2.0**	**2.75**	✓	X	✓	✓	X	✓	✓	✓
L_d	Core depth [mm]	**36.6**	**65.0**	X	X	X	X	X	X	X	X
F_h	Fin height [mm]	**7.0**	**10.0**	X	✓	✓	✓	✓	X	X	X

b	Fin thickness [mm]	**0.15**	**0.2**	X	X	X	X	X	X	X	X

Table 38- Correlation 5 parametrical range-Condensers

Correlation 6

Authors: Kijung Ryu, Kwan-Soo Lee [2015]

This correlation describes the heat transfer characteristics of the entire area of the louvered fin rather than a specific area. The correlation is dimensionless and suitable for a general fin.

The fin parameters field is $\frac{Fp}{Lp} > 1 \; and \; \frac{Fp}{Lp} < 1$

Correlation 7

Authors: Davenport [1983b]

Sym	Description	min	max	C1	C2	C3	C4	C5	C6	C7	C8
L_p	Louver pitch [mm]	**1.5**	**3.0**	X	X	X	X	X	X	X	X
L_a	Louver angle [°]	**8**	**36**	✓	✓	✓	✓	✓	✓	✓	✓
F_p	Fin pitch [mm]	**1.0**	**1.6**	X	X	X	X	X	X	X	X
$\frac{L_p}{F_p}$	Louver pitch/Fin pitch	**0.94**	**2.24**	X	X	X	X	X	X	X	X

Table 39- Correlation 7 parametrical range-Condensers

Correlation 8

Authors: Nae-Hyun Kim & Jin-Pyo Cho [2007]

Sym	Description	min	max	C1	C2	C3	C4	C5	C6	C7	C8
L_a	Louver angle [°]	**15**	**27**	X	X	X	X	✓	✓	✓	X
F_p	Fin pitch [mm]	**1.0**	**1.4**	X	X	X	X	X	X	X	X

Table 40- Correlation 8 parametrical range-Condensers

3.1.2. Choise of the reference correlation.

The aim of this point is to evaluate and compare the correlation that better approximates the heat transfer coefficient behavior obtained by MFCondenser that have been developed with the standard procedures described in the previous chapter.

The Colburn factor in function of the Reynolds number is analyzed for the eight types of Condenser fins, neglecting for the moment that some fins do not satisfy the application ranges of the fin parameters given by each correlation, therefore in the following graphs are plotted the correlations comparing with the experimental tests.

The correlations are calculated with an average temperature of 50˚C, and the air velocity considered for the Reynolds numbers calculation is the air inlet air velocity.

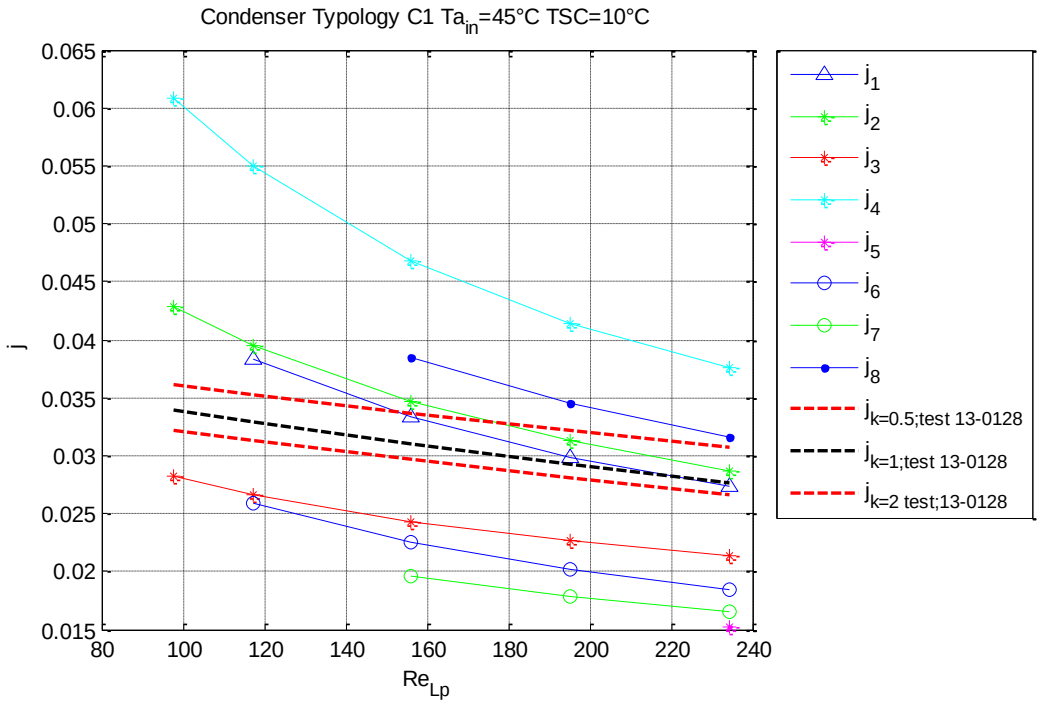

Figure 62-Comparison between correlations and experimental test –C1

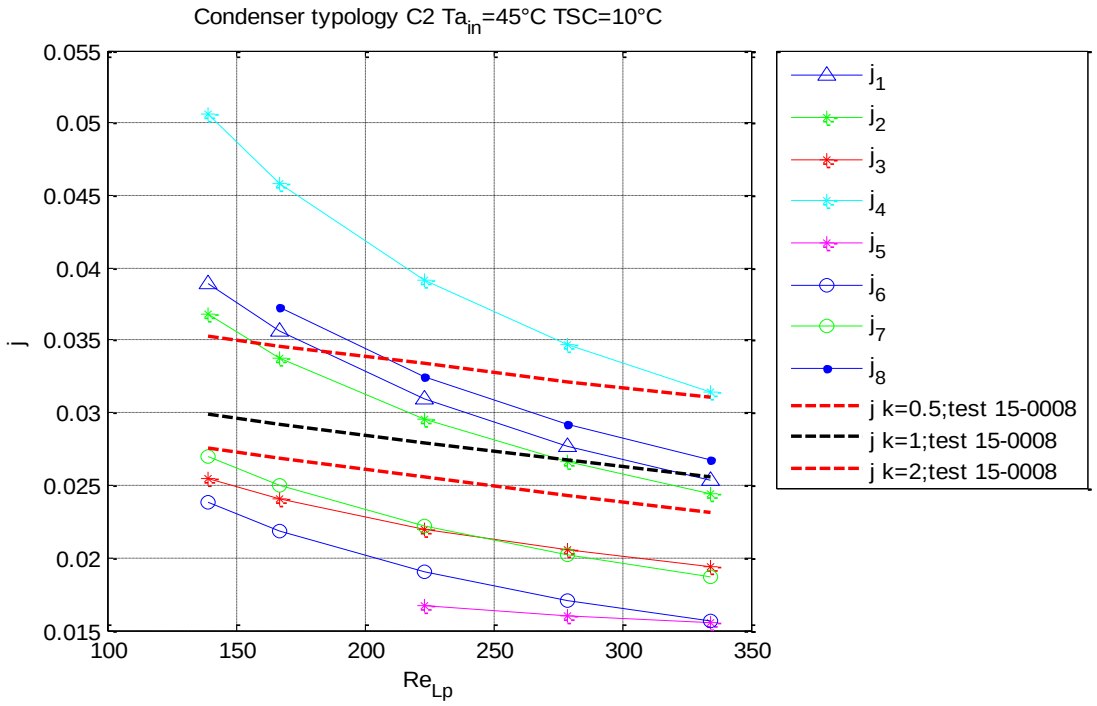

Figure 63-Comparison between correlations and experimental test –C2

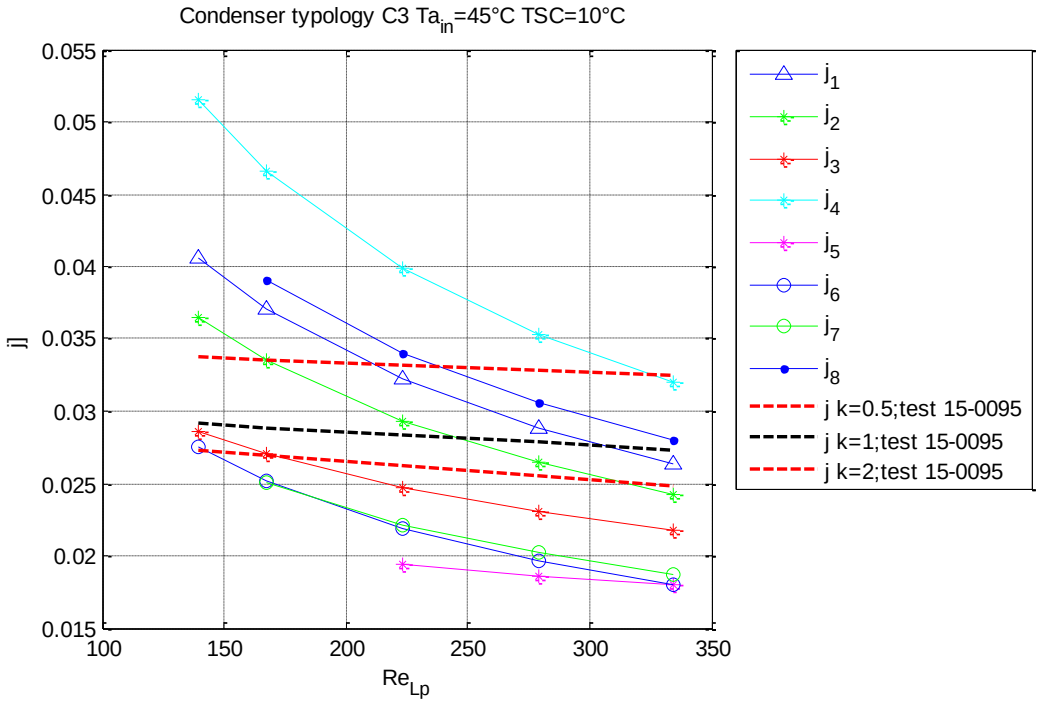

Figure 64-Comparison between correlations and experimental test –C3

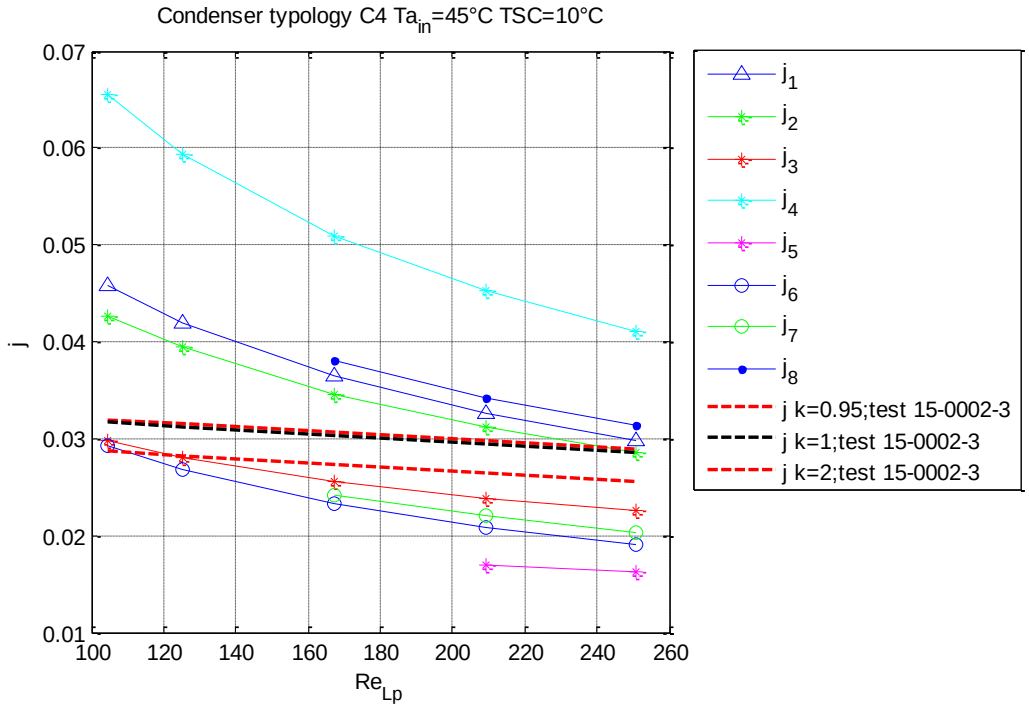

Figure 65-Comparison between correlations and experimental test –C4

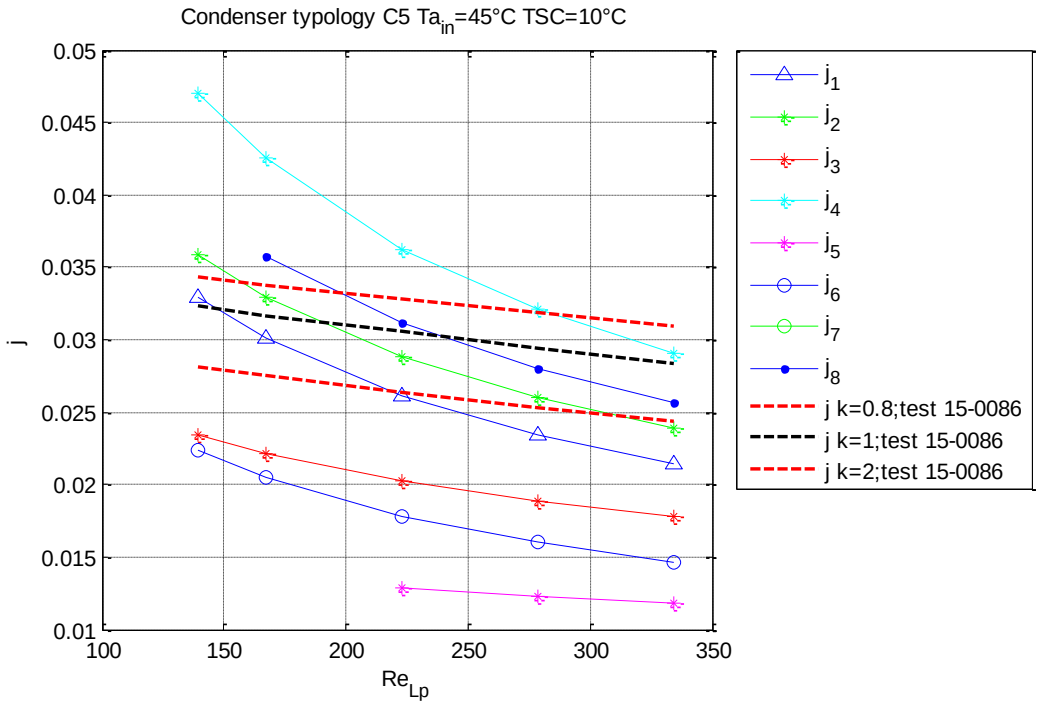

Figure 66-Comparison between correlations and experimental test –C5

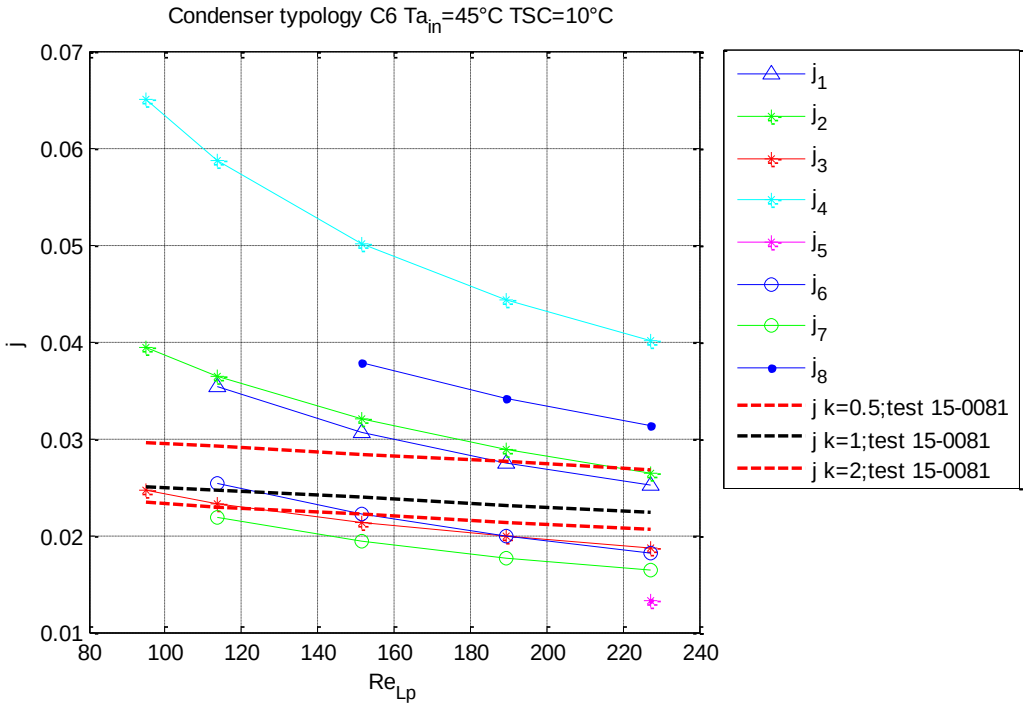

Figure 67-Comparison between correlations and experimental test –C6

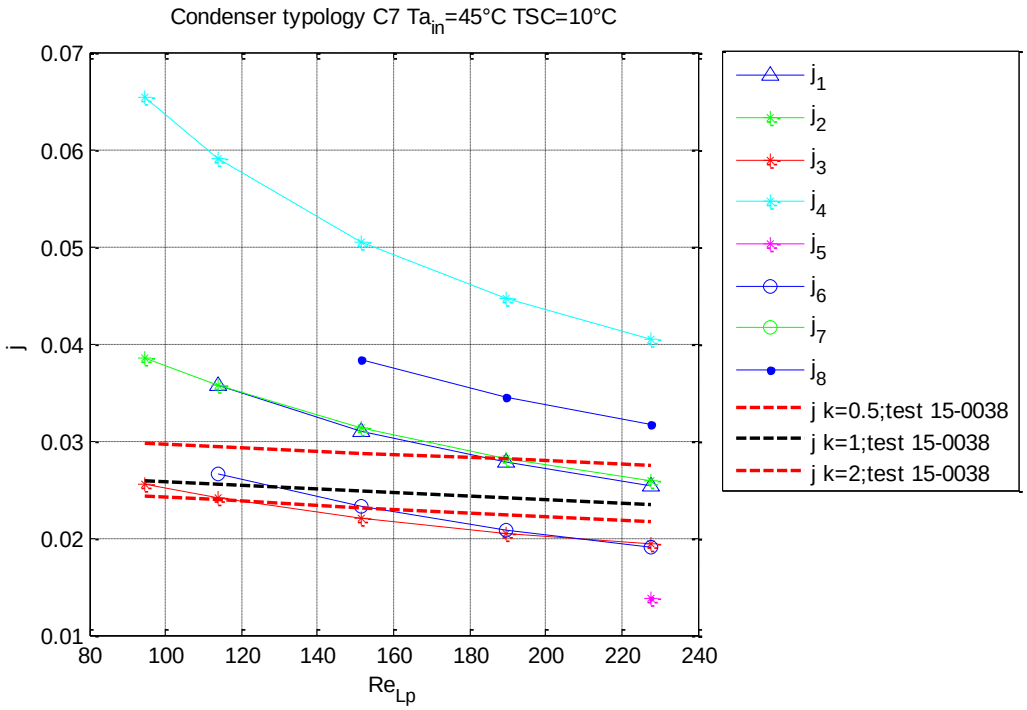

Figure 68-Comparison between correlations and experimental test –C7

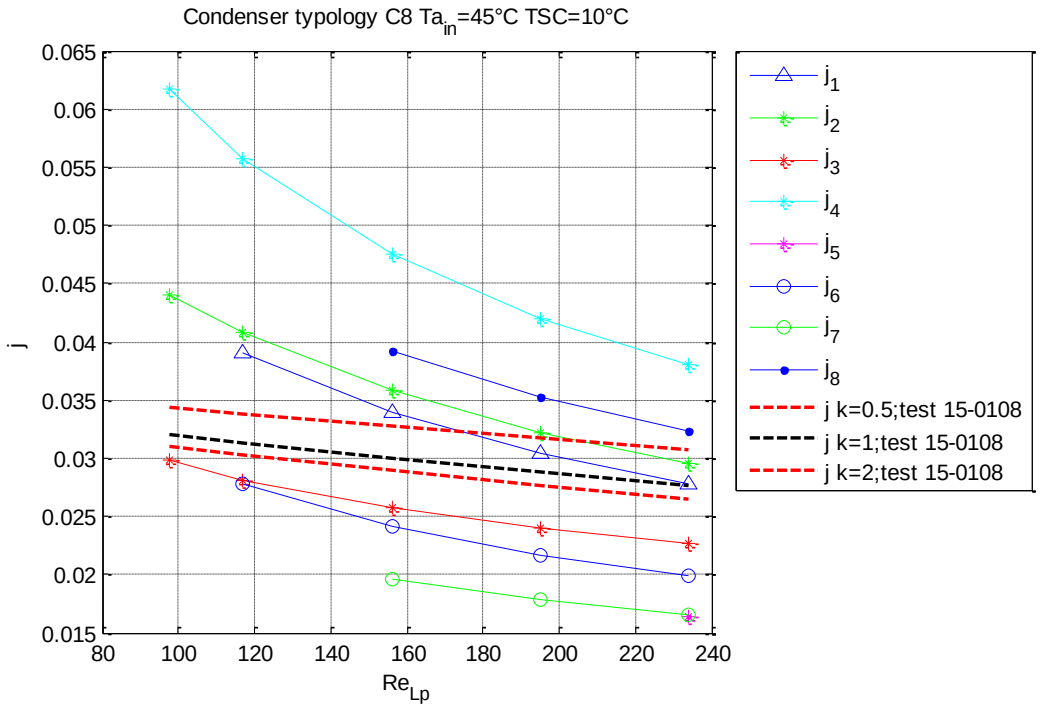

Figure 69-Comparison between correlations and experimental test –C8

It can be observed that evaluating all the article correlations, the figures from 62 to 69 show that the correlation 1 and 2 approximate more accurately to the MFCondenser curves, but with a different slope.

The choice between these two correlations has been considered mostly due to the parametric analysis that has been done in the chapter 2, because as can be observed the correlation 2 has the presence of a periodical behavior with the louver pitch and louver angle variation, hence is not possible to apply this correlation having a different behavior.

Consequently the correlation 1 is the one that has been considered for the study, having a normal behavior with the parametric variations and in addition approximate to the MFcondenser curves with certain trend.

In the following summary table are reported for each fin some comparative characteristics of the experimental test respect of the correlation 1 curves.

Fin	Test number	Inside all the Reynolds the range	Intersection between [2.5 and 6 m/s]	% Difference at 2.5 m/s	% Difference at 3 m/s	% Difference at 4 m/s	% Difference at 5m/s	% Difference at 6m/s
C1	***13-0128***	***NO***	$\approx 6m/s$	-	16.6%	7.43%	2.03%	-1.27%
C2	***15-0008***	***YES***	$\approx 6m/s$	30.12%	21.74%	10.59%	3.60%	-1.05%
C3	***15-0095***	***YES***	$\approx 6m/s$	39.19%	28.46%	13.62%	3.71%	-3.43%
C4	***15-0002-3***	***YES***	/	44.37%	34.09%	20.11%	10.99%	4.61%
C5	***15-0086***	***YES***	$\approx 2.6\ m/s$	2.00%	-4.95%	-14.33%	-20.34%	-24.48%
C6	***15-0081***	***NO***	/	-	43.09%	28.30%	18.69%	11.98%
C7	***15-0038***	***NO***	/	-	39.95%	25.15%	15.47%	8.66%
C8	***15-0108***	***NO***	/	-	24.65%	12.98%	5.61%	0.66%

Table 41 - Summary / Comparative Chart – Condenser Fins

It is possible to plot in the following figures the percentage differences in function of Reynolds number of the correlation 1 with the experimental test.

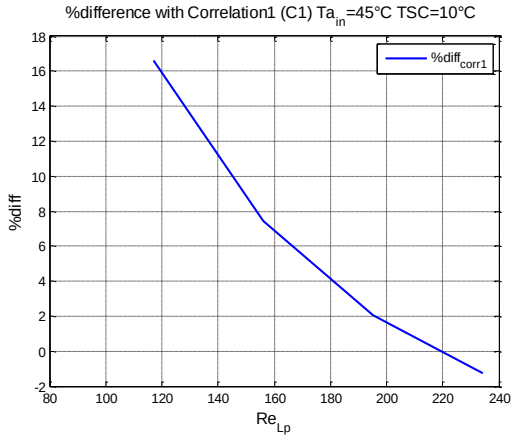

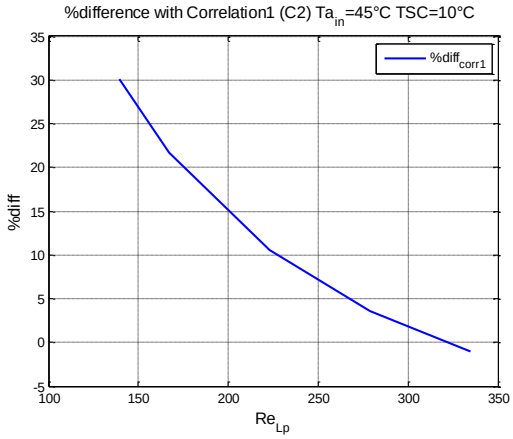

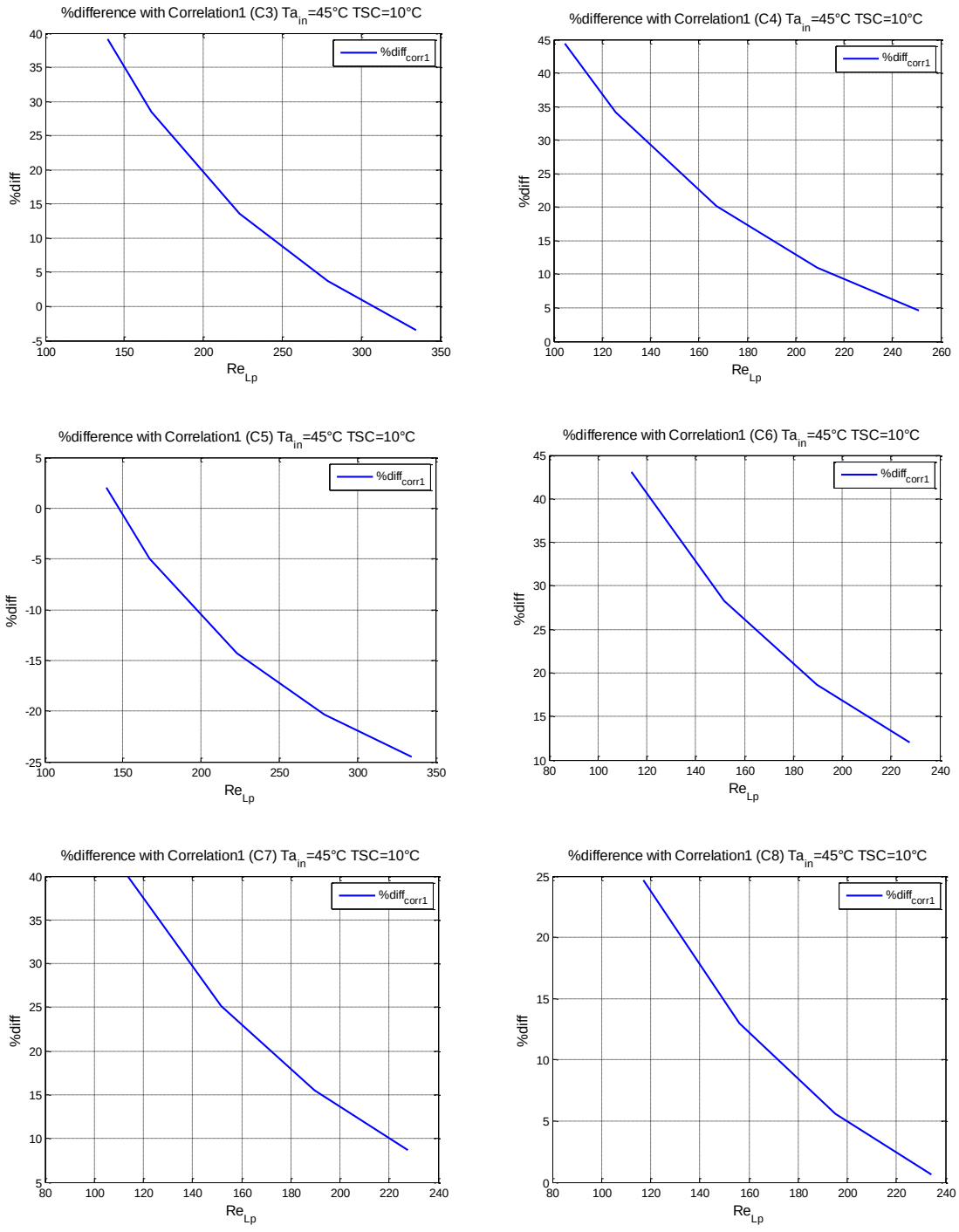

Figure 70- % Difference of the experimental test with correlation 1.

It can be noticed from the graphs that the condenser type which has the lower percentage differences is the C1, even if the fin height, core depth and tube pitch are not inside the

application range and at 2.5 m/s the Reynolds value is not inside the range allowed by the correlation.

The correlation overestimates the value of air heat transfer coefficient in almost all the range of air velocity, except the case of the C5 in which overestimates until more or less $Re_{Lp} \approx 140$.

3.1.3 Dependence of the chosen correlation on the geometrical and physical parameters

Correlation 1 depends on several fin geometrical parameters and physical parameters such as:

$$j = Re_{Lp}^{-0.49}\left(\frac{\theta}{90}\right)^{0.27}\left(\frac{F_p}{Lp}\right)^{-0.14}\left(\frac{F_h}{L_p}\right)^{-0.29}\left(\frac{L_d}{L_p}\right)^{-0.23}\left(\frac{L_h}{L_p}\right)^{0.68}\left(\frac{T_p}{L_p}\right)^{-0.28}\left(\frac{b}{L_p}\right)^{-0.05}$$

- ✓ $Re_{Lp} = \frac{u.L_p}{v_o}\begin{cases} Kinematics\ viscosity: v_0 = v_0\,(Temp) \\ Louver\ pitch:\ L_p \\ Air\ velocity: u \end{cases}$
- ✓ $Louver\ angle: L_a$
- ✓ $Fin\ pitch:\ F_p$
- ✓ $Fin\ heigth:\ F_h$
- ✓ $Louver\ heigth:\ L_h$
- ✓ $Louver\ pitch:\ L_p$
- ✓ $Fin\ length:\ L_d$
- ✓ $Tube\ pitch:\ T_p$
- ✓ $Fin\ thickness:\ b$

$$h_o = \frac{j\rho u c_p}{Pr^{\frac{2}{3}}}\begin{cases} Colburn\ factor:\ j \\ Air\ density:\ \rho = \rho(Temp) \\ Air\ velocity: u \\ Heat\ capacity:\ c_p = c_p(Temp) \\ Prandtl\ Number:\ Pr = \Pr(Temp) \end{cases}$$

Thus, can be observed that the correlation behavior is directly dependent on:

- The fin geometric parameters.
- The Temperature.

Temperature influence

The Correlations have been evaluated with a mean temperature of 50 °C, therefore is possible to observe if there is an influence due to the Temperature. Thus in the following figure 71 can be observed the difference evaluating the correlations at two different temperatures, the inlet air temperature 45°C and the mean temperature 50°C, against the experimental tests

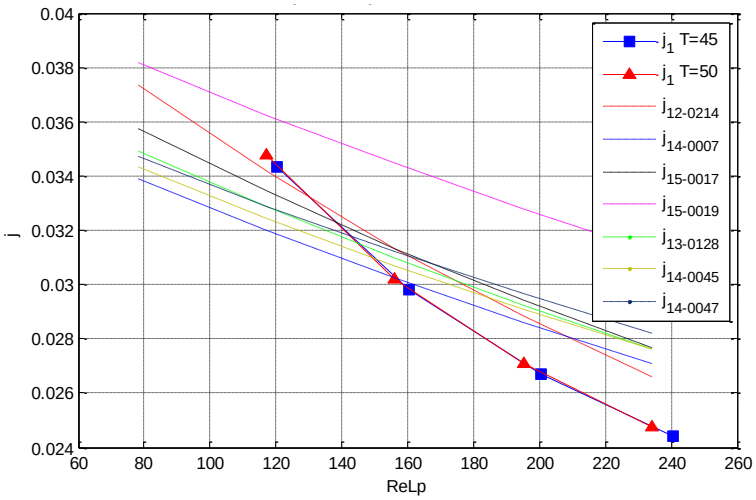

Figure 71- Temperature sensitivity C1 at T1=45C and T2=50C

The difference between Colburn factor of the Correlation 1 at 45°C and 50°C is approximately 0.13%, therefore is an almost neglected difference.

3.1.4. Function study.

Firstly is important to verify the behavior of the chosen correlation with varying the parameters of our interest, at this point is possible beginning with varying the two parameters Core depth and Fin height.

Then has been necessary to consider the application range given by the article in which has been studied the present correlation.

Fixed parameters		
Fin thickness	$b\ [mm]$	0.07
Fin pitch	$Fp\ [mm]$	2.3
Louver pitch	$Lp\ [mm]$	0.7
Louver angle	La	28
Tube height	$Th\ [mm]$	1.51

Variable parameters			Step
Core depth	Ld [mm]	15.6mm – 50mm	**2**
Fin height	Fh [mm]	6mm – 20mm	**1**
Tube pitch	$T_p[mm]$	7.51mm-21.51mm	**Fh+Th**
Louver height	$Lh\ [mm]$	5mm-19mm	**Fh-1**

Table 42- Function study - Geometrical parameters

The evaluation is conducted in two velocities, at 3m/s and 5 m/s.

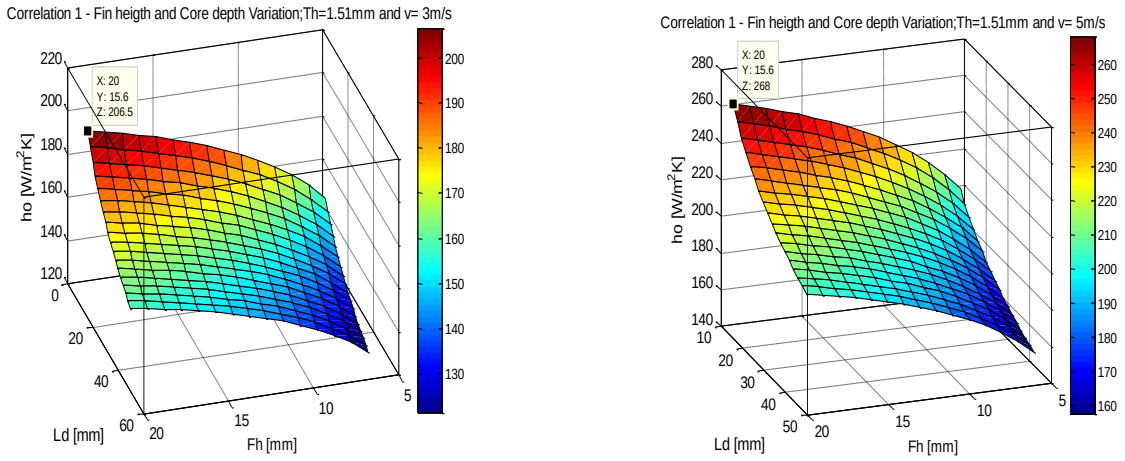

Figure 72-Function study- Surfaces Ld vs Fh a) 3m/s; b) 5m/s

As shown in the table below the highest values of air heat transfer coefficient are found with the smallest values of Core depth and highest value of Fin height. For two velocities the results are:

	v = 3 m/s	v = 5 m/s
$ho\ \left[\frac{W}{m^2K}\right]$	**206.5**	**268**
$Fh\ [mm]$	20	20
$Ld\ [mm]$	15.6	15.6

Table 43-Function study - HTC air at two velocities.

3.1.5. Optimization

At this point is possible to study the Condensers optimization, in order to reduce the fin geometries obtaining iso-thermal loads or even higher than the C1 thermal load, therefore the parameters of new condensers were hypothesized.

Previously it has been noticed the parametric analysis of the fin height and core depth inside the application range of the correlation 1, observing that reaching high values of fin height and decreasing the core depth are obtained higher values of air heat transfer coefficient, in our case the aim is to reduce the dimensions, therefore as a starting point has been considered lower values of fin height and core depth respect of those from the (C1).

Variable parameters			
Core depth	$Ld\ [mm]$	10 – 11.5	***Step 0.1***
Fin height	$Fh\ [mm]$	4 – 5	***Step 0.05***
Tube pitch	$Tp\ [mm]$	5.4 – 6.4	***Fh + Th***
Louver height	$Lh\ [mm]$	3-4	***Fh - 1***

Table 44- Variable parameters

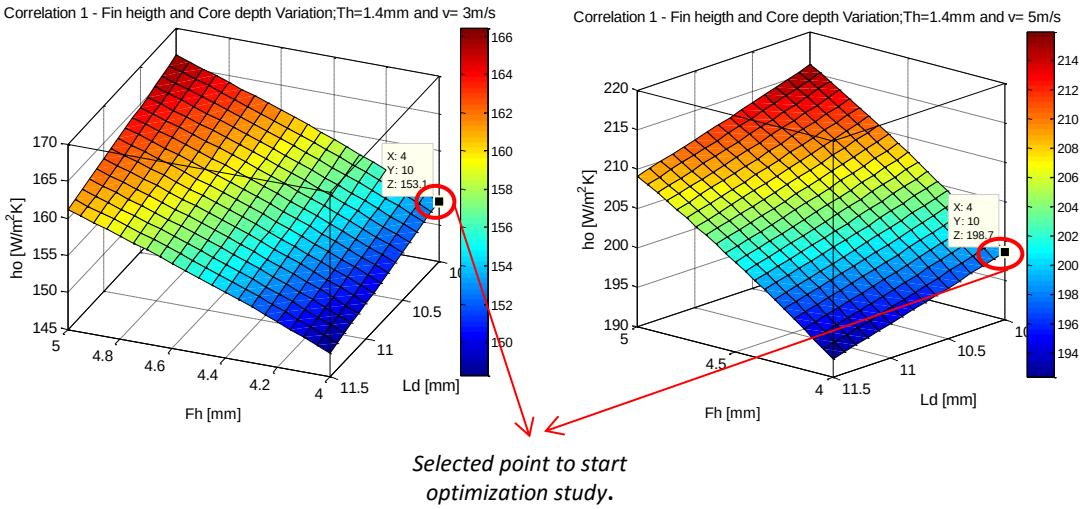

Figure 73-Surfaces- selected point to start optimization.

he internal dimensions of the tube were set starting from the C1 in order to reach the same internal flow area (with same total dimension of condenser) and similar hydraulic diameter of the tube.

New parameters		Value
Core depth	$\boldsymbol{Ld}$ [mm]	10
Fin height	$\boldsymbol{Fh}$ [mm]	4
Tube height	$\boldsymbol{T_h[mm]}$	1.4
Tube pitch	$\boldsymbol{T_p[mm]}$	5.4
Louver height	$\boldsymbol{Lh}$ $[\boldsymbol{mm}]$	3

Table 45-New parameters

The values of HTC_{air} were calculated at 3 m/s and 5 m/s with the correlation 1.

	v = 3 m/s	v = 5 m/s
$\boldsymbol{ho}\ \left[\frac{\boldsymbol{W}}{\boldsymbol{m^2K}}\right]$	153.1	198.7
$\boldsymbol{Fh}\ [\boldsymbol{mm}]$	4	4
$\boldsymbol{Ld}\ [\boldsymbol{mm}]$	10	10

Table 46 -HTC air at two velocities.

Then these values of air heat transfer coefficients in the two velocities are interpolated with the model function used by MFCondenser. Therefore a system of equations has been presented as follows:

$$\begin{cases} 153.1\dfrac{W}{m^2K} = a.\left[1 - e^{(-b.3)}\right] \\ 198.7\dfrac{W}{m^2K} = a.\left[1 - e^{(-b.5)}\right] \end{cases}$$

Hence the calculation of the coefficients a and b are performed for this new condenser geometry.

$$\begin{cases} a = 0.250849 \\ b = 0.314150 \end{cases}$$

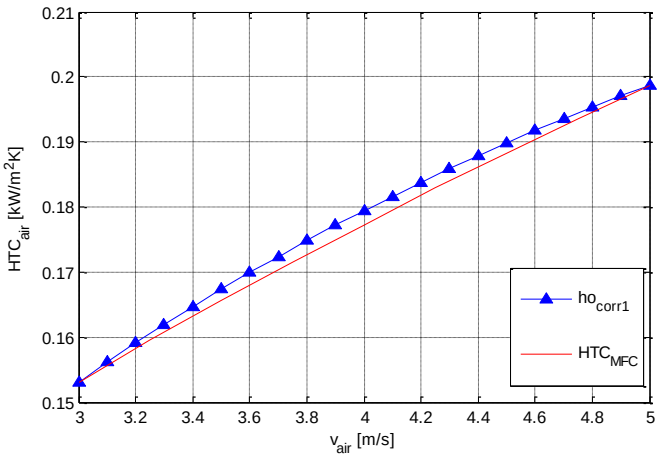

Figure 74-Calibration at two velocities.

Then it is possible to insert the inputs in MFCondenser, the coefficients a and b, the new geometry, in order to obtain the simulation of an experimental test with performance parameters results, one of them is the heat rejection.

In the following figure 75 are plotted the heat rejections of the original C1 experimental test,the simulation of the C1 by the correlation 1 (blue curve), and the simulation of the new condenser ($Ld = 10\ and\ Fh = 4\ with\ Tp = 5.4$) the green curve.

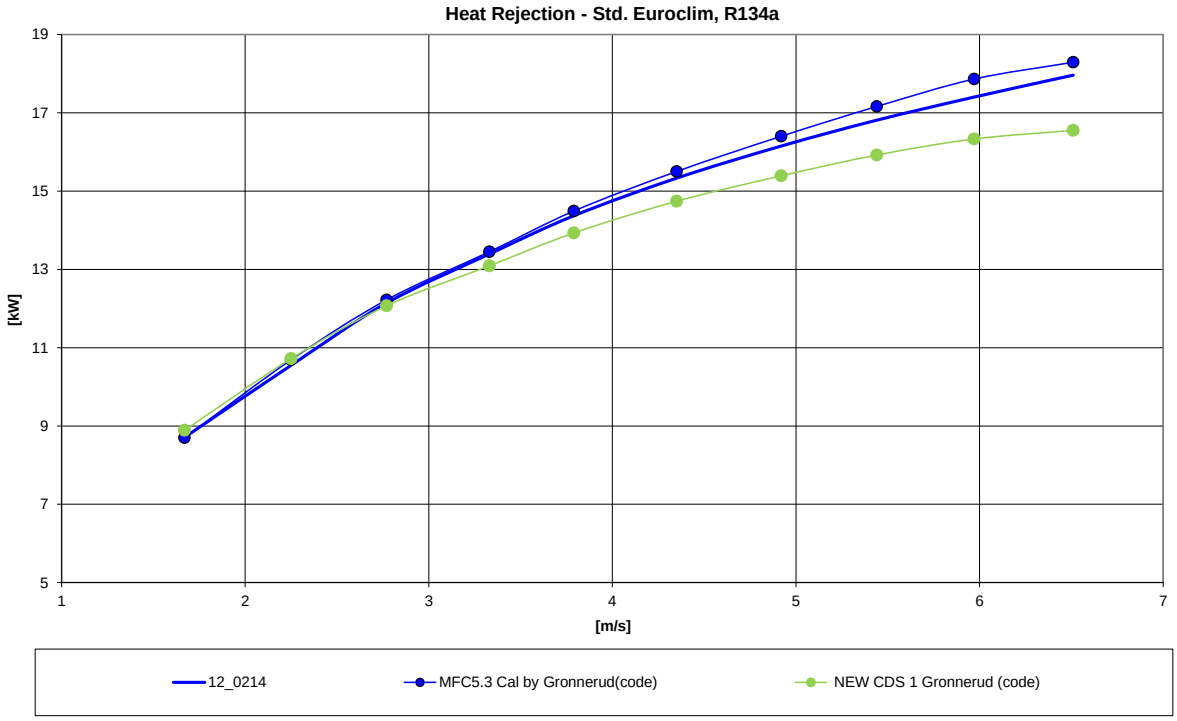

Figure 75-Heat rejection trial optimization

The optimized condenser simulated (green curve) obtains worse performances respect to the C1, but further optimizations can be obtained.

Other condenser configurations

Following the same procedure described previously, are considered other condenser types:

	C1(Ref)	NREC133	NREC134	NREC135	NREC132	NREC129	NREC131	NREC130
$Ld[mm]$	11.5	10	10	10	10	10	10	10
$Tp[mm]$	6.4	5.3	5.3	5.3	5.4	6	6	6
$Th[mm]$	1.4	1.2	1.2	1.2	1.2	1.2	1.2	1.2
$La[°]$	28	30	30	30	30	30	30	30
$Lp[mm]$	0.7	0.64	0.64	0.64	0.64	0.64	0.64	0.64
$Fp[mm]$	2.3	2.3	2.2	2.1	2.2	2.3	2.2	2.1

Table 47- New Condenser geometries

Where,

$$Fh = Tp - Th$$

$$Lh = Fh - 1$$

The other geometrical parameters of the fin are considered like the C1 typology.

The air heat transfer coefficients are obtained by the correlation 1 on two different velocities (v=3 and 5 m/s), then is possible to obtain the coefficients a and b, keeping the same C1 core dimensions (core width and height):

The height of the core is forced to be more or less the same, but changing the fin height and the tube pitch, the number of tubes in the core change with the following expression.

$$Nt = \frac{Hc_{REC} - Fh}{Tp}$$

Then the core height is calculated:

$$Hc = (Nt.Th) + (Nt + 1).Fh$$

Therefore the value is approximated as the C1 core height, but due to the small difference in the comparison with the others is necessary neglect the effect due to this variation.

Once all the geometries of the new condensers are defined, and the coefficients a and b, it is possible to do the simulations in MFCondenser, and obtain the performance parameters.

The air thermal loads in function of air velocity are obtained for each condenser, thus the analysis has been done in two fixed air velocities, in order to plot in the same graph the trend of the heat rejection as a function of the tube pitch variation at specifics tube heights, in addition the graphs are studied at same core depth values.

The following figures from 76 to 81 represent the specific heat rejection based on the tube pitch variation at 3.5 m/s and 5m/s, with core depth of 10 , 11.5 and 16 mm, and in each graph are represented the curves with the different tube height values from 1 mm to 2 mm.

The specific heat rejection has been respect of the core area, in order to neglect the influence due to the little variations in each condenser configuration.

To obtain these graphs more accurately and reduce calculations, the calculations have been optimized, for the tube height 1.2 the calibrations with MFCondenser have been done for each tube pitch configuration, and this curve has been verified with a trend line which as results the differences are less than 0.12% (see Appendix).

Therefore the calculations have been realized first obtaining some points of the curve with the MFCondenser, then can be obtained a trend line in order to plot the values of specific heat rejection with all the tube pitches.

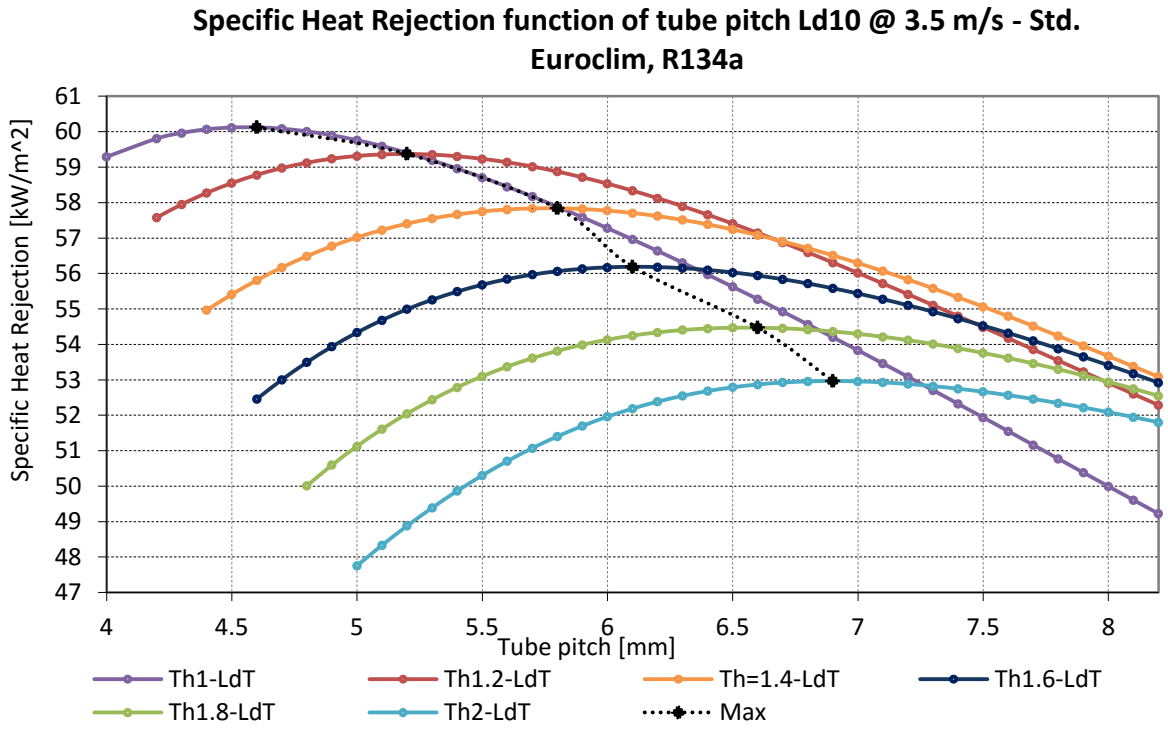

Figure 76- Specific heat rejection function of tube pitch Ld=10 v=3.5m/s

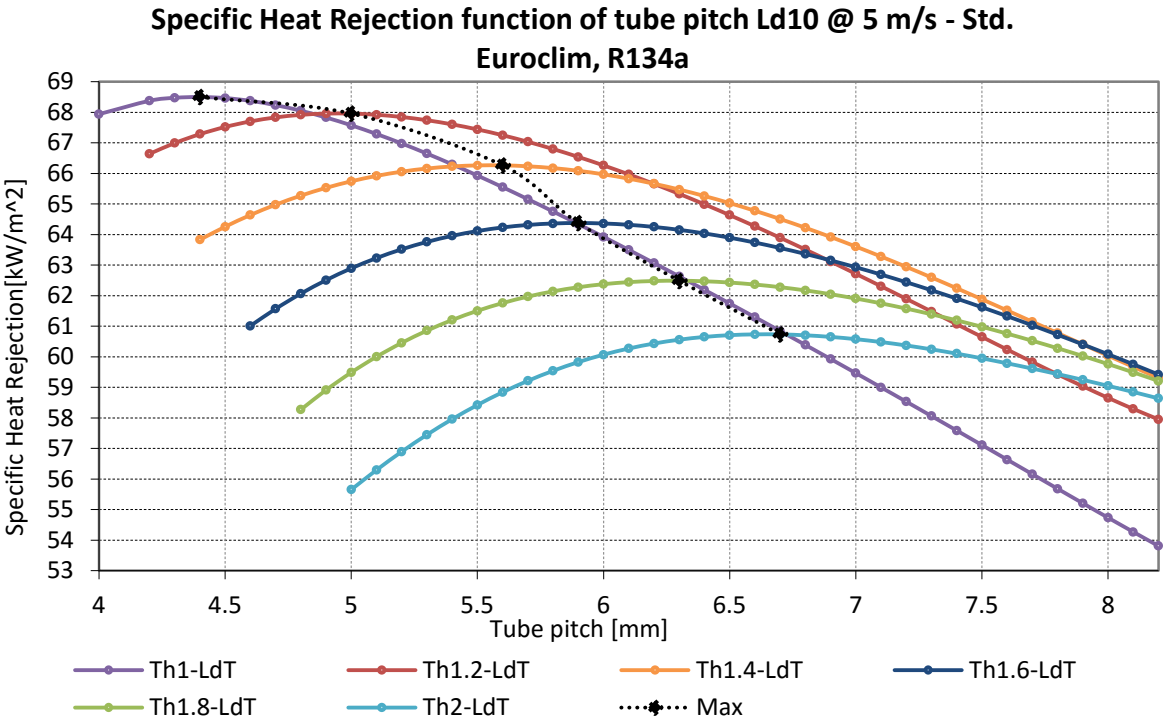

Figure 77- Specific heat rejection function of tube pitch Ld=10 v=5m/s

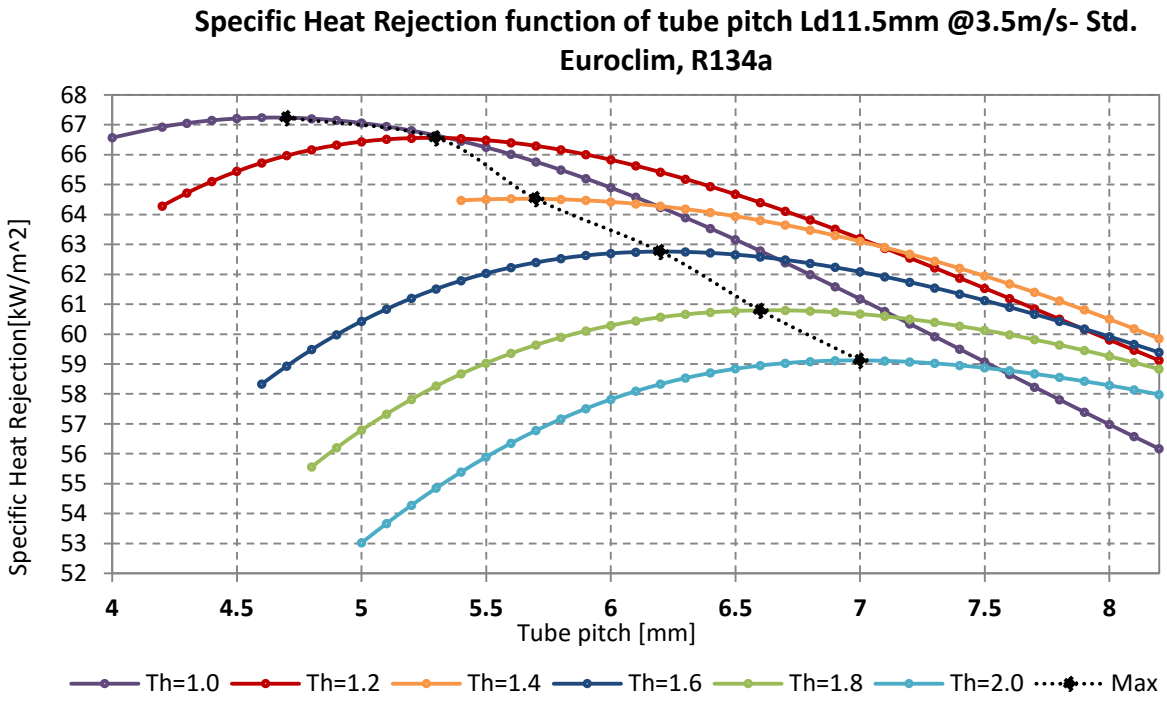

Figure 78- Specific heat rejection function of tube pitch Ld=11.5 v=3.5m/s

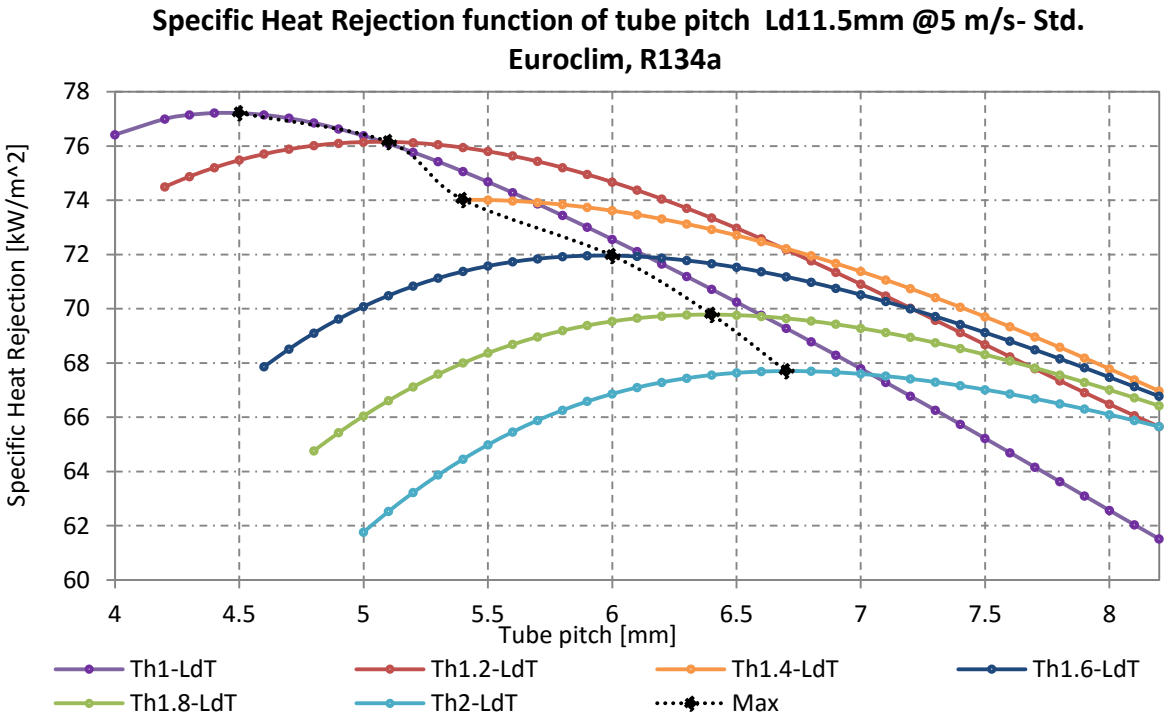

Figure 79- Specific heat rejection function of tube pitch Ld=11.5 v=5m/s

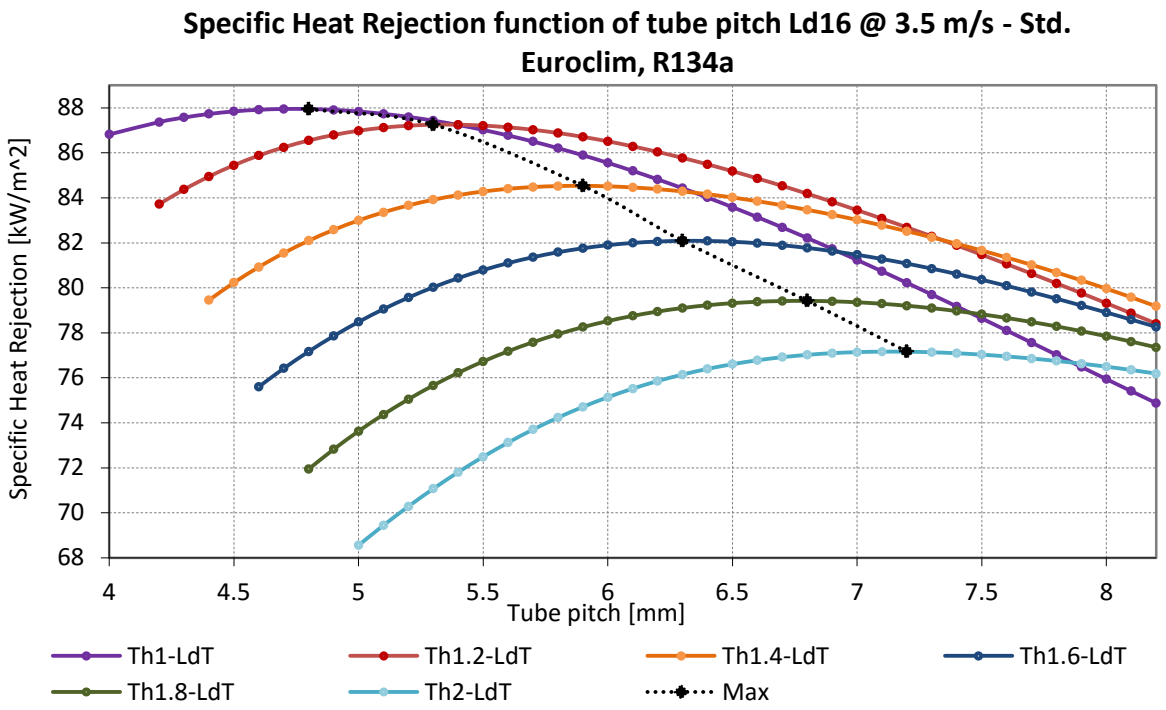

Figure 80- Specific heat rejection function of tube pitch Ld=16 v=3.5m/s

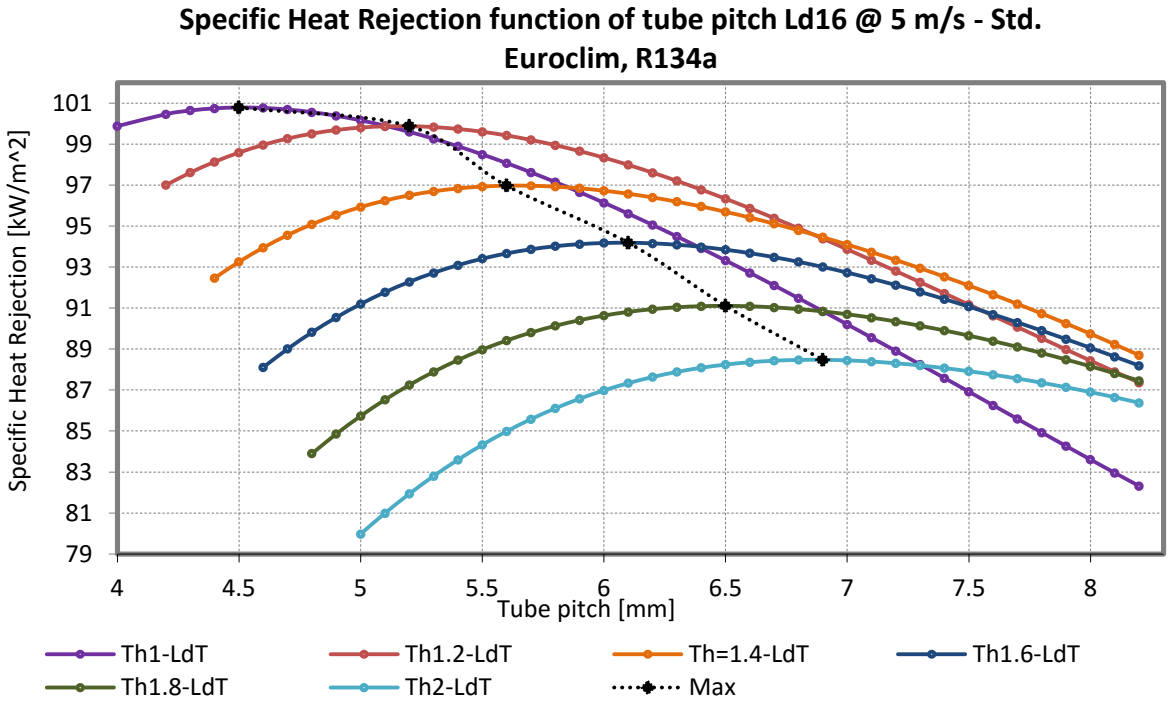

Figure 81- Specific heat rejection function of tube pitch Ld=16 v=5m/s

From the previous graphs is possible to conclude:

- The dependence that exits between the tube pitch and the tube height, because at each tube height there is an optimum value of tube pitch that reaches the highest thermal load this is valid for each core depth and for each of the two velocities.
- The general study noticed that the tube pitch that optimizes the heat transfer decrease with the tube height decreasing.

In the following table are represented the optimum tube pitches for each tube height on the three core depths and the two velocities.

Th	Ld=10		Ld=11.5		Ld=16	
	v=3.5m/s	v=5m/s	v=3.5m/s	v=5m/s	v=3.5m/s	v=5m/s
	Max tube pitch [mm]	Max tube pitch [mm]	Max tube pitch [mm]	Max tube pitch [mm]	Max tube pitch [mm]	Max tube pitch [mm]
1.0	4.6	4.4	4.7	4.5	4.8	4.5
1.2	5.2	5	5.3	5.1	5.3	5.2
1.4	5.8	5.6	5.7	5.4	5.9	5.6

1.6	6.1	5.9	6.2	6	6.3	6.1
1.8	6.6	6.3	6.6	6.4	6.8	6.5
2.0	6.9	6.7	7	6.9	7.2	6.9

Table 48-Optimum tube pitches for each tube height, with the different core depths and the two velocities.

From this information is possible to study the possibility of an optimum and common tube pitch that would be valid for each core depth and each air velocity, with a condition of difference < 0.5 % of the chosen optimum tube pitch with respect of the maximum specific heat rejection for each configuration.

Verification that for each tube pitch the maximum heat exchange is around 0.5% of maximum value (for each core depth and each air velocity)											
Ld=10				**Ld=11.5**				**Ld=16**			
v=3.5m/s		**v=5m/s**		**v=3.5m/s**		**v=5m/s**		**v=3.5m/s**		**v=5m/s**	
Max tube pitch [mm]	**%vs max vs choice**	**Max tube pitch [mm]**	**%vs max vs choice**	**Max tube pitch [mm]**	**%vs max vs choice**	**Max tube pitch [mm]**	**%vs max vs choice**	**Max tube pitch [mm]**	**%vs max vs choice**	**Max tube pitch [mm]**	**%vs max vs choice**
4.6	0.06%	4.4	0.4%	4.7	0.00%	4.5	0.3%	4.8	0.0%	4.5	0.1%
5.2	0.03%	5.0	0.3%	5.3	0.00%	5.1	0.1%	5.3	0.0%	5.2	0.0%
5.8	0.04%	5.6	0.3%	5.7	0.08%	5.4	0.4%	5.9	0.0%	5.6	0.1%
6.1	0.07%	5.9	0.3%	6.2	0.02%	6.0	0.2%	6.3	0.0%	6.1	0.1%
6.6	0.00%	6.3	0.2%	6.6	0.00%	6.4	0.1%	6.8	0.0%	6.5	0.0%
6.9	0.00%	6.7	0.1%	7.0	0.01%	6.9	0.1%	7.2	0.1%	6.9	0.0%

Table 49- Verification that for each tube pitch the maximum heat exchange is around 0.5% of maximum value(for each core depth and each air velocity).

The following table 50 shows the common optimum tube pitches.

Optimum (and common) tube pitch that is valid for each core depth and each air velocity.	
Tube height [mm]	**Tube pitch [mm]**
1.0	4.7
1.2	5.3
1.4	5.9
1.6	6.3
1.8	6.6
2.0	6.9

Table 50- Optimum tube pitch for each tube height, valid for ach core depth and air velocity.

The following figure 82 shows the tube pitch dependence on tube height, for each core depth and each air velocity.

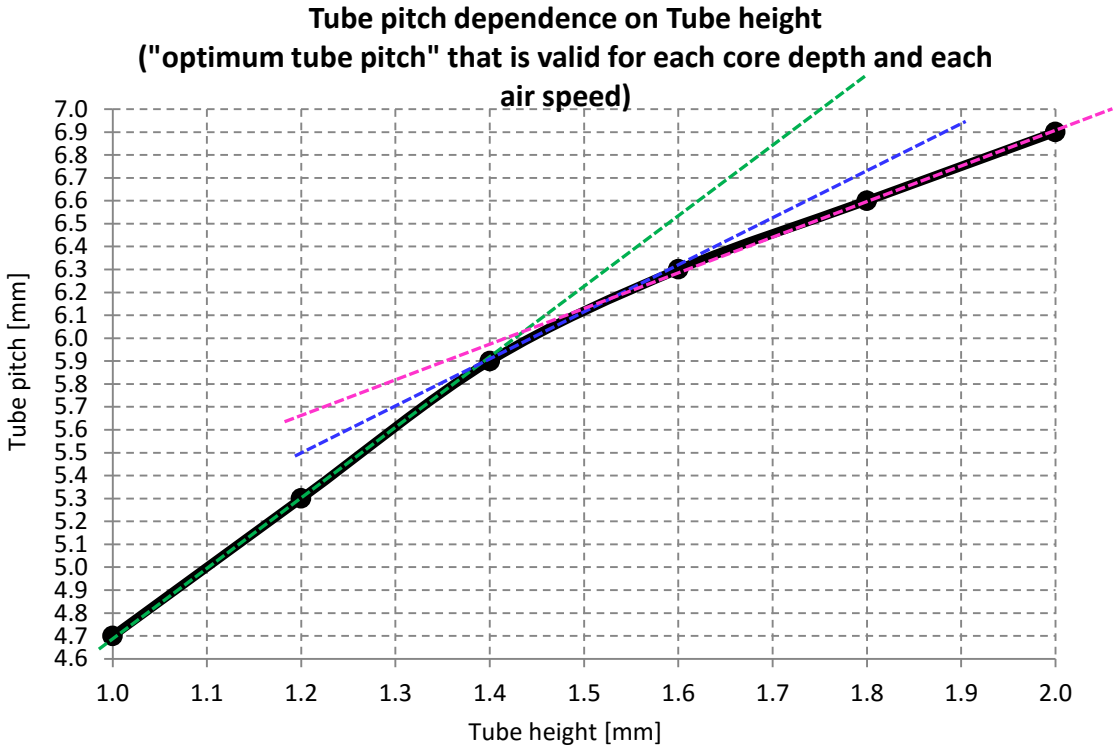

Figure 82-Tube pitch vs Tube height for each Ld and velocity

From the figure can be noticed that the tube pitch optimum raises with increasing of tube height, but it is evident a slightly different slope, from tube height from 1 to 1.4 there is a higher slope, then the slope changes.

Starting point

The optimization of the condenser geometries starts selecting these two dimensions in order to reduce the geometry:

- Core depth ➔ $Ld = 10mm$.
- Tube height ➔ $Th = 1.2mm$.

Starting with these two parameters further tube pitches have been analyzed with MFCondenser, and consequently reach more accurately the optimum, in which the heat

rejection is the maximum. In the following figure are plotted the thermal loads in function of tube pitch for the two curves at two different velocities and are compared with the C1 points.

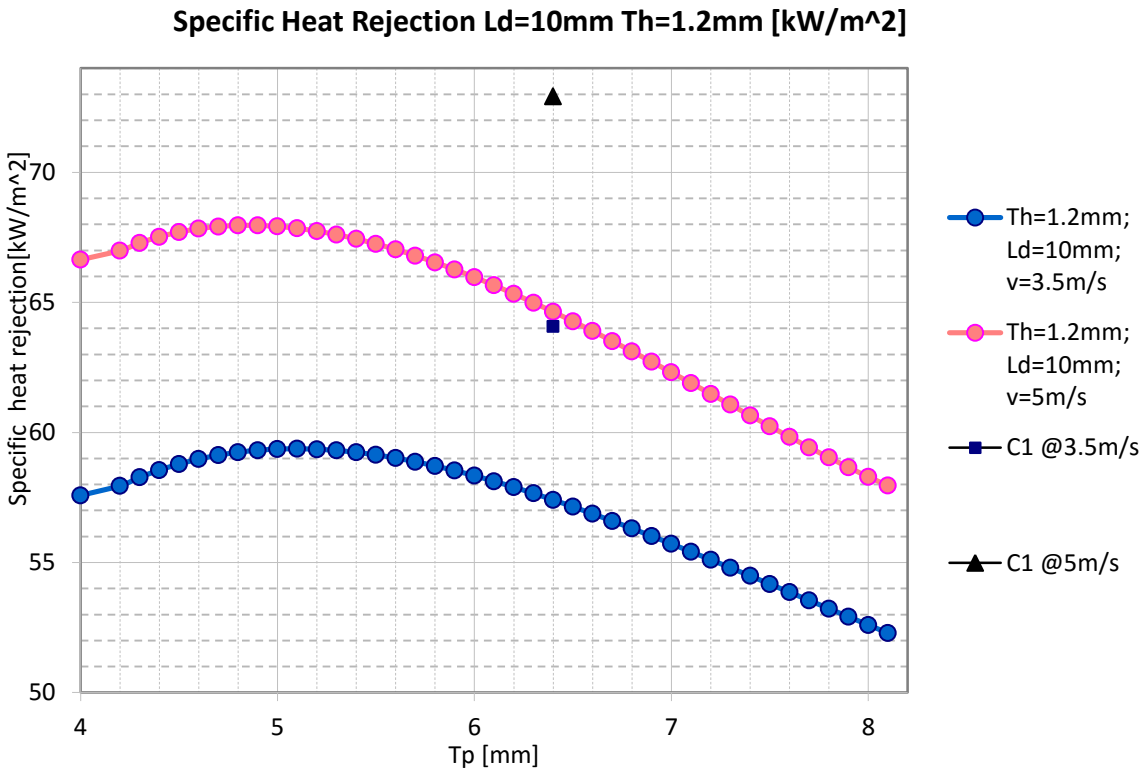

Figure 83-Specific heat rejection Ld=10 Th=1.2

It is noticed that the maximum thermal load of both curves are lower than the C1 points, at this point is necessary to optimize with other fin geometrical parameters.

The tube pitch optimum for a $Th = 1.2mm$ where there is the maximum heat rejection is $Tp = 5.3mm$.

- Tube pitch ➔ $Tp = 5.3mm$.

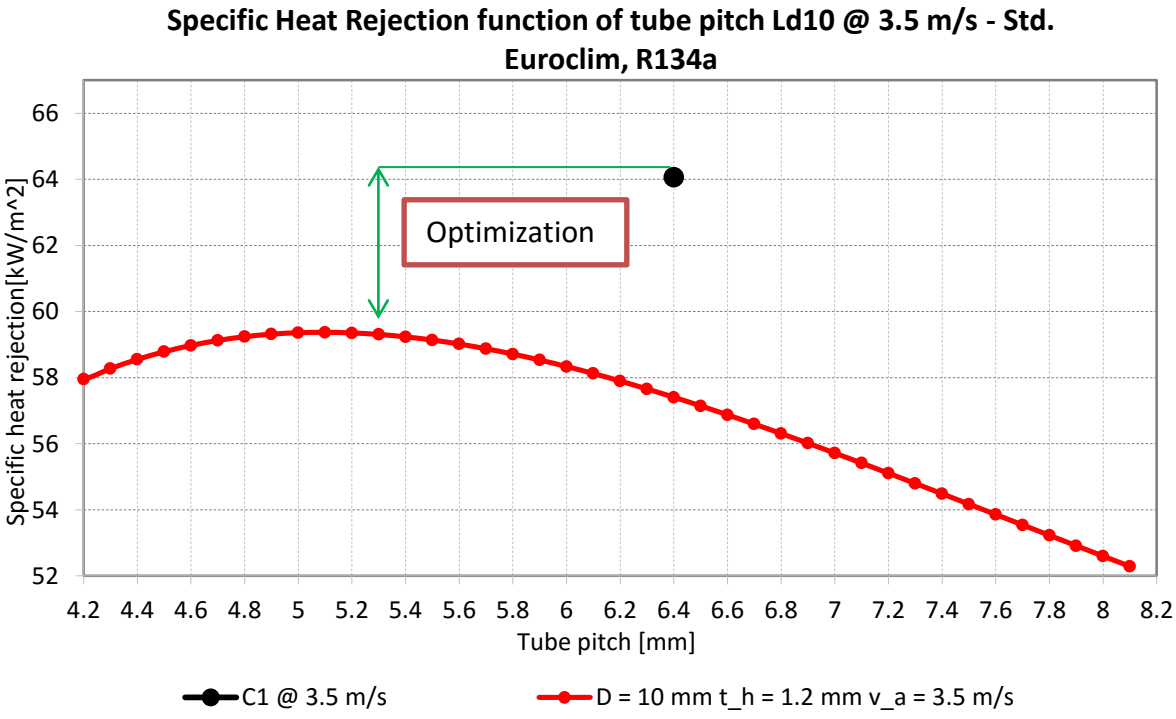

Figure 84-Specific heat rejection Ld=10, optimization begins Tp=5.3

3.1.5.1. First optimization

The first optimization has been considered varying the following parameters:

- Louver pitch ➔ $Lp = 0.64mm$
- Louver angle ➔ $La = 30^{\circ}$

The louver angle has been increased from 28° to 30°, and the louver pitch decreased from 0.7 to 0.64 in order to enhance the thermal load. The following figure 85 represents the thermal load with the first optimization respect of the C1.

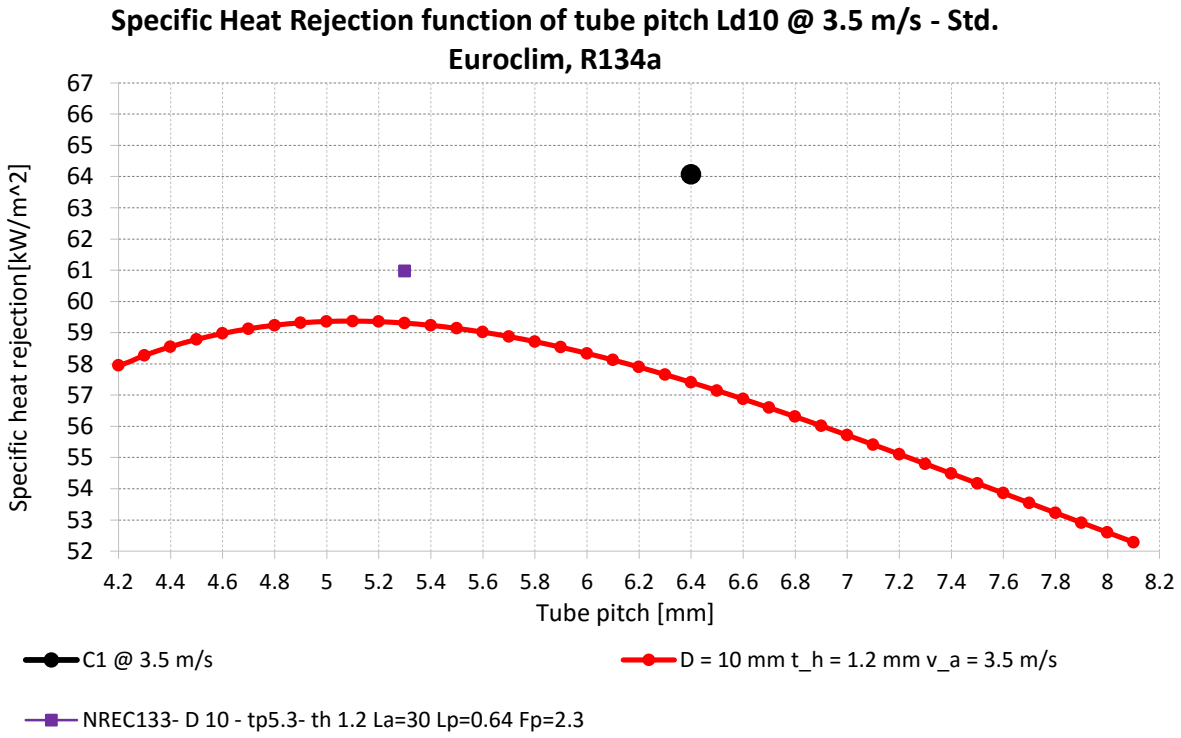

Figure 85- First optimization - Condensers

Further optimizations are required to reach higher thermal loads.

3.1.5.2 Second optimization

The second optimization has been considered varying the following parameters:

- Louver pitch ➔ $Lp = 0.64mm$
- Louver angle ➔ $La = 30^{\circ}$
- Fin pitch ➔ $Fp = 2.2mm$

The fin pitch reduction leads the louver height variation considering the following expression:

- $Lh = Fh - \left(\frac{Fp}{2}\right) + 0.15$

The following figure 86 represents the thermal load with the second optimization.

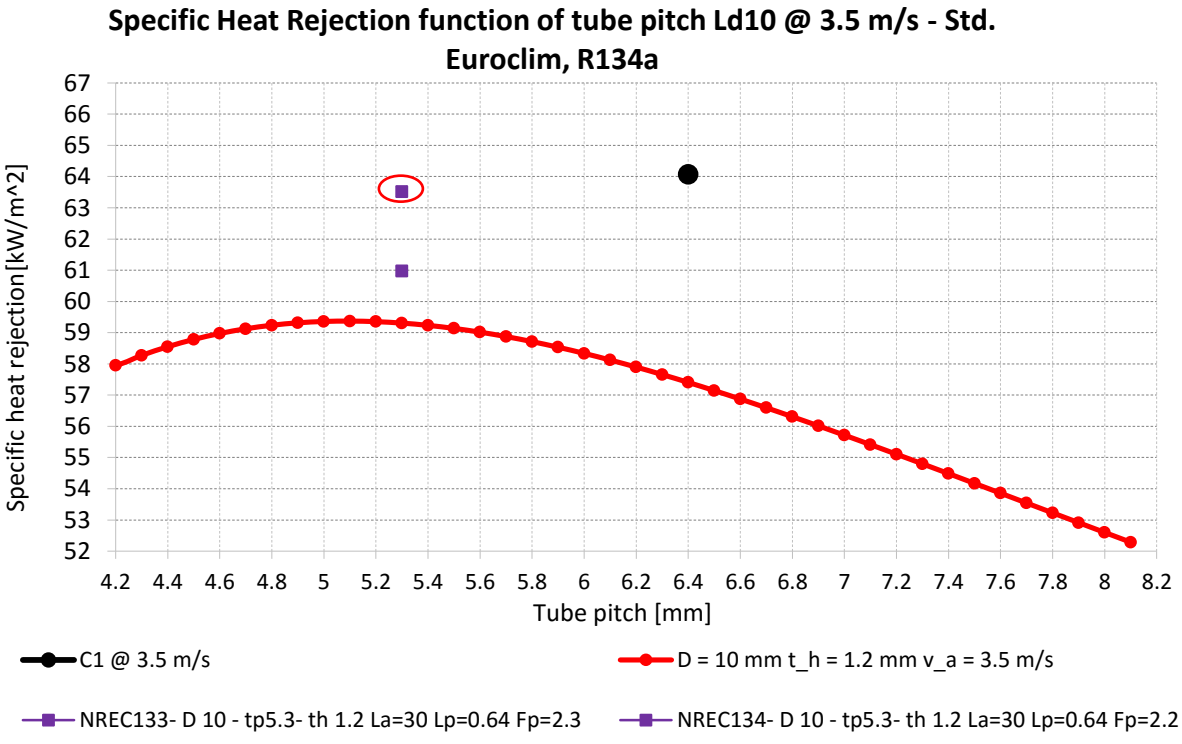

Figure 86-Second optimization-Condensers

The optimization of the other fin parameters induce a result that do not reach the same heat rejection as C1, therefore is necessary to continue optimizing.

3.1.5.3 Third optimization

The third optimization has been considered varying the following parameters:

- Louver pitch ➔ $Lp = 0.64mm$
- Louver angle ➔ $La = 30^{\circ}$
- Fin pitch ➔ $Fp = 2.1mm$

The following figure 87 represents the thermal load with the third optimization.

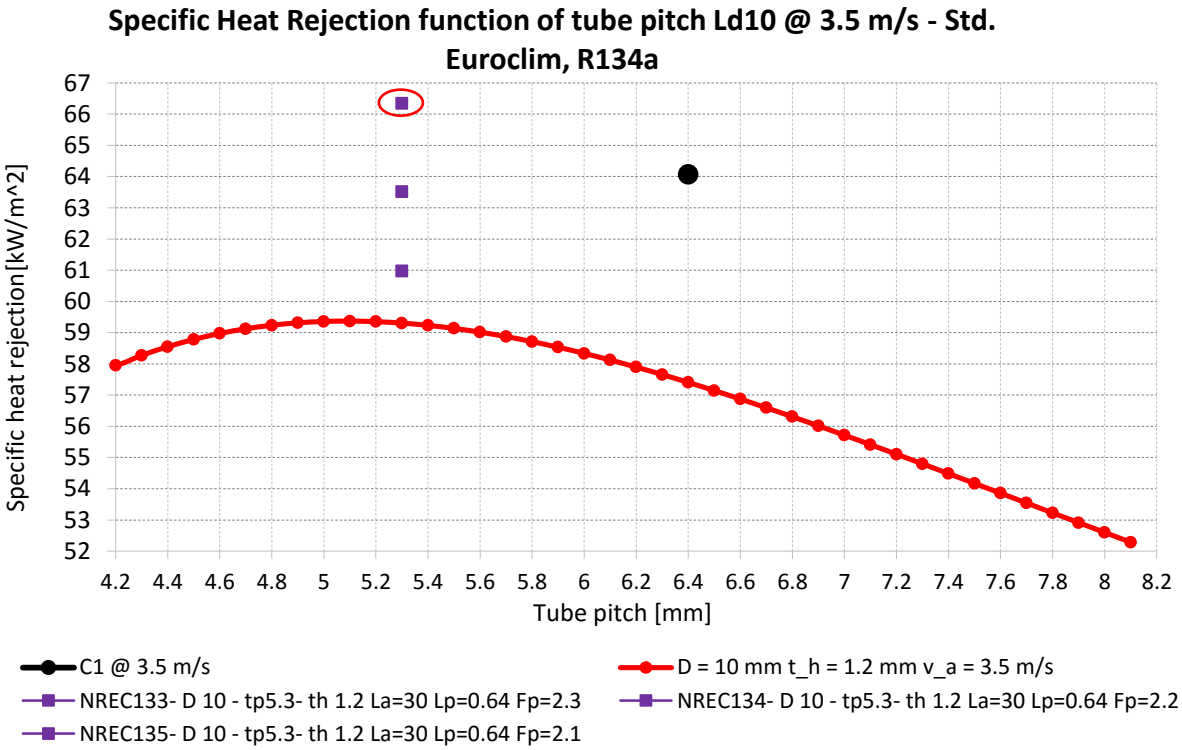

Figure 87-Third optimization-Condensers

From the figure can be noticed that the third optimization with decreasing the fin pitch the thermal load raises, and is higher than the C1 value.

Is possible to continue optimizing in order to obtain other options that reach higher or the same heat rejection as the actual C1 condenser typology.

3.1.5.4 Fourth optimization

The fourth optimization has been considered varying the following parameters:

- Louver pitch ➔ $Lp = 0.64mm$
- Louver angle ➔ $La = 30^{\circ}$
- Fin pitch ➔ $Fp = 2.3mm$

And considering a higher tube pitch.

- Tube pitch ➔ $Tp = 5.4mm$

The following figure 88 represent the thermal load with the fourth optimization respect to the others.

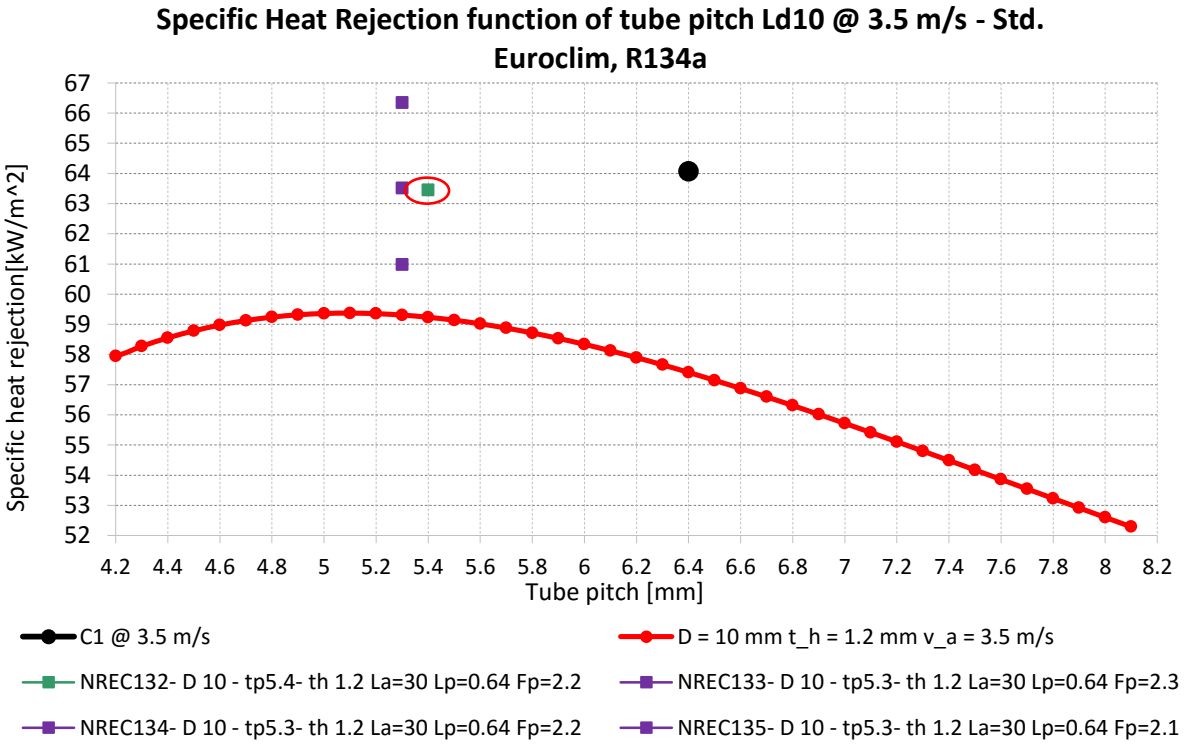

Figure 88-Fourth optimization-Condensers

The figure shows that the fourth optimization, with increasing the tube pitch the thermal load is lower than the C1, then further optimizations can be considered with other tube pitch.

3.1.5.5 Fifth optimization

The fifth optimization has been considered varying the following parameters:

- Louver pitch ➔ $Lp = 0.64mm$
- Louver angle ➔ $La = 30^{\circ}$
- Fin pitch ➔ $Fp = 2.3mm$

And considering a higher tube pitch.

- Tube pitch ➔ $Tp = 6mm$

The following figure 89 represent the thermal load with the fifth optimization respect to the others.

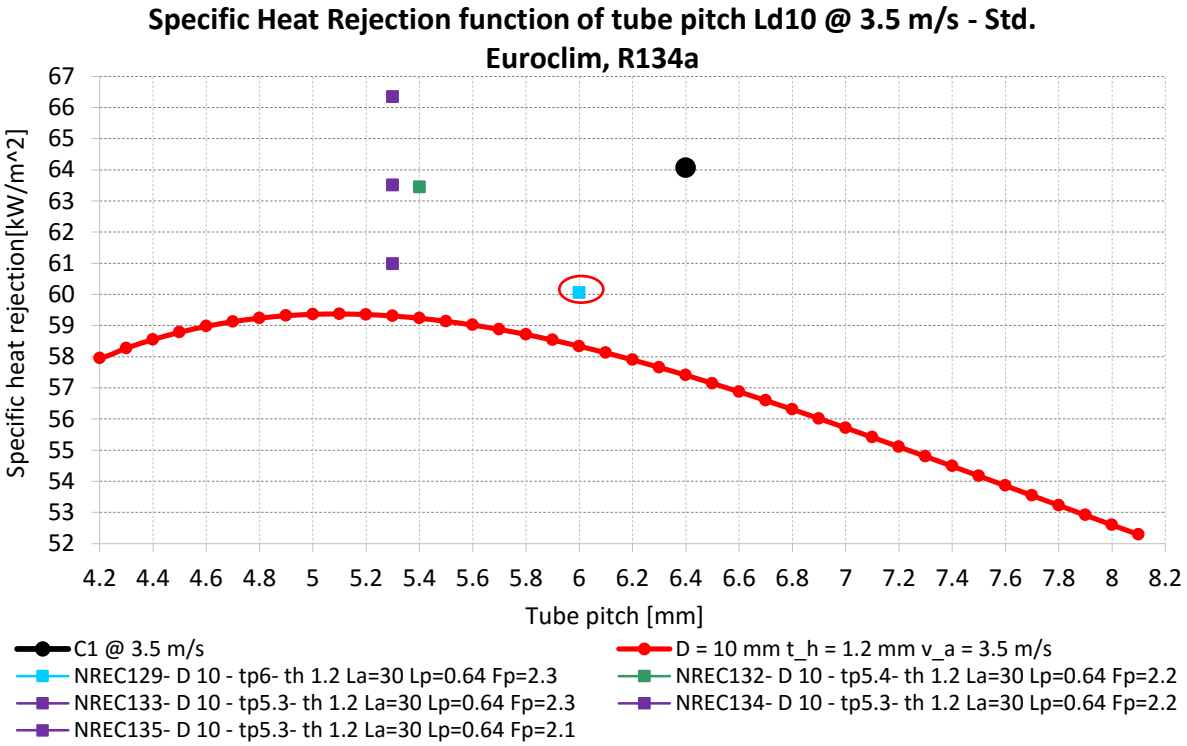

Figure 89-Fifth optimization-Condensers

From the figure, can be noticed that is possible further reductions on the fin pitch to obtain higher heat rejections.

3.1.5.6 Sixth optimization.

The fifth optimization has been considered varying the following parameters:

- Louver pitch ➔ $Lp = 0.64mm$
- Louver angle ➔ $La = 30^{\circ}$
- Fin pitch ➔ $Fp = 2.2mm$

And considering a higher tube pitch.

- Tube pitch ➔ $Tp = 6mm$

The following figure 90 represent the thermal load with the sixth optimization respect to the others.

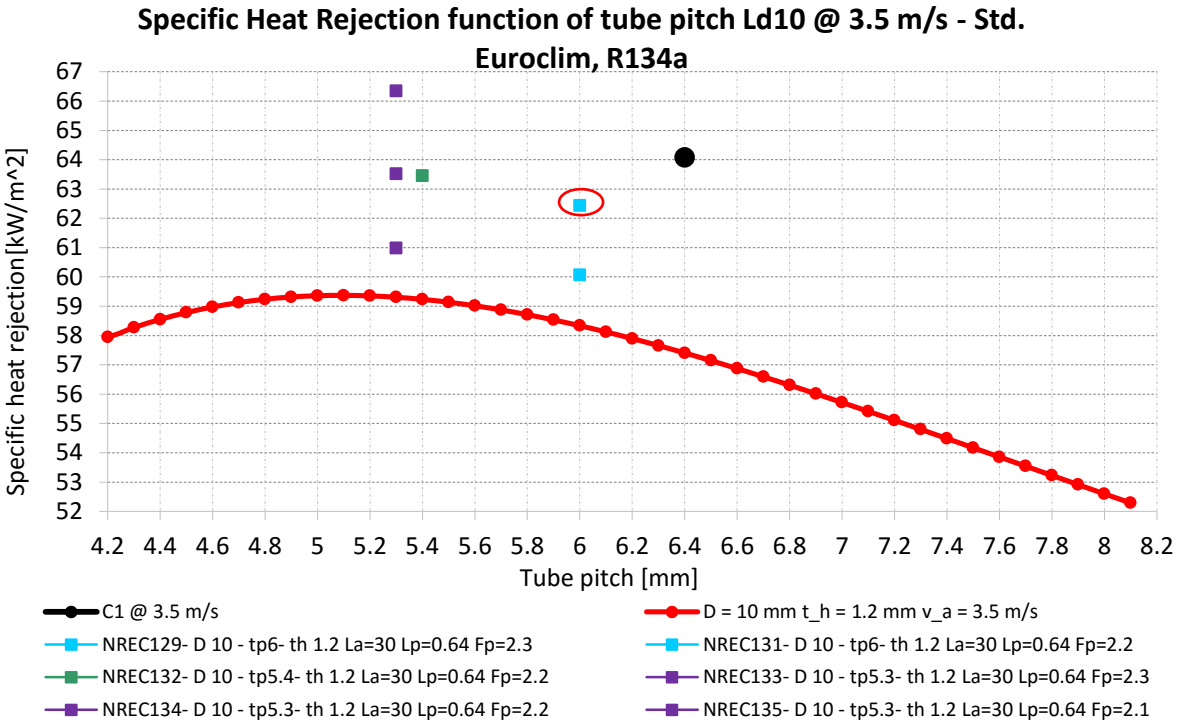

Figure 90-Sixth optimization-Condensers

3.1.5.7 Seventh optimization.

The seventh optimization has been considered varying the following parameters:

- Louver pitch ➔ $Lp = 0.64mm$
- Louver angle ➔ $La = 30^{\circ}$
- Fin pitch ➔ $Fp = 2.1mm$

And considering a higher tube pitch.

- Tube pitch ➔ $Tp = 6mm$

The following figure 91 represent the thermal load with the actual optimization respect to the others.

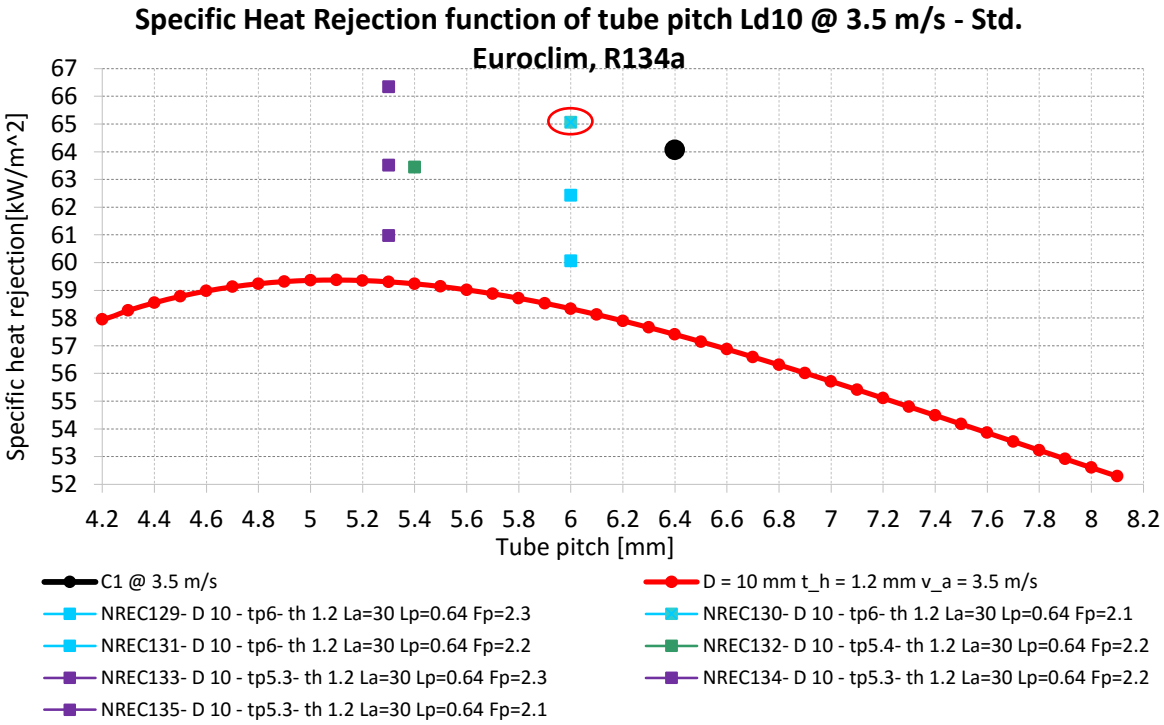

Figure 91-Seventh optimization-Condensers

3.1.5.8 Selected optimal option.

Once all the optimizations have been studied is possible to observe from the following graph that the chosen option is the condenser NREC134. Considering a band of C1 value of heat rejection with ±1% in which can be considered the optimizations.

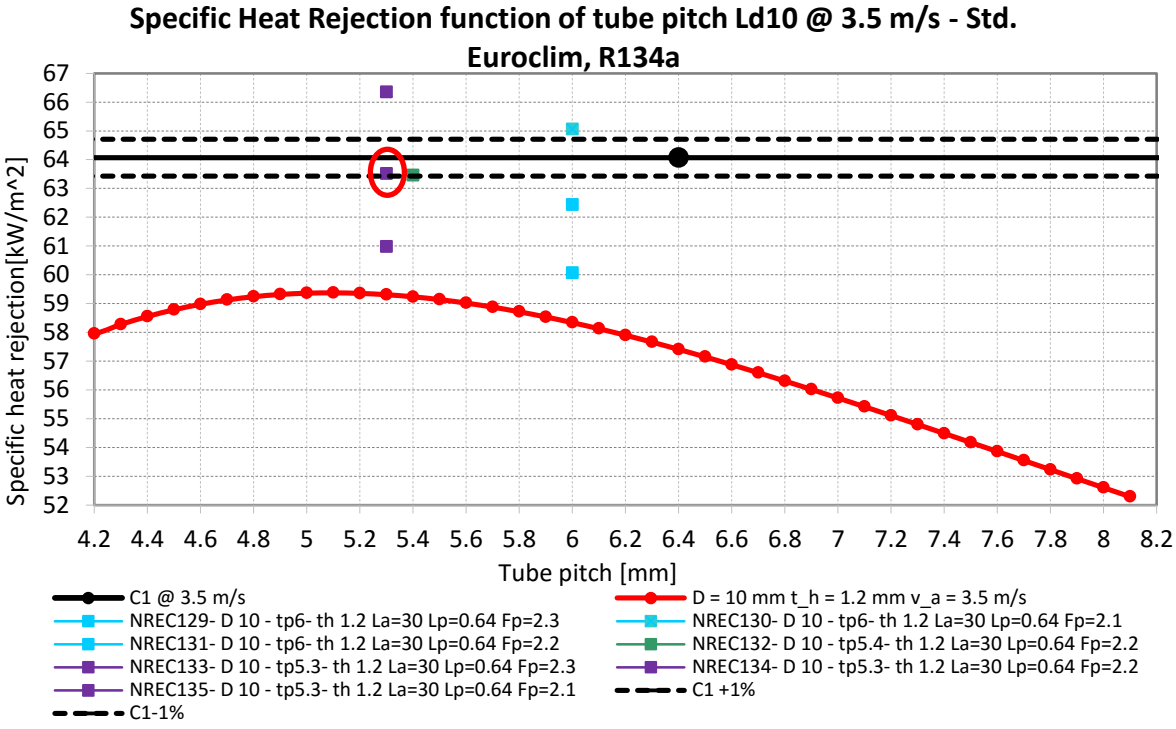

Figure 92-Selected optimization-Condensers

From this graph is possible to observe that the two optimizations, that can be considered are:

1) Optimization with $Tp = 5.3mm$ and Fp=2.2 (NR134) which is the optimum that maximize the heat rejection for $Th = 1.2mm$.

2) Optimization with $Tp = 6mm$ with Fp=2.1 (NR130) that is easier to obtain with current process technology.

The percentage difference between the NR134 and C1 heat rejection is about 1%, and due to the small difference can be consider as a good result of optimization.

Finally the selected optimized condenser is the NREC134 (second optimization) which has the following characteristics:

- Core depth ➔ $Ld = 10mm.$
- Tube pitch ➔ $Tp = 5.3mm.$
- Tube height ➔ $Th = 1.2mm.$
- Louver pitch ➔ $Lp = 0.64mm.$
- Louver angle ➔ $La = 30^{\circ}.$
- Fin pitch ➔ $Fp = 2.2mm.$

3.2. RADIATORS

3.2.1. Comparison between the application range of correlations and experimental data.

As performed for the condenser geometries, it is necessary to verify if the Radiator fins geometries under analysis are in agreement with the application range of each correlation.

In the tables from 51 to 57, are reported, for each correlation, a complete list of geometric parameters with their descriptions and the agreement between the correlation range and the analyzed radiators range.

Correlation 1

Authors: Chang and Wang [1997]

Sym	Description	min	max	R1	R2	R3	R4	R5
L_p	Louver pitch [mm]	**0.5**	**3**	✓	✓	✓	✓	✓
L_h	Louver height [mm]	**0.94**	**18.5**	✓	✓	✓	✓	✓
L_a	Louver angle [°]	**8.43**	**35**	✓	✓	✓	✓	✓
F_p	Fin pitch [mm]	**0.51**	**3.33**	✓	✓	✓	✓	✓
L_d	Core depth [mm]	**15.6**	**50**	✓	✓	X	X	X
F_h	Fin height [mm]	**6**	**20**	X	X	✓	✓	X
b	Fin thickness [mm]	**0.04**	**0.16**	✓	✓	✓	✓	✓
T_p	Tube pitch [mm]	**7.51**	**25**	X	X	✓	✓	X
D_h	Hydraulic Diameter[mm]	**0.824**	**4.94**	✓	✓	✓	✓	✓

Table 51-Correlation 1 parametrical range-Radiators

Correlation 2

Authors:Park and Jacobi [2009a]

Sym	Description	min	max	R1	R2	R3	R4	R5
L_p	Louver pitch [mm]	**0.5**	**3**	✓	✓	✓	✓	✓
L_h	Louver height [mm]	**0.94**	**18.5**	✓	✓	✓	✓	✓
L_a	Louver angle [°]	**8.43**	**35**	✓	✓	✓	✓	✓
F_p	Fin pitch [mm]	**0.51**	**5.08**	✓	✓	✓	✓	✓
L_d	Core depth [mm]	**15.6**	**57.4**	✓	✓	X	X	✓
F_h	Fin height [mm]	**2.84**	**20**	✓	✓	✓	✓	✓
b	Fin thickness [mm]	**0.0254**	**0.16**	✓	✓	✓	✓	✓
T_p	Tube pitch [mm]	**3.76**	**25**	✓	✓	✓	✓	✓

Table 52-Correlation 2 parametrical range pt1 -Radiators

Sym	Correlation 2 - Inclusive range of heat exchangers parameters.						
	min	max	R1	R2	R3	R4	R5
Fp/Lp	**0.45**	**4.44**	✓	✓	✓	✓	✓
Fh/Lp	**2.6**	**16**	✓	✓	✓	✓	✓
Lh/Fh	**0.63**	**0.96**	✓	✓	✓	✓	✓
La	**8.4**	**35.9**	✓	✓	✓	✓	✓
Ld/Fp	**5**	**40**	✓	✓	✓	✓	✓
Tp/Fh	**1.12**	**1.37**	✓	✓	✓	✓	✓
b/Lp	**0.025**	**0.155**	✓	✓	✓	✓	✓
NLB	**1**	**4**	✓	✓	✓	✓	✓

Table 53-Correlation 2 parametrical range pt2-Radiators

Correlation 3

Authors: Park and Jacobi [2009b]

Sym	Description	min	max	R1	R2	R3	R4	R5
L_p	Louver pitch [mm]	**0.95**	**2.66**	X	X	X	X	X
L_h	Louver height [mm]	**6.15**	**11.15**	X	X	X	X	X
L_a	Louver angle [°]	**15**	**42**	✓	✓	✓	✓	✓
F_p	Fin pitch [mm]	**1.0**	**5.08**	✓	✓	✓	✓	✓
L_d	Core depth [mm]	**15.6**	**57.4**	✓	✓	X	X	✓
F_h	Fin height [mm]	**7.93**	**12.43**	X	X	X	X	X
b	Fin thickness [mm]	**0.08**	**0.15**	X	X	X	X	X

T_p	Tube pitch [mm]	**9.7**	**15.7**	X	X	X	X	X

Table 54-Correlation 3 parametrical range-Radiators

Correlation 4

Authors: A.Vaisi, M.Esmaeilpour, H.Taherian

The present correlation is a theoretical model that has been developed for only one type of heat exchanger.

Correlation 5

Authors: Junqi.D,Jiangping Chen, Zhijiu Chen,Wenfeng Zhang, Yimin Zhou [2007]

Sym	Description	min	max	R1	R2	R3	R4	R5
L_a	Louver angle [°]	**22**	**28**	✓	✓	✓	✓	✓
F_p	Fin pitch [mm]	**2.0**	**2.75**	✓	✓	✓	✓	✓
L_d	Core depth [mm]	**36.6**	**65.0**	X	X	X	X	X
F_h	Fin height [mm]	**7.0**	**10.0**	X	X	X	X	X
b	Fin thickness [mm]	**0.15**	**0.2**	X	X	X	X	X

Table 55-Correlation 5 parametrical range-Radiators

Correlation 6

Authors: Kijung Ryu, Kwan-Soo Lee [2015]

This correlation describes the heat transfer characteristics of the entire area of the louvered fin rather than a specific area. The correlation is dimensionless and suitable for a general fin.

The fin parameters field is $\frac{Fp}{Lp} > 1 \; and \; \frac{Fp}{Lp} < 1.$

Correlation 7

Authors: Davenport [1983b]

Sym	Description	min	max	R1	R2	R3	R4	R5
L_p	Louver pitch [mm]	**1.5**	**3.0**	X	X	X	X	X

L_a	Louver angle [°]	**8**	**36**	✓	✓	✓	✓	✓
F_p	Fin pitch [mm]	**1.0**	**1.6**	X	X	X	X	X
$\frac{L_p}{F_p}$	Louver pitch/Fin pitch	**0.94**	**2.24**	X	X	X	X	X

Table 56-Correlation 7 parametrical range - Radiators

Correlation 8

Authors: Nae-Hyun Kim & Jin-Pyo Cho [2007]

Sym	Description	min	max	R1	R2	R3	R4	R5
L_a	Louver angle [°]	**15**	**27**	✓	✓	X	X	✓
F_p	Fin pitch [mm]	**1.0**	**1.4**	X	X	X	X	X

Table 57-Correlation 8 parametrical range-Radiators

3.2.2. Choise of the reference correlation.

The aim of this paragraph is to identify the correlation that better approximates the heat experimental transfer coefficient.

The Colburn factor, plotted as a function of the Reynolds number in the following figures, is analyzed for the five types of Radiator fins.

The calculated uncertainties of the heat transfer coefficient by HEX (shown in the chapter 2) has been plotted in order to consider the band of uncertainty.

Therefore in the following figures from 93 to 97 are plotted the comparison between the correlations and experimental tests for each Radiator fin. All the correlation are evaluated considering constant air properties, at a mean temperature of 40 °C. The air velocity, considered for the Reynolds numbers calculation, is the inlet air velocity.

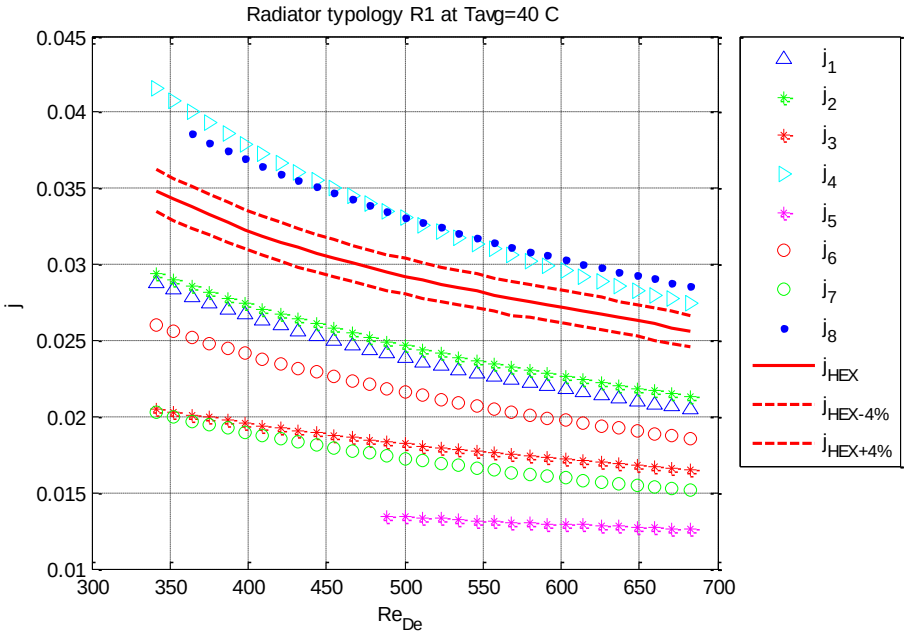

Figure 93 - Comparison between correlations and experimental test –R1

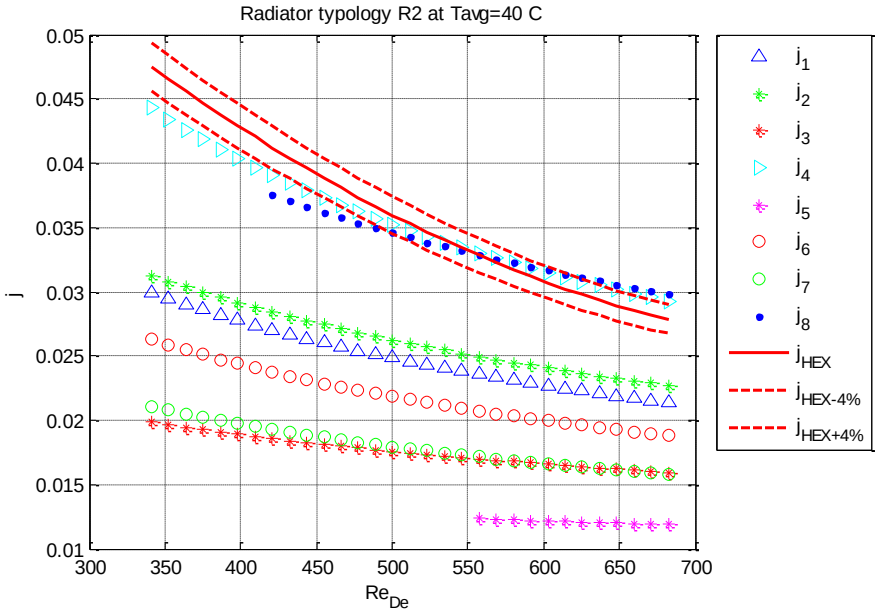

Figure 94 - Comparison between correlations and experimental test –R2

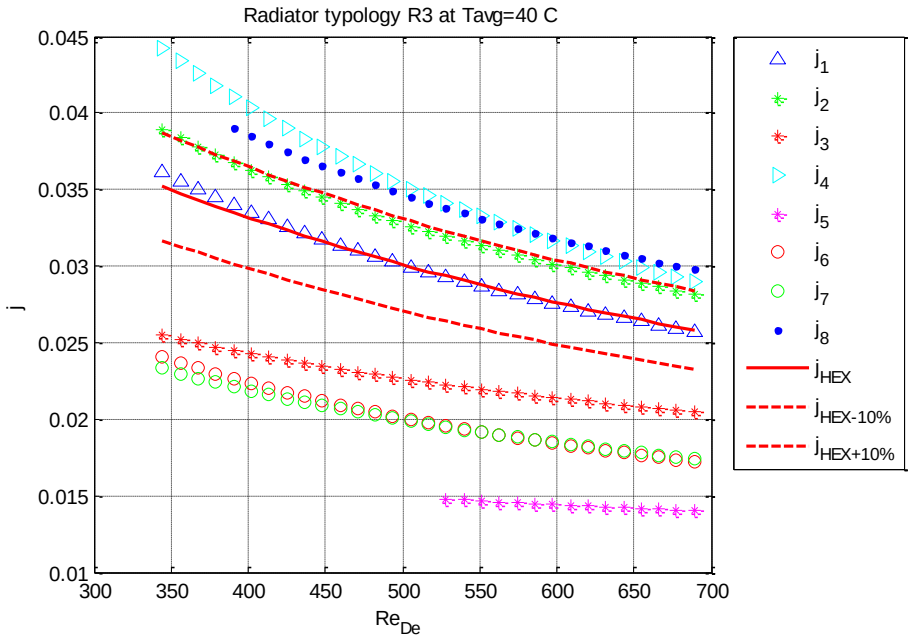

Figure 95 - Comparison between correlations and experimental test –R3

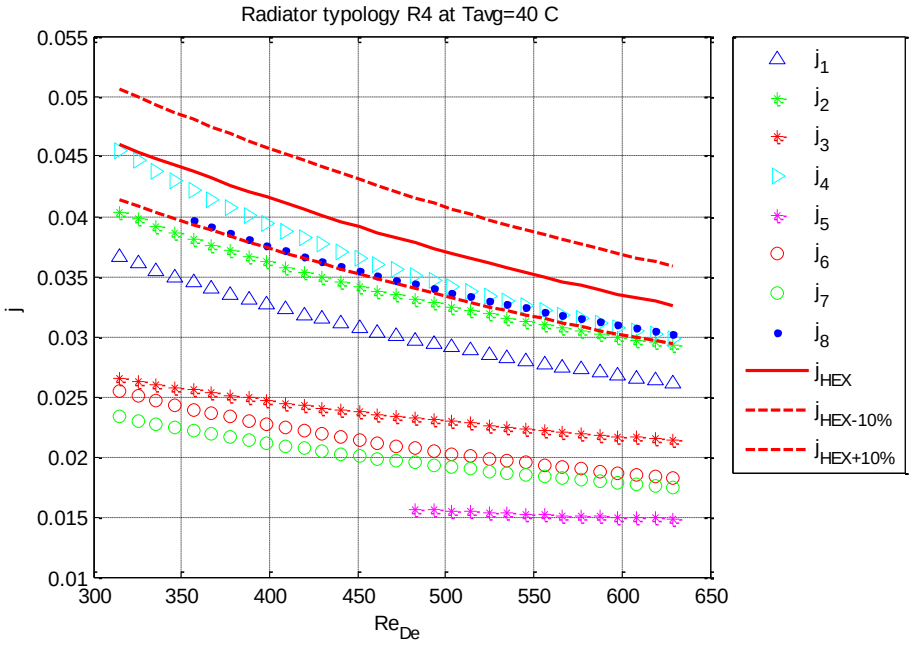

Figure 96 - Comparison between correlations and experimental test –R4

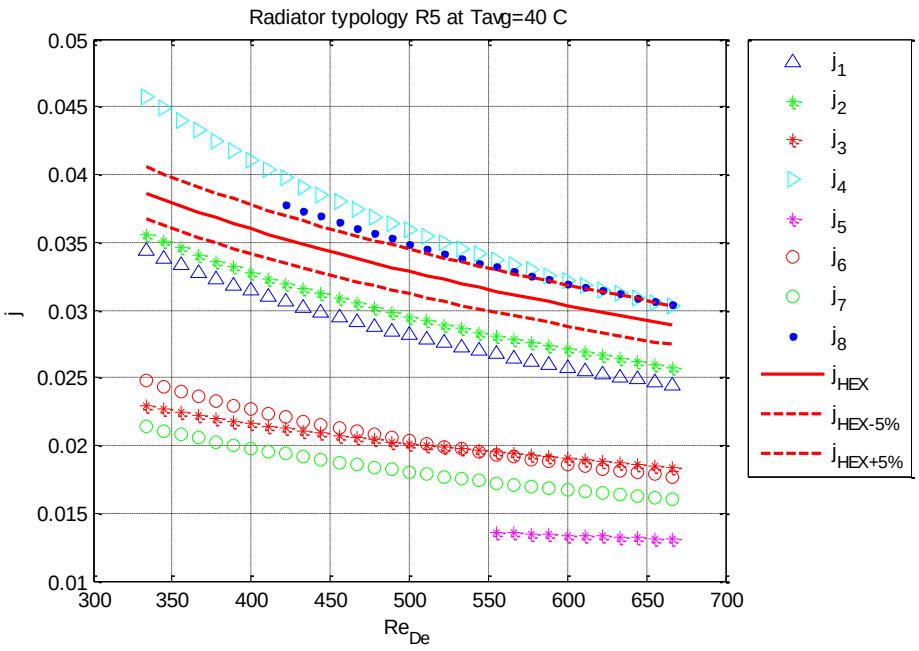

Figure 97 - Comparison between correlations and experimental test –R5

It can be observed that, the correlations that approximate more accurately to the experimental data are the correlations 1, 2, 4 and 8.

- The correlation 8 may not be considered because the parametric analysis shows that the equations have not dependence on the fin height, louver height and core depth parameters.
- The correlation 2 may not be considered due to the periodical behavior with the louver pitch and louver angle variation.
- The correlation 4 that presents a theoretical approach, may not be considered because with the fin height variation and core depth variation presents a behavior not clearly understood, therefore does not provide a suitable performance.

Hence the correlation 1 has been considered for the Radiator analysis, which presents a slope slightly similar to the experimental test curves.

In the following summary table 58 is reported for each fin some comparative characteristics of the experimental test curves respect of correlation 1.

Fin	Inside all the Reynolds the range	Intersection between [3 and 6 m/s]	% Difference at 3 m/s	% Difference at 4 m/s	% Difference at 5 m/s	% Difference at 6m/s
R1	***YES***	/	-17.44%	-17.75%	-19.38%	-20.00%
R2	***YES***	/	-36.82%	-32.93%	-27.59%	-23.34%
R3	***YES***	/	2.69%	0.33%	-0.30%	-0.42%
R4	***YES***	/	-20.19%	-21.52%	-20.93%	-19.94%
R5	***YES***	/	-11.08	-13.44	-14.80	-15.30

Table 58 - Summary / Comparative Chart – Radiator Fins

In the following figures, are shown the percentage differences between the selected correlation and the experimental data as a function of the Reynolds number.

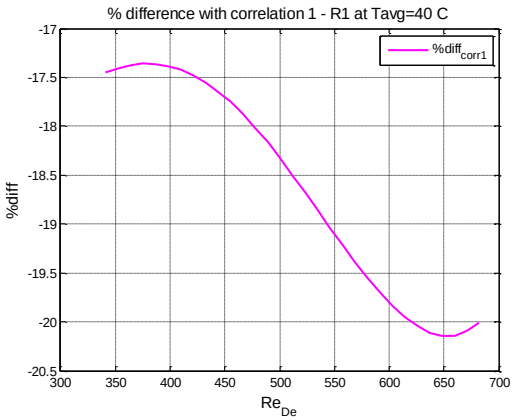

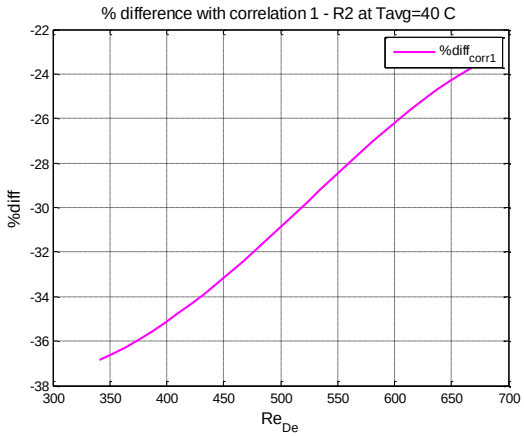

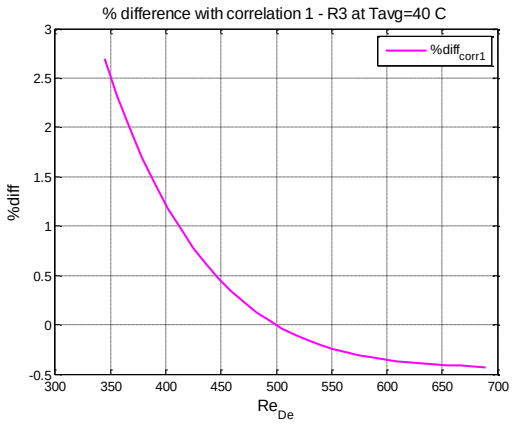

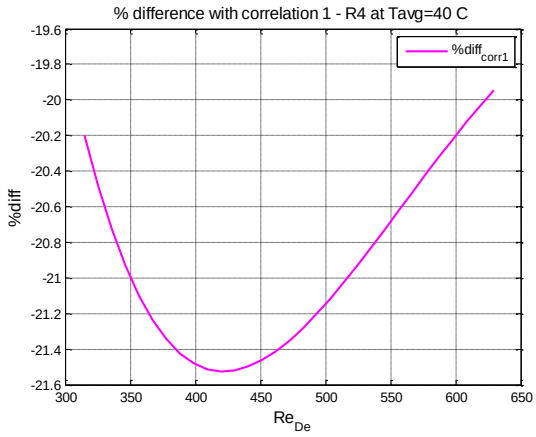

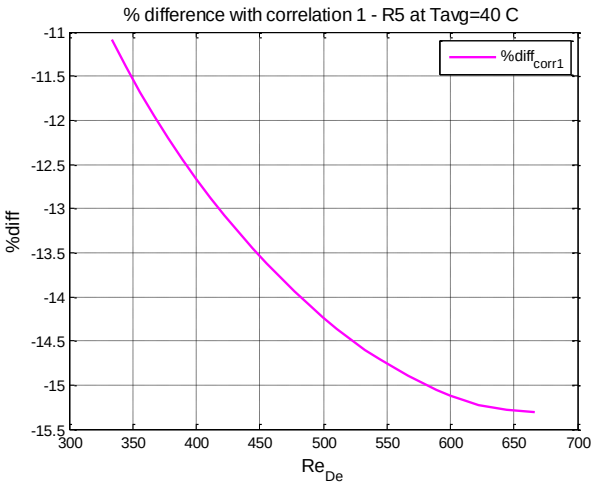

Figure 98-%Differences of the experimental tests with correlation 1.

It can be noticed from the graphs that the radiator geometry which has the lower percentage differences is the R3 .

3.2.3. Dependence of the chosen correlation from the geometrical and physical parameters.

The correlation chosen for the Radiators study is the same as the Condensers and this analysis has been already done in the previous Condensers section.

3.2.4. Function study

As shown before for the Condensers, the correlation 1 predicts the value of air heat transfer coefficient with higher values with decreasing the core depth and increasing the value of Fin height.

3.2.5. Optimization

The optimization in the case of Radiators has been performed inside the actual core depth range, with varying the tube heights and the tube pitches, trying to reach at least the same thermal load or higher than the existing geometries.

Thus a number of 24 new Radiator geometries have been considered, with two different tube pitches with three core depths (12.5, 16, 22), and varying the tube heights (1.2 to 1.8).

- With $\boldsymbol{Tp = 6.4\ mm}$

		$Ld\ [mm]$		
		12.5	**16**	**22**
$Th\ [mm]$	**1.2**	NR19	NR21	NR23
	1.4	NR4	NR10	NR16
	1.6	NR5	NR11	NR17
	1.8	NR6	NR12	NR18

Table 59- Radiator configurations with Tp=6.4

- With $\boldsymbol{Tp = 7.8mm}$

		$Ld\ [mm]$		
		12.5	**16**	**22**
$Th\ [mm]$	**1.2**	NR20	NR22	NR24
	1.4	NR1	NR7	NR13
	1.6	NR2	NR8	NR14
	1.8	NR3	NR9	NR15

Table 60- Radiator configurations with Tp=7.8

The fin height and the louver height vary as consequence.

$$Fh = Tp - Th$$

$$Lh = Fh - 1$$

The other fin parameters have been considered constants.

The values of Colburn factor j were calculated in the velocity range 3 to 6 m/s. The HEX software requires in input both the colburn factor and the air friction factor values, which have been calculated with the following equation:

$$f = 4.\frac{\Delta P D_h 2}{Ld.\, v_a^2 \rho.\, 4}$$

The air pressure drops are calculated by a simulation program in which are required all the radiator dimensions, the air velocities, among others.

Finally once all the j and f factors are calculated, can be inserted in the HEX software including the geometrical parameters, the hydraulic Reynolds numbers and a coolant mass flow rate defined in all the cases equal to 6000 l/h.

Then the HEX is able to simulate a test, that allows to obtain the performance parameters of the new radiator.

The thermal loads as a function of the air velocity have been plotted in the following figures from 99 to 101, for each investigated core depth. Each curve represents a specific tube height and a specific tube pitch.

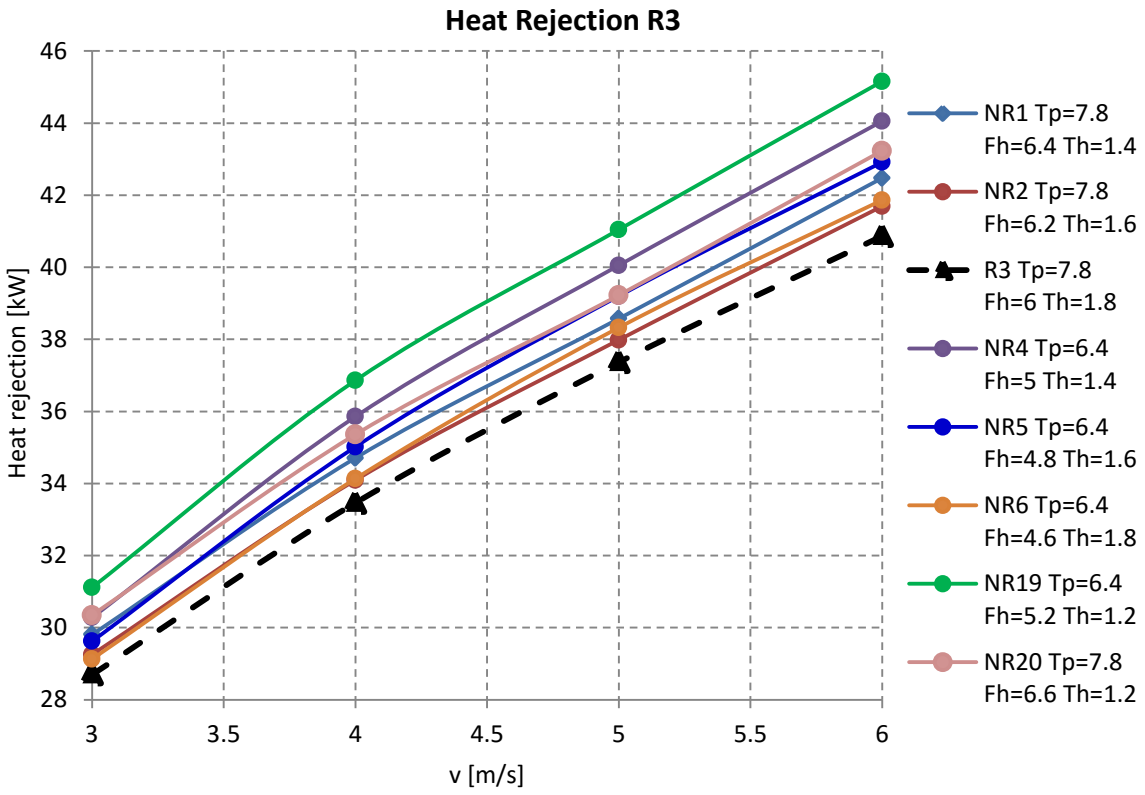

Figure 99- Heat rejection R3 Ld=12.5

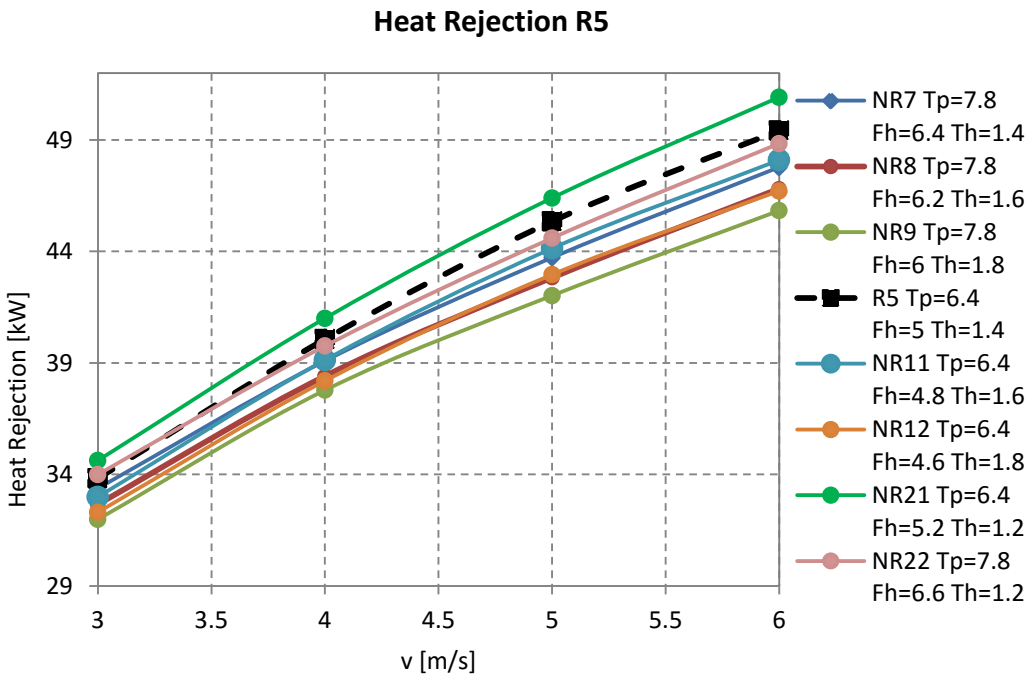

Figure 100- Heat rejection R5 Ld=16.

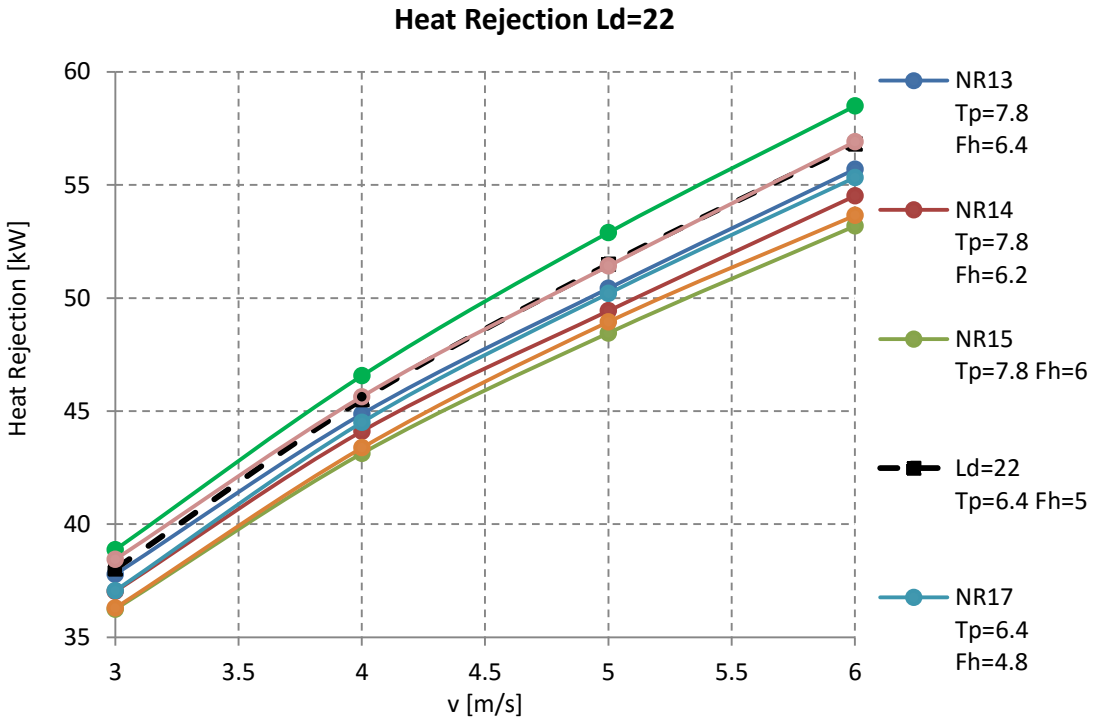

Figure 101- Heat rejection Ld=22.

From the previous graphs can be noticed that:

- The higher thermal loads are obtained with lower tube heights and lower fin heights.
- Therefore it is possible to conclude that in the thermal load calculations, because the coolant does not presents a phase change, as in the case of Condensers, the coolant physical properties remain approximately constant therefore there is not impact on the heat transfer, on the other hand the condensers obtain the optimum points with highest thermal loads with specific combinations between tube height and tube pitch.

Thus is necessary to consider the analysis with other performance parameters, one of them is the Qv (In vehicle performance index) which is a parameter that consider the effect of the air pressure drop on the thermal load.

$$Qv = \frac{Q[kW]}{\Delta P_{air}^{0.2}[Pa]}$$

The following graphs show for each core depth typology the Qv in each air velocity value.

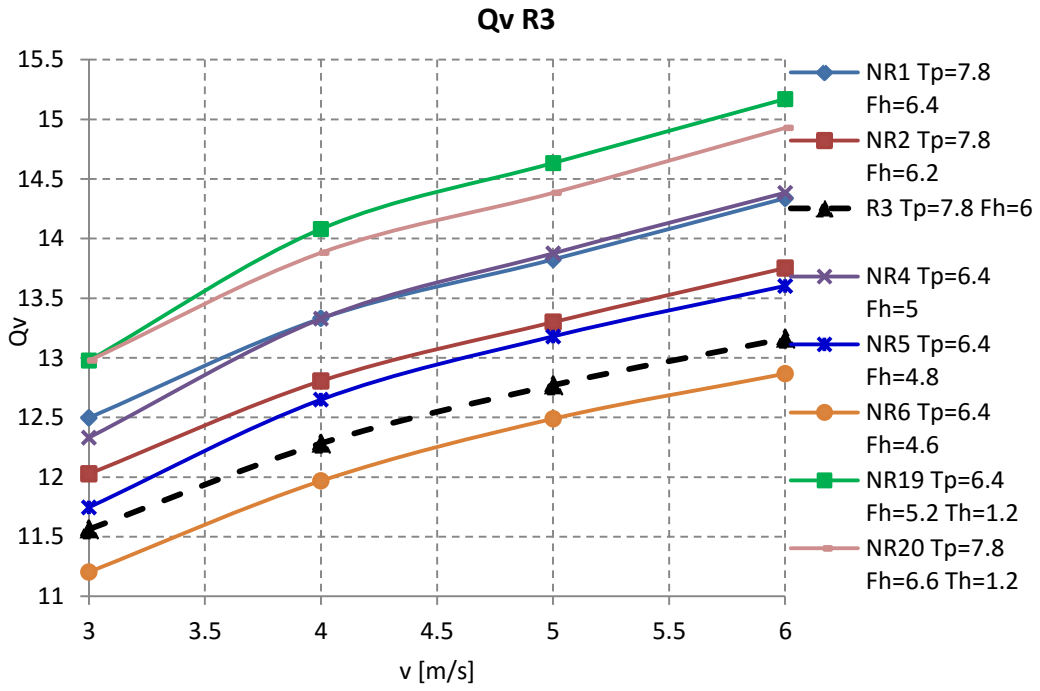

Figure 102- Qv of R3 Ld=12.5

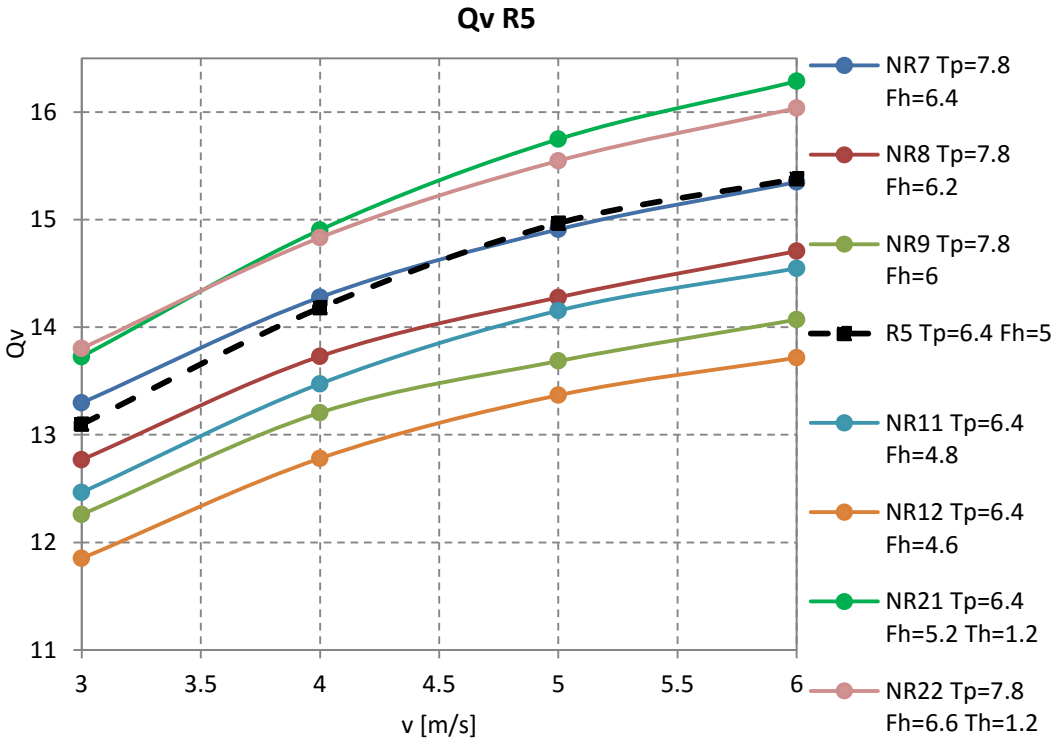

Figure 103- Qv of R5 Ld=16.

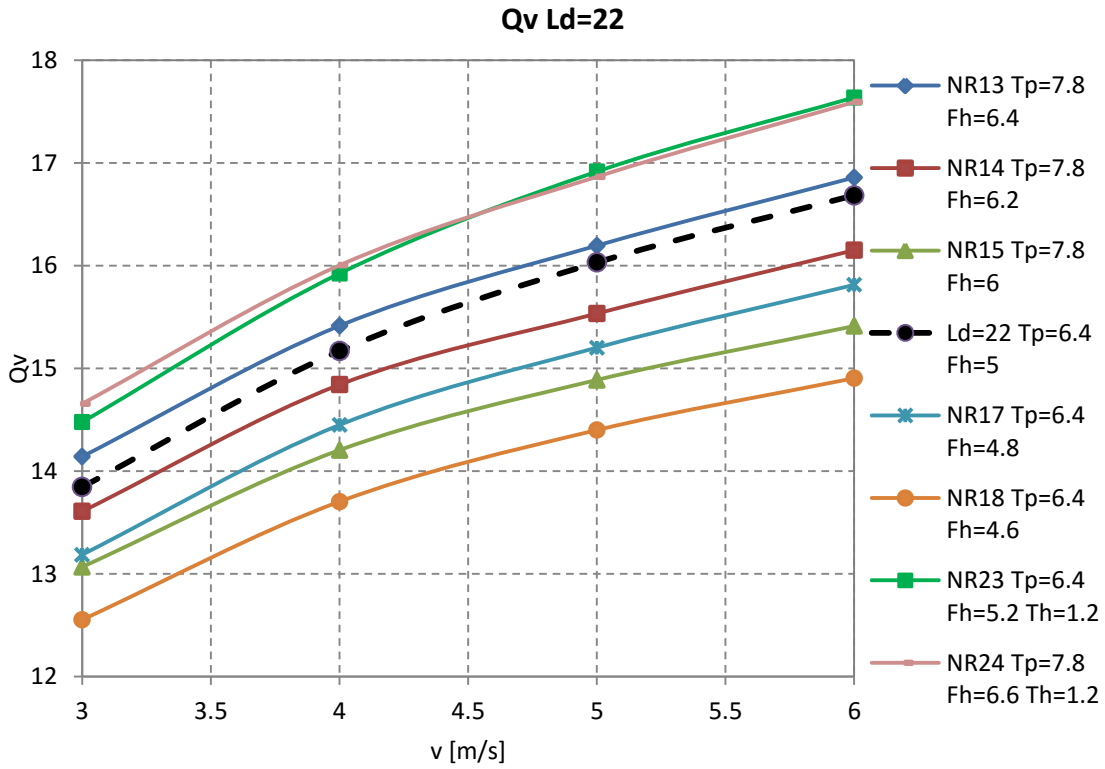

Figure 104- Qv of Ld=22

From the previous figures can be observed that the effects of the air pressure drops are evident, it is noticed that with higher fin height values the air pressure drops are smaller, therefore with higher Qv, and the influence of a lower tube height is still having better performances also with the Qv.

In addition to all the previous analysis, is necessary to add the influence that has the coolant pressure drops in choosing the better Radiator typology, thus the coolant pressure drops have been calculated only for the $Ld = 12.5\ mm$ core depth typology. The figure 105 shows the coolant pressure drops in percentage differences respect of the original N12.5, for each of the new radiator typologies of core depth 12.5.

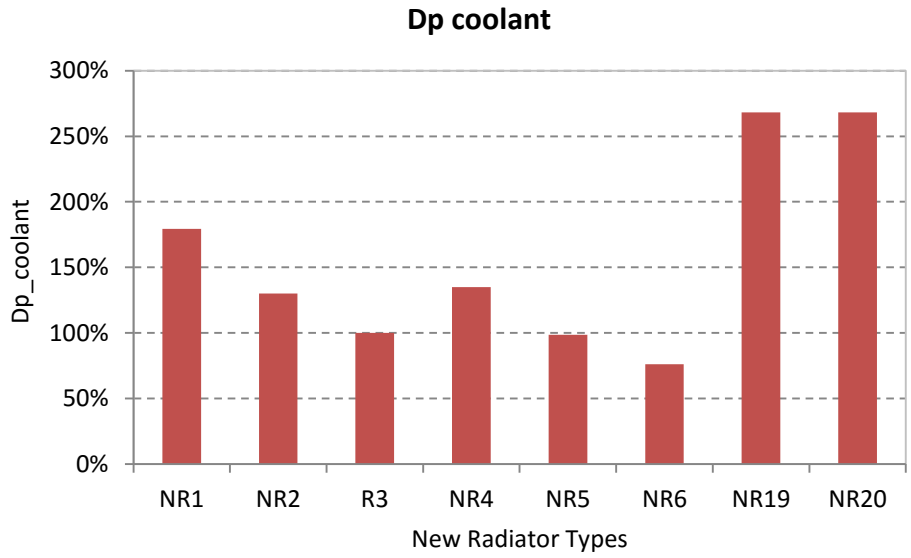

Figure 105- Coolant pressure drop for all the new radiators

The NR6 radiator presents the lowest coolant pressure drop respect of the N12, the NR6 has a fin height of Fh=4.6mm, and a Tube height 1.8 mm, therefore a low value of tube pitch of 6.4, on the other hand the highest coolant $\triangle p$ are the NR19 and NR20 having the smallest tube height values of 1.2 mm that consequently render the highest pressure drops.

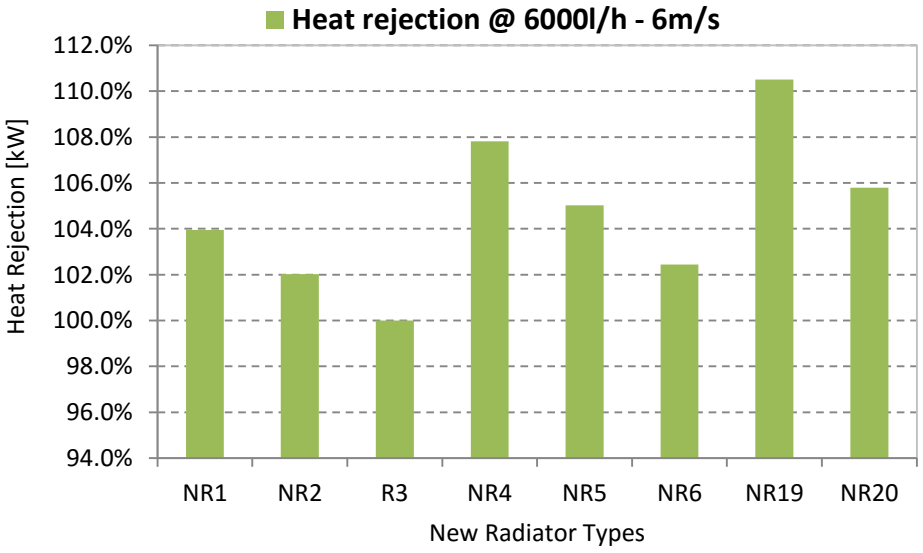

Figure 106- Heat rejection for all the new radiators

The heat rejections respect of the N12 have been plotted in the figure 106 above, and as was expected the highest heat rejection has the NR19 typology with the lowest tube height value and tube pitch 6.4mm like have been observed before. In fact from the figure can be noticed that all the new radiators have higher thermal loads.

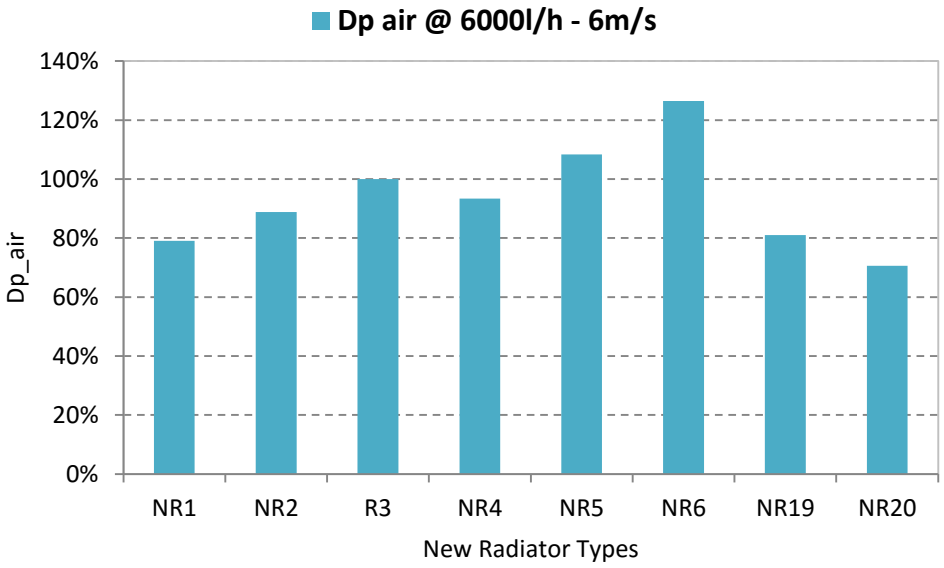

Figure 107- Air pressure drop for all the new radiators

The air pressure drops have been plotted in the figure 107 above, the NR6 typology has the highest value due to the lowest fin height respect to the others(the fin height is the minimal respect to others). The influence of air pressure drop is mostly due to the dimension of the fin height.

The following figure 108 represents all the three performance parameter that has been considered to the selection of an optimized radiator.

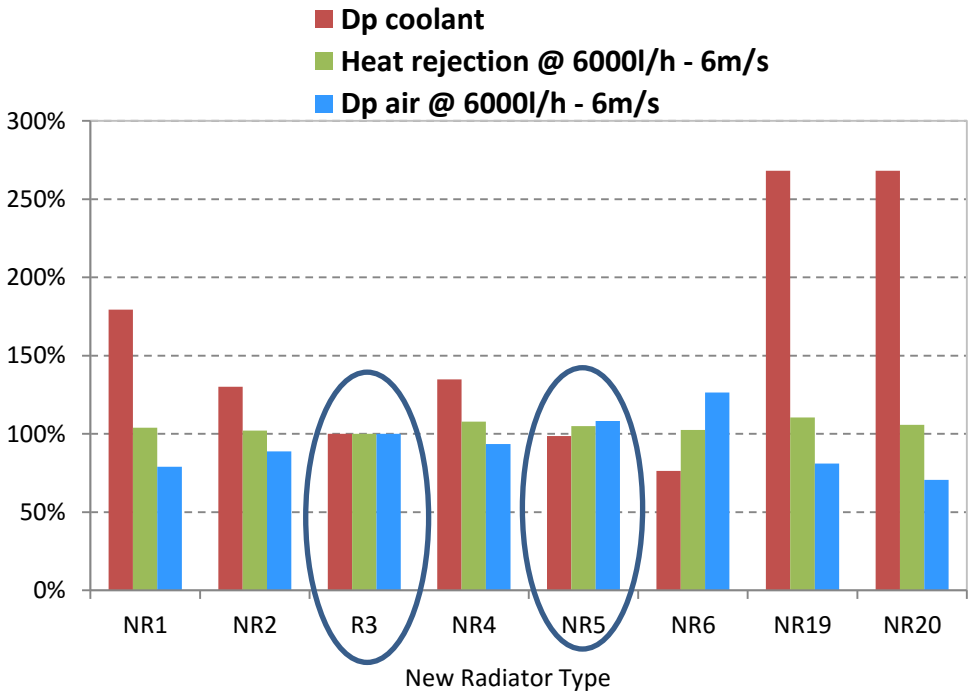

Figure 108- Performance parameters for each new radiator.

From the figure 108 can be observed that the optimum radiators still being the actual radiator R3 and the NR5, because even if the heat rejection as seen previously is not the best respect to the other new radiator types, the effects due to the coolant pressure drop and air pressure drop compensate the fact of a better performance.

An additional figure has been plotted, in order to observe the compensation between the Qv parameter and the coolant pressure drop.

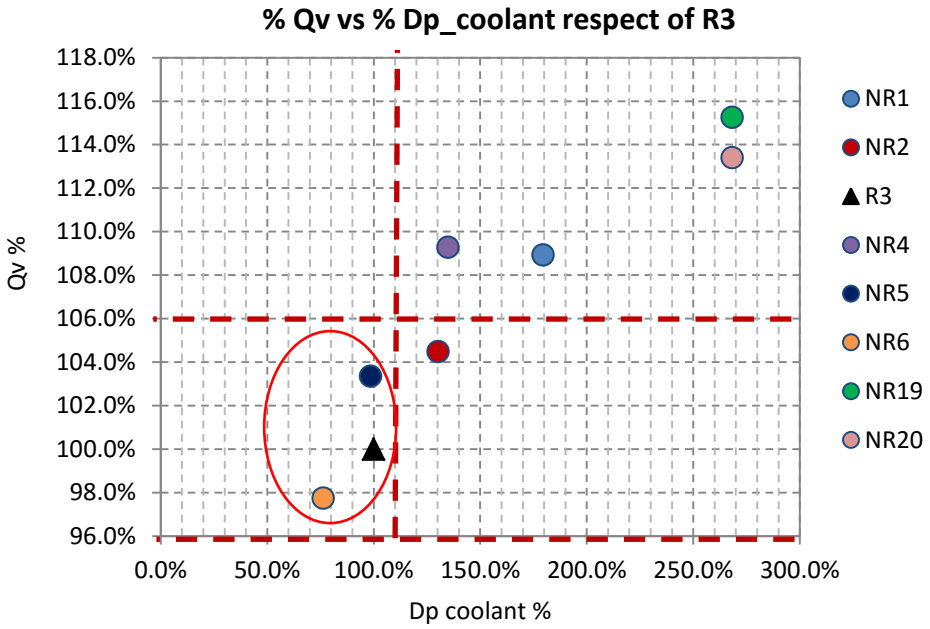

Figure 109- %Qv versus %Dp coolant for all new radiators

From this figure 109 can be observed that considering a +10% of coolant pressure drop respect of the R3 (reference radiator), and a +6% of Qv, the additional radiator that is inside these limits is the NR6. Hence, the radiators that are optimized respect of the R3 (reference radiator) are the following:

- The NR5.
- The NR6.
- The actual radiator R3.

At this point is possible to conclude that further analysis may be realized to select depending on the requested radiator conditions, it is possible to do an economic analysis, and consider the weight reduction as a consequence.

4. Results and Conclusions

The results obtained are the following:

- The correlation 1 has been selected for the Condensers and Radiators study.
- The function study for the Radiators. Main subjects:

  1. The heat rejection increase with lower tube dimensions.
  2. The vehicle performance index which takes into account the air pressure drop, increase with lower tube heights and lower fin heights.
  3. The coolant pressure drop increase with lower tube heights.

  Therefore, the possible optimizations are the Radiators NR5, NR6, and the reference R3, and further optimization steps can be performed, such as cost analysis.

- The function study for the Condensers: Main subjects:

  1. The general study noticed that the tube pitch that optimizes the heat transfer decrease with the tube height decreasing.
  2. The tube pitch does not depend on the core depth, nor the air velocity.
  3. From the general study, selecting the core depth 10mm and the tube height $1.2mm$, have been considered the following optimizations:

     1) Optimization with $Tp = 5.3mm$ with Fp=2.2mm, that obtains higher performances for the $Th = 1.2mm$.

     2) Optimization with $Tp = 6mm$ that reaches the C1(reference) performances with a fin pitch tighter ($2.1mm$ instead of $2.2mm$), it is easier to obtain with the current process technology.

- The results obtained with Radiators and Condensers are quite different, due to the fact that the Condenser presents a two-phase flow, the pressure drops induce the change of the fluid properties and affect directly the heat transfer, instead the impact of coolant pressure drop in a single phase flow that is the case on Radiators, is not considerable.

APPENDIX

The trend line calculations for each tube pitch for the three different core depths and the two velocities, and calculation of the respective maximum values of specific heat rejection at an optimum tube pitch.

1) Tube height ➔ Th=1.0mm

Th=1mm; Ld=10mm; v=3.5m/s		Th=1mm; Ld=10mm; v=5m/s		Th=1mm; Ld=11.5mm; v=3.5m/s		Th=1mm; Ld=11.5mm; v=5m/s		Th=1mm; Ld=16mm; v=3.5m/s		Th=1mm; LD=16mm; v=5m/s	
Tp [mm]	Tp with LdT	Tp [mm]	Tp with LdT	Tp [mm]	Tp with LdT	Tp [mm]	Tp with LdT	Tp [mm]	Tp with LdT	Tp [mm]	Tp with LdT
4	59.292	**4**	67.940	**4**	66.570	**4**	76.416	**4**	86.819	**4**	99.876
4.2	59.806	**4.2**	68.375	**4.2**	66.927	**4.2**	76.995	**4.2**	87.367	**4.2**	100.462
4.3	59.965	**4.3**	68.472	**4.3**	67.053	**4.3**	77.145	**4.3**	87.570	**4.3**	100.638
4.4	60.068	**4.4**	68.499	**4.4**	67.147	**4.4**	77.214	**4.4**	87.727	**4.4**	100.743
4.5	60.119	**4.5**	68.464	**4.5**	67.208	**4.5**	77.211	**4.5**	87.842	**4.5**	100.783
4.6	60.123	**4.6**	68.374	**4.6**	67.237	**4.6**	77.144	**4.6**	87.915	**4.6**	100.762
4.7	60.085	**4.7**	68.234	**4.7**	67.236	**4.7**	77.021	**4.7**	87.950	**4.7**	100.685
4.8	60.009	**4.8**	68.050	**4.8**	67.205	**4.8**	76.847	**4.8**	87.947	**4.8**	100.556
4.9	59.900	**4.9**	67.829	**4.9**	67.145	**4.9**	76.630	**4.9**	87.909	**4.9**	100.379
5	59.760	**5**	67.573	**5**	67.058	**5**	76.374	**5**	87.837	**5**	100.158
5.1	59.593	**5.1**	67.289	**5.1**	66.944	**5.1**	76.085	**5.1**	87.732	**5.1**	99.896
5.2	59.402	**5.2**	66.979	**5.2**	66.805	**5.2**	75.767	**5.2**	87.597	**5.2**	99.595
5.3	59.190	**5.3**	66.647	**5.3**	66.641	**5.3**	75.423	**5.3**	87.432	**5.3**	99.260
5.4	58.959	**5.4**	66.297	**5.4**	66.453	**5.4**	75.058	**5.4**	87.238	**5.4**	98.892
5.5	58.711	**5.5**	65.930	**5.5**	66.243	**5.5**	74.674	**5.5**	87.018	**5.5**	98.495
5.6	58.448	**5.6**	65.549	**5.6**	66.012	**5.6**	74.275	**5.6**	86.773	**5.6**	98.071
5.7	58.171	**5.7**	65.156	**5.7**	65.760	**5.7**	73.862	**5.7**	86.502	**5.7**	97.621
5.8	57.883	**5.8**	64.753	**5.8**	65.490	**5.8**	73.437	**5.8**	86.208	**5.8**	97.147
5.9	57.585	**5.9**	64.342	**5.9**	65.202	**5.9**	73.002	**5.9**	85.892	**5.9**	96.653
6	57.277	**6**	63.923	**6**	64.897	**6**	72.559	**6**	85.555	**6**	96.138
6.1	56.960	**6.1**	63.498	**6.1**	64.576	**6.1**	72.108	**6.1**	85.198	**6.1**	95.606
6.2	56.636	**6.2**	63.066	**6.2**	64.241	**6.2**	71.650	**6.2**	84.821	**6.2**	95.056
6.3	56.305	**6.3**	62.630	**6.3**	63.892	**6.3**	71.186	**6.3**	84.426	**6.3**	94.491
6.4	55.968	**6.4**	62.190	**6.4**	63.532	**6.4**	70.717	**6.4**	84.014	**6.4**	93.912
6.5	55.624	**6.5**	61.745	**6.5**	63.160	**6.5**	70.242	**6.5**	83.586	**6.5**	93.320
6.6	55.276	**6.6**	61.297	**6.6**	62.779	**6.6**	69.762	**6.6**	83.143	**6.6**	92.717

	6.7	54.922	**6.7**	60.844	**6.7**	62.388	**6.7**	69.277	**6.7**	82.686	**6.7**	92.102
	6.8	54.563	**6.8**	60.389	**6.8**	61.990	**6.8**	68.787	**6.8**	82.215	**6.8**	91.478
	6.9	54.200	**6.9**	59.929	**6.9**	61.585	**6.9**	68.291	**6.9**	81.733	**6.9**	90.844
	7	53.832	**7**	59.467	**7**	61.174	**7**	67.791	**7**	81.239	**7**	90.204
	7.1	53.460	**7.1**	59.001	**7.1**	60.759	**7.1**	67.286	**7.1**	80.735	**7.1**	89.556
	7.2	53.085	**7.2**	58.533	**7.2**	60.341	**7.2**	66.776	**7.2**	80.222	**7.2**	88.903
	7.3	52.706	**7.3**	58.062	**7.3**	59.920	**7.3**	66.262	**7.3**	79.701	**7.3**	88.245
	7.4	52.323	**7.4**	57.588	**7.4**	59.497	**7.4**	65.743	**7.4**	79.174	**7.4**	87.583
	7.5	51.939	**7.5**	57.113	**7.5**	59.074	**7.5**	65.219	**7.5**	78.642	**7.5**	86.919
	7.6	51.552	**7.6**	56.636	**7.6**	58.651	**7.6**	64.693	**7.6**	78.105	**7.6**	86.254
	7.7	51.163	**7.7**	56.159	**7.7**	58.229	**7.7**	64.163	**7.7**	77.566	**7.7**	85.589
	7.8	50.773	**7.8**	55.683	**7.8**	57.810	**7.8**	63.632	**7.8**	77.025	**7.8**	84.925
	7.9	50.384	**7.9**	55.208	**7.9**	57.393	**7.9**	63.100	**7.9**	76.484	**7.9**	84.264
	8	49.995	**8**	54.737	**8**	56.980	**8**	62.568	**8**	75.946	**8**	83.608
	8.1	49.609	**8.1**	54.270	**8.1**	56.572	**8.1**	62.040	**8.1**	75.410	**8.1**	82.958
	8.2	49.226	**8.2**	53.811	**8.2**	56.168	**8.2**	61.516	**8.2**	74.879	**8.2**	82.316
MAX	4.6	60.12266415	4.4	68.499	4.7	67.237	4.5	77.214	4.8	87.950	4.5	100.783
Scelto	4.7	60.08479182	4.7	68.234	4.7	67.236	4.7	77.021	4.7	87.950	4.7	100.685
Diff. Max - scelto		0.063%		0.389%		0.002%		0.251%		0.000%		0.097%

2) Tube height ➔ Th=1.2mm

Th=1.2mm; Ld=10mm; v=3.5m/s		Th=1.2mm; Ld=10mm; v=5m/s		Th=1.2mm; Ld=11.5mm; v=3.5m/s		Th=1.2mm; Ld=11.5mm; v=5m/s		Th=1.2mm; Ld=16mm; v=3.5m/s		Th=1.2mm; Ld=16mm; v=5m/s	
Tp [mm]	Tp with LdT	Tp [mm]	Tp with LdT	Tp [mm]	Tp with LdT	Tp [mm]	Tp with LdT	Tp [mm]	Tp with LdT	Tp [mm]	Tp with LdT
4.2	57.578	**4.2**	66.639	**4.2**	64.284	**4.2**	74.493	**4.2**	83.719	**4.2**	97.003
4.3	57.950	**4.3**	66.992	**4.3**	64.722	**4.3**	74.873	**4.3**	84.372	**4.3**	97.609
4.4	58.273	**4.4**	67.284	**4.4**	65.107	**4.4**	75.201	**4.4**	84.948	**4.4**	98.136
4.5	58.550	**4.5**	67.519	**4.5**	65.442	**4.5**	75.476	**4.5**	85.449	**4.5**	98.585
4.6	58.783	**4.6**	67.700	**4.6**	65.728	**4.6**	75.702	**4.6**	85.881	**4.6**	98.962
4.7	58.974	**4.7**	67.831	**4.7**	65.968	**4.7**	75.879	**4.7**	86.246	**4.7**	99.269
4.8	59.125	**4.8**	67.916	**4.8**	66.164	**4.8**	76.011	**4.8**	86.549	**4.8**	99.509
4.9	59.238	**4.9**	67.956	**4.9**	66.319	**4.9**	76.099	**4.9**	86.793	**4.9**	99.687
5	59.315	**5**	67.956	**5**	66.434	**5**	76.144	**5**	86.982	**5**	99.804
5.1	59.359	**5.1**	67.918	**5.1**	66.511	**5.1**	76.149	**5.1**	87.119	**5.1**	99.865
5.2	59.371	**5.2**	67.845	**5.2**	66.553	**5.2**	76.115	**5.2**	87.208	**5.2**	99.872
5.3	59.353	**5.3**	67.739	**5.3**	66.561	**5.3**	76.045	**5.3**	87.250	**5.3**	99.828
5.4	59.306	**5.4**	67.603	**5.4**	66.538	**5.4**	75.939	**5.4**	87.251	**5.4**	99.737
5.5	59.234	**5.5**	67.439	**5.5**	66.484	**5.5**	75.801	**5.5**	87.211	**5.5**	99.600
5.6	59.137	**5.6**	67.248	**5.6**	66.402	**5.6**	75.630	**5.6**	87.135	**5.6**	99.421
5.7	59.016	**5.7**	67.034	**5.7**	66.294	**5.7**	75.430	**5.7**	87.024	**5.7**	99.202
5.8	58.875	**5.8**	66.797	**5.8**	66.162	**5.8**	75.203	**5.8**	86.882	**5.8**	98.947
5.9	58.713	**5.9**	66.539	**5.9**	66.006	**5.9**	74.949	**5.9**	86.710	**5.9**	98.657
6	58.533	**6**	66.262	**6**	65.829	**6**	74.670	**6**	86.512	**6**	98.336
6.1	58.336	**6.1**	65.967	**6.1**	65.631	**6.1**	74.369	**6.1**	86.288	**6.1**	97.984
6.2	58.124	**6.2**	65.656	**6.2**	65.416	**6.2**	74.046	**6.2**	86.042	**6.2**	97.606
6.3	57.897	**6.3**	65.329	**6.3**	65.184	**6.3**	73.704	**6.3**	85.775	**6.3**	97.203
6.4	57.657	**6.4**	64.989	**6.4**	64.936	**6.4**	73.344	**6.4**	85.488	**6.4**	96.778
6.5	57.406	**6.5**	64.636	**6.5**	64.674	**6.5**	72.969	**6.5**	85.185	**6.5**	96.331
6.6	57.144	**6.6**	64.270	**6.6**	64.399	**6.6**	72.578	**6.6**	84.865	**6.6**	95.867
6.7	56.873	**6.7**	63.895	**6.7**	64.112	**6.7**	72.175	**6.7**	84.531	**6.7**	95.386
6.8	56.594	**6.8**	63.509	**6.8**	63.815	**6.8**	71.761	**6.8**	84.184	**6.8**	94.891
6.9	56.307	**6.9**	63.116	**6.9**	63.509	**6.9**	71.337	**6.9**	83.825	**6.9**	94.383
7	56.014	**7**	62.715	**7**	63.194	**7**	70.905	**7**	83.456	**7**	93.865
7.1	55.716	**7.1**	62.308	**7.1**	62.873	**7.1**	70.466	**7.1**	83.076	**7.1**	93.337
7.2	55.413	**7.2**	61.897	**7.2**	62.545	**7.2**	70.023	**7.2**	82.688	**7.2**	92.802
7.3	55.107	**7.3**	61.482	**7.3**	62.212	**7.3**	69.576	**7.3**	82.291	**7.3**	92.261
7.4	54.797	**7.4**	61.066	**7.4**	61.875	**7.4**	69.127	**7.4**	81.887	**7.4**	91.716

	7.5	54.485	**7.5**	60.650	**7.5**	61.535	**7.5**	68.678	**7.5**	81.475	**7.5**	91.168
	7.6	54.172	**7.6**	60.237	**7.6**	61.192	**7.6**	68.231	**7.6**	81.057	**7.6**	90.619
	7.7	53.857	**7.7**	59.828	**7.7**	60.848	**7.7**	67.786	**7.7**	80.632	**7.7**	90.070
	7.8	53.543	**7.8**	59.427	**7.8**	60.502	**7.8**	67.345	**7.8**	80.201	**7.8**	89.522
	7.9	53.228	**7.9**	59.035	**7.9**	60.156	**7.9**	66.909	**7.9**	79.763	**7.9**	88.976
	8	52.913	**8**	58.656	**8**	59.810	**8**	66.481	**8**	79.319	**8**	88.433
	8.1	52.600	**8.1**	58.295	**8.1**	59.465	**8.1**	66.061	**8.1**	78.868	**8.1**	87.895
	8.2	52.288	**8.2**	57.953	**8.2**	59.121	**8.2**	65.651	**8.2**	78.410	**8.2**	87.362
MAX	5.2	59.371	5	67.956	5.3	66.561	5.1	76.149	5.3	87.251	5.2	99.872
Scelto	5.3	59.353	5.3	67.739	5.3	66.561	5.3	76.045	5.3	87.250	5.3	99.828
Diff. Max - scelto		0.0305%		0.3204 %		0.0000%		0.1370%		0.00%		0.0439 %

3) Tube height ➔ Th=1.4mm

Th=1.4mm; Ld=10mm; v=3.5m/s		**Th=1.4mm; Ld=10mm; v=5m/s**		**Th=1.4mm; Ld=11.5mm; v=3.5m/s**		**Th=1.4mm; Ld=11.5mm; v=5m/s**		**Th=1.4mm; Ld=16mm; v=3.5m/s**		**Th=1.4mm; Ld=16mm; v=5m/s**	
Tp [mm]	**Tp with LdT**	**Tp [mm]**	**Tp with LdT**	**Tp [mm]**	**Tp with LdT**	**Tp [mm]**	**Tp with LdT**	**Tp [mm]**	**Tp with LdT**	**Tp [mm]**	**Tp with LdT**
4.2		**4.2**		**4.2**		**4.2**		**4.2**		**4.2**	
4.3		**4.3**		**4.3**		**4.3**		**4.3**		**4.3**	
4.4	54.968	**4.4**	63.830	**4.4**		**4.4**		**4.4**	79.455	**4.4**	92.470
4.5	55.410	**4.5**	64.256	**4.5**		**4.5**		**4.5**	80.231	**4.5**	93.254
4.6	55.810	**4.6**	64.638	**4.6**		**4.6**		**4.6**	80.926	**4.6**	93.949
4.7	56.169	**4.7**	64.976	**4.7**		**4.7**		**4.7**	81.546	**4.7**	94.559
4.8	56.489	**4.8**	65.272	**4.8**		**4.8**		**4.8**	82.095	**4.8**	95.089
4.9	56.771	**4.9**	65.527	**4.9**		**4.9**		**4.9**	82.577	**4.9**	95.544
5	57.017	**5**	65.742	**5**		**5**		**5**	82.997	**5**	95.928
5.1	57.228	**5.1**	65.918	**5.1**		**5.1**		**5.1**	83.357	**5.1**	96.245
5.2	57.406	**5.2**	66.057	**5.2**		**5.2**		**5.2**	83.663	**5.2**	96.499
5.3	57.551	**5.3**	66.159	**5.3**		**5.3**		**5.3**	83.916	**5.3**	96.695
5.4	57.665	**5.4**	66.227	**5.4**	64.472	**5.4**	74.019	**5.4**	84.122	**5.4**	96.836
5.5	57.750	**5.5**	66.261	**5.5**	64.506	**5.5**	74.008	**5.5**	84.282	**5.5**	96.926
5.6	57.806	**5.6**	66.263	**5.6**	64.523	**5.6**	73.974	**5.6**	84.401	**5.6**	96.969
5.7	57.835	**5.7**	66.233	**5.7**	64.522	**5.7**	73.917	**5.7**	84.480	**5.7**	96.967
5.8	57.839	**5.8**	66.173	**5.8**	64.505	**5.8**	73.837	**5.8**	84.524	**5.8**	96.924
5.9	57.818	**5.9**	66.085	**5.9**	64.472	**5.9**	73.735	**5.9**	84.534	**5.9**	96.843
6	57.773	**6**	65.969	**6**	64.422	**6**	73.612	**6**	84.513	**6**	96.726
6.1	57.706	**6.1**	65.828	**6.1**	64.357	**6.1**	73.469	**6.1**	84.463	**6.1**	96.576

	6.2	57.619	**6.2**	65.661	**6.2**	64.276	**6.2**	73.306	**6.2**	84.386	**6.2**	96.396
	6.3	57.511	**6.3**	65.472	**6.3**	64.179	**6.3**	73.123	**6.3**	84.285	**6.3**	96.188
	6.4	57.385	**6.4**	65.260	**6.4**	64.068	**6.4**	72.923	**6.4**	84.161	**6.4**	95.953
	6.5	57.241	**6.5**	65.028	**6.5**	63.942	**6.5**	72.705	**6.5**	84.016	**6.5**	95.695
	6.6	57.080	**6.6**	64.777	**6.6**	63.802	**6.6**	72.469	**6.6**	83.852	**6.6**	95.414
	6.7	56.904	**6.7**	64.507	**6.7**	63.648	**6.7**	72.218	**6.7**	83.669	**6.7**	95.113
	6.8	56.714	**6.8**	64.222	**6.8**	63.480	**6.8**	71.951	**6.8**	83.469	**6.8**	94.793
	6.9	56.510	**6.9**	63.921	**6.9**	63.298	**6.9**	71.669	**6.9**	83.253	**6.9**	94.454
	7	56.294	**7**	63.607	**7**	63.103	**7**	71.373	**7**	83.022	**7**	94.099
	7.1	56.067	**7.1**	63.280	**7.1**	62.896	**7.1**	71.063	**7.1**	82.776	**7.1**	93.728
	7.2	55.829	**7.2**	62.943	**7.2**	62.676	**7.2**	70.740	**7.2**	82.517	**7.2**	93.341
	7.3	55.582	**7.3**	62.596	**7.3**	62.444	**7.3**	70.406	**7.3**	82.244	**7.3**	92.941
	7.4	55.326	**7.4**	62.242	**7.4**	62.199	**7.4**	70.060	**7.4**	81.959	**7.4**	92.526
	7.5	55.063	**7.5**	61.882	**7.5**	61.943	**7.5**	69.703	**7.5**	81.660	**7.5**	92.097
	7.6	54.794	**7.6**	61.516	**7.6**	61.676	**7.6**	69.337	**7.6**	81.348	**7.6**	91.655
	7.7	54.519	**7.7**	61.147	**7.7**	61.398	**7.7**	68.961	**7.7**	81.023	**7.7**	91.198
	7.8	54.239	**7.8**	60.777	**7.8**	61.108	**7.8**	68.576	**7.8**	80.684	**7.8**	90.728
	7.9	53.955	**7.9**	60.406	**7.9**	60.809	**7.9**	68.184	**7.9**	80.331	**7.9**	90.244
	8	53.667	**8**	60.036	**8**	60.499	**8**	67.784	**8**	79.963	**8**	89.744
	8.1	53.378	**8.1**	59.670	**8.1**	60.179	**8.1**	67.378	**8.1**	79.579	**8.1**	89.229
	8.2	53.087	**8.2**	59.307	**8.2**	59.850	**8.2**	66.966	**8.2**	79.179	**8.2**	88.697
MAX	5.8	57.839	5.6	66.263	5.7	64.523	5.4	74.019	5.9	84.534	5.6	96.969
Scelto	6.1	57.706	6.1	65.828	6.1	64.357	6.1	73.469	6.1	84.463	6.1	96.576
Diff. Max - scelto		0.002		0.007		0.003		0.007		0.001		0.004
MAX	5.8	57.839	5.6	66.263	5.7	64.523	5.4	74.019	5.9	84.534	5.6	96.969
Scelto	5.9	57.818	5.9	66.085	5.9	64.472	5.9	73.735	5.9	84.534	5.9	96.843
Diff. Max - scelto		0.04%		0.27%		0.08%		0.38%		0.00%		0.13%

4) Tube height ➔ Th=1.6mm

Th=1.6mm; Ld=10mm; v=3.5m/s		**Th=1.6mm; Ld=10mm; v=5m/s**		**Th=1.6mm; Ld=11.5mm; v=3.5m/s**		**Th=1.6mm; Ld=11.5mm; v=5m/s**		**Th=1.6mm; Ld=16mm; v=3.5m/s**		**Th=1.6mm; Ld=16mm; v=5m/s**	
Tp [mm]	**Tp with LdT**	**Tp [mm]**	**Tp with LdT**	**Tp [mm]**	**Tp with LdT**	**Tp [mm]**	**Tp with LdT**	**Tp [mm]**	**Tp with LdT**	**Tp [mm]**	**Tp with LdT**
4.2		**4.2**		**4.2**		**4.2**		**4.2**		**4.2**	
4.3		**4.3**		**4.3**		**4.3**		**4.3**		**4.3**	
4.4		**4.4**		**4.4**		**4.4**		**4.4**		**4.4**	

	4.5		**4.5**		**4.5**		**4.5**		**4.5**		**4.5**	
	4.6	52.460	**4.6**	61.012	**4.6**	58.331	**4.6**	67.861	**4.6**	75.605	**4.6**	88.114
	4.7	53.004	**4.7**	61.568	**4.7**	58.933	**4.7**	68.514	**4.7**	76.420	**4.7**	89.008
	4.8	53.495	**4.8**	62.066	**4.8**	59.482	**4.8**	69.099	**4.8**	77.171	**4.8**	89.817
	4.9	53.938	**4.9**	62.507	**4.9**	59.981	**4.9**	69.621	**4.9**	77.858	**4.9**	90.545
	5	54.333	**5**	62.894	**5**	60.431	**5**	70.081	**5**	78.485	**5**	91.196
	5.1	54.684	**5.1**	63.229	**5.1**	60.836	**5.1**	70.484	**5.1**	79.054	**5.1**	91.773
	5.2	54.992	**5.2**	63.517	**5.2**	61.196	**5.2**	70.832	**5.2**	79.567	**5.2**	92.279
	5.3	55.259	**5.3**	63.758	**5.3**	61.513	**5.3**	71.127	**5.3**	80.026	**5.3**	92.718
	5.4	55.489	**5.4**	63.957	**5.4**	61.790	**5.4**	71.374	**5.4**	80.433	**5.4**	93.093
	5.5	55.682	**5.5**	64.114	**5.5**	62.029	**5.5**	71.573	**5.5**	80.790	**5.5**	93.408
	5.6	55.841	**5.6**	64.232	**5.6**	62.230	**5.6**	71.728	**5.6**	81.099	**5.6**	93.664
	5.7	55.968	**5.7**	64.314	**5.7**	62.396	**5.7**	71.842	**5.7**	81.362	**5.7**	93.866
	5.8	56.064	**5.8**	64.361	**5.8**	62.529	**5.8**	71.916	**5.8**	81.582	**5.8**	94.017
	5.9	56.132	**5.9**	64.376	**5.9**	62.630	**5.9**	71.954	**5.9**	81.760	**5.9**	94.118
	6	56.173	**6**	64.361	**6**	62.701	**6**	71.957	**6**	81.897	**6**	94.173
	6.1	56.188	**6.1**	64.318	**6.1**	62.744	**6.1**	71.927	**6.1**	81.996	**6.1**	94.185
	6.2	56.180	**6.2**	64.248	**6.2**	62.759	**6.2**	71.867	**6.2**	82.060	**6.2**	94.156
	6.3	56.150	**6.3**	64.153	**6.3**	62.749	**6.3**	71.779	**6.3**	82.088	**6.3**	94.088
	6.4	56.099	**6.4**	64.036	**6.4**	62.715	**6.4**	71.664	**6.4**	82.084	**6.4**	93.985
	6.5	56.029	**6.5**	63.896	**6.5**	62.659	**6.5**	71.524	**6.5**	82.049	**6.5**	93.847
	6.6	55.941	**6.6**	63.737	**6.6**	62.581	**6.6**	71.362	**6.6**	81.985	**6.6**	93.678
	6.7	55.837	**6.7**	63.560	**6.7**	62.483	**6.7**	71.178	**6.7**	81.893	**6.7**	93.480
	6.8	55.717	**6.8**	63.365	**6.8**	62.366	**6.8**	70.975	**6.8**	81.775	**6.8**	93.255
	6.9	55.582	**6.9**	63.154	**6.9**	62.232	**6.9**	70.754	**6.9**	81.633	**6.9**	93.004
	7	55.434	**7**	62.929	**7**	62.082	**7**	70.516	**7**	81.468	**7**	92.730
	7.1	55.274	**7.1**	62.690	**7.1**	61.917	**7.1**	70.262	**7.1**	81.283	**7.1**	92.434
	7.2	55.103	**7.2**	62.439	**7.2**	61.738	**7.2**	69.995	**7.2**	81.077	**7.2**	92.119
	7.3	54.921	**7.3**	62.177	**7.3**	61.545	**7.3**	69.715	**7.3**	80.854	**7.3**	91.785
	7.4	54.729	**7.4**	61.904	**7.4**	61.341	**7.4**	69.423	**7.4**	80.614	**7.4**	91.435
	7.5	54.529	**7.5**	61.621	**7.5**	61.126	**7.5**	69.120	**7.5**	80.359	**7.5**	91.069
	7.6	54.320	**7.6**	61.329	**7.6**	60.901	**7.6**	68.808	**7.6**	80.091	**7.6**	90.690
	7.7	54.103	**7.7**	61.028	**7.7**	60.667	**7.7**	68.487	**7.7**	79.810	**7.7**	90.298
	7.8	53.879	**7.8**	60.720	**7.8**	60.425	**7.8**	68.157	**7.8**	79.518	**7.8**	89.895
	7.9	53.649	**7.9**	60.405	**7.9**	60.176	**7.9**	67.820	**7.9**	79.216	**7.9**	89.481
	8	53.412	**8**	60.083	**8**	59.919	**8**	67.476	**8**	78.906	**8**	89.059
	8.1	53.169	**8.1**	59.754	**8.1**	59.657	**8.1**	67.126	**8.1**	78.589	**8.1**	88.628
	8.2	52.920	**8.2**	59.419	**8.2**	59.389	**8.2**	66.770	**8.2**	78.267	**8.2**	88.190
MAX	6.1	56.188	5.9	64.376	6.2	62.759	6	71.957	6.3	82.088	6.1	94.185
Scelto	6.3	56.150	6.3	64.153	6.3	62.749	6.3	71.779	6.3	82.088	6.3	94.088
Diff. Max - scelto		0.068%		0.348%		0.016%		0.248%		0.000%		0.103%

5) Tube height ➔ Th=1.8mm

Th=1.8mm; Ld=16mm; v=5m/s		Th=1.8mm; Ld=16mm; v=3.5m/s		Th=1.8mm; Ld=11.5mm; v=5m/s		Th=1.8mm; Ld=11.5mm; v=3.5m/s		Th=1.8mm; Ld=10mm; v=5m/s		Th=1.8mm; Ld=10mm; v=3.5m/s	
Tp [mm]	Tp with LdT	Tp [mm]	Tp with LdT	Tp [mm]	Tp with LdT	Tp [mm]	Tp with LdT	Tp [mm]	Tp with LdT	Tp [mm]	Tp with LdT
4.2		**4.2**		**4.2**		**4.2**		**4.2**		**4.2**	
4.3		**4.3**		**4.3**		**4.3**		**4.3**		**4.3**	
4.4		**4.4**		**4.4**		**4.4**		**4.4**		**4.4**	
4.5		**4.5**		**4.5**		**4.5**		**4.5**		**4.5**	
4.6		**4.6**		**4.6**		**4.6**		**4.6**		**4.6**	
4.7		**4.7**		**4.7**		**4.7**		**4.7**		**4.7**	
4.8	83.901	**4.8**	71.945	**4.8**	64.764	**4.8**	55.561	**4.8**	58.270	**4.8**	50.014
4.9	84.859	**4.9**	72.823	**4.9**	65.432	**4.9**	56.200	**4.9**	58.912	**4.9**	50.596
5	85.734	**5**	73.630	**5**	66.047	**5**	56.788	**5**	59.488	**5**	51.128
5.1	86.527	**5.1**	74.371	**5.1**	66.610	**5.1**	57.327	**5.1**	60.001	**5.1**	51.610
5.2	87.244	**5.2**	75.048	**5.2**	67.122	**5.2**	57.819	**5.2**	60.456	**5.2**	52.046
5.3	87.888	**5.3**	75.665	**5.3**	67.584	**5.3**	58.266	**5.3**	60.856	**5.3**	52.438
5.4	88.463	**5.4**	76.224	**5.4**	67.998	**5.4**	58.669	**5.4**	61.204	**5.4**	52.789
5.5	88.971	**5.5**	76.729	**5.5**	68.364	**5.5**	59.032	**5.5**	61.504	**5.5**	53.100
5.6	89.416	**5.6**	77.182	**5.6**	68.684	**5.6**	59.355	**5.6**	61.758	**5.6**	53.373
5.7	89.802	**5.7**	77.585	**5.7**	68.959	**5.7**	59.640	**5.7**	61.969	**5.7**	53.611
5.8	90.132	**5.8**	77.942	**5.8**	69.192	**5.8**	59.890	**5.8**	62.141	**5.8**	53.816
5.9	90.408	**5.9**	78.254	**5.9**	69.383	**5.9**	60.105	**5.9**	62.275	**5.9**	53.989
6	90.635	**6**	78.524	**6**	69.535	**6**	60.289	**6**	62.375	**6**	54.133
6.1	90.813	**6.1**	78.755	**6.1**	69.649	**6.1**	60.441	**6.1**	62.442	**6.1**	54.249
6.2	90.947	**6.2**	78.948	**6.2**	69.727	**6.2**	60.564	**6.2**	62.479	**6.2**	54.339
6.3	91.038	**6.3**	79.105	**6.3**	69.771	**6.3**	60.660	**6.3**	62.488	**6.3**	54.405
6.4	91.090	**6.4**	79.228	**6.4**	69.783	**6.4**	60.730	**6.4**	62.471	**6.4**	54.448
6.5	91.105	**6.5**	79.320	**6.5**	69.764	**6.5**	60.774	**6.5**	62.429	**6.5**	54.469
6.6	91.085	**6.6**	79.381	**6.6**	69.718	**6.6**	60.796	**6.6**	62.364	**6.6**	54.470
6.7	91.032	**6.7**	79.414	**6.7**	69.644	**6.7**	60.795	**6.7**	62.278	**6.7**	54.452
6.8	90.948	**6.8**	79.421	**6.8**	69.546	**6.8**	60.773	**6.8**	62.172	**6.8**	54.416
6.9	90.836	**6.9**	79.401	**6.9**	69.425	**6.9**	60.732	**6.9**	62.048	**6.9**	54.364
7	90.696	**7**	79.358	**7**	69.283	**7**	60.672	**7**	61.906	**7**	54.297
7.1	90.532	**7.1**	79.292	**7.1**	69.121	**7.1**	60.595	**7.1**	61.749	**7.1**	54.215
7.2	90.344	**7.2**	79.205	**7.2**	68.941	**7.2**	60.501	**7.2**	61.577	**7.2**	54.119
7.3	90.134	**7.3**	79.097	**7.3**	68.744	**7.3**	60.392	**7.3**	61.391	**7.3**	54.010
7.4	89.904	**7.4**	78.970	**7.4**	68.532	**7.4**	60.268	**7.4**	61.192	**7.4**	53.890
7.5	89.654	**7.5**	78.825	**7.5**	68.307	**7.5**	60.130	**7.5**	60.980	**7.5**	53.758
7.6	89.387	**7.6**	78.662	**7.6**	68.069	**7.6**	59.979	**7.6**	60.757	**7.6**	53.615

	7.7	89.102	**7.7**	78.482	**7.7**	67.819	**7.7**	59.816	**7.7**	60.523	**7.7**	53.461
	7.8	88.801	**7.8**	78.287	**7.8**	67.559	**7.8**	59.641	**7.8**	60.279	**7.8**	53.298
	7.9	88.486	**7.9**	78.076	**7.9**	67.289	**7.9**	59.454	**7.9**	60.026	**7.9**	53.125
	8	88.156	**8**	77.850	**8**	67.009	**8**	59.257	**8**	59.763	**8**	52.942
	8.1	87.812	**8.1**	77.611	**8.1**	66.720	**8.1**	59.049	**8.1**	59.491	**8.1**	52.750
	8.2	87.455	**8.2**	77.358	**8.2**	66.422	**8.2**	58.832	**8.2**	59.210	**8.2**	52.549
MAX	6.5	91.105	6.8	79.421	6.4	69.783	6.6	60.796	6.3	62.488	6.6	54.470
Scelto	6.6	91.085	6.6	79.381	6.6	69.718	6.6	60.796	6.6	62.364	6.6	54.470
Diff. Max - scelto		0.022%		0.050%		0.094%		0.000%		0.199%		0.000%

6) Tube height ➔ Th=2.0 mm

Th=2mm; Ld=16mm; v=5m/s		**Th=2mm; Ld=16mm; v=3.5m/s**		**Th=2mm; Ld=11.5mm; v=5m/s**		**Th=2mm; Ld=11.5mm; v=3.5m/s**		**Th=2mm; Ld=10mm; v=5m/s**		**Th=2mm; Ld=10mm; v=3.5m/s**	
Tp [mm]	**Tp with LdT**	**Tp [mm]**	**Tp with LdT**	**Tp [mm]**	**Tp with LdT**	**Tp [mm]**	**Tp with LdT**	**Tp [mm]**	**Tp with LdT**	**Tp [mm]**	**Tp with LdT**
4.2		**4.2**		**4.2**		**4.2**		**4.2**		**4.2**	
4.3		**4.3**		**4.3**		**4.3**		**4.3**		**4.3**	
4.4		**4.4**		**4.4**		**4.4**		**4.4**		**4.4**	
4.5		**4.5**		**4.5**		**4.5**		**4.5**		**4.5**	
4.6		**4.6**		**4.6**		**4.6**		**4.6**		**4.6**	
4.7		**4.7**		**4.7**		**4.7**		**4.7**		**4.7**	
4.8		**4.8**		**4.8**		**4.8**		**4.8**		**4.8**	
4.9		**4.9**		**4.9**		**4.9**		**4.9**		**4.9**	
5	79.978	**5**	68.559	**5**	61.767	**5**	53.022	**5**	55.654	**5**	47.758
5.1	80.994	**5.1**	69.447	**5.1**	62.526	**5.1**	53.667	**5.1**	56.297	**5.1**	48.336
5.2	81.936	**5.2**	70.285	**5.2**	63.226	**5.2**	54.278	**5.2**	56.896	**5.2**	48.880
5.3	82.804	**5.3**	71.073	**5.3**	63.868	**5.3**	54.853	**5.3**	57.450	**5.3**	49.390
5.4	83.600	**5.4**	71.808	**5.4**	64.454	**5.4**	55.391	**5.4**	57.959	**5.4**	49.865
5.5	84.327	**5.5**	72.492	**5.5**	64.984	**5.5**	55.892	**5.5**	58.423	**5.5**	50.304
5.6	84.985	**5.6**	73.124	**5.6**	65.460	**5.6**	56.354	**5.6**	58.841	**5.6**	50.706
5.7	85.577	**5.7**	73.703	**5.7**	65.884	**5.7**	56.777	**5.7**	59.213	**5.7**	51.073
5.8	86.106	**5.8**	74.232	**5.8**	66.257	**5.8**	57.162	**5.8**	59.541	**5.8**	51.403
5.9	86.574	**5.9**	74.710	**5.9**	66.582	**5.9**	57.509	**5.9**	59.826	**5.9**	51.699
6	86.983	**6**	75.139	**6**	66.861	**6**	57.819	**6**	60.069	**6**	51.960
6.1	87.336	**6.1**	75.520	**6.1**	67.095	**6.1**	58.092	**6.1**	60.270	**6.1**	52.188
6.2	87.635	**6.2**	75.856	**6.2**	67.288	**6.2**	58.329	**6.2**	60.433	**6.2**	52.384
6.3	87.884	**6.3**	76.148	**6.3**	67.440	**6.3**	58.532	**6.3**	60.559	**6.3**	52.548

	6.4	88.085	**6.4**	76.398	**6.4**	67.556	**6.4**	58.702	**6.4**	60.650	**6.4**	52.683
	6.5	88.242	**6.5**	76.608	**6.5**	67.636	**6.5**	58.841	**6.5**	60.707	**6.5**	52.790
	6.6	88.356	**6.6**	76.780	**6.6**	67.684	**6.6**	58.949	**6.6**	60.734	**6.6**	52.869
	6.7	88.431	**6.7**	76.918	**6.7**	67.702	**6.7**	59.030	**6.7**	60.732	**6.7**	52.924
	6.8	88.469	**6.8**	77.023	**6.8**	67.692	**6.8**	59.084	**6.8**	60.703	**6.8**	52.956
	6.9	88.473	**6.9**	77.097	**6.9**	67.656	**6.9**	59.114	**6.9**	60.651	**6.9**	52.966
	7	88.446	**7**	77.144	**7**	67.597	**7**	59.121	**7**	60.576	**7**	52.956
	7.1	88.389	**7.1**	77.164	**7.1**	67.516	**7.1**	59.106	**7.1**	60.482	**7.1**	52.928
	7.2	88.306	**7.2**	77.162	**7.2**	67.416	**7.2**	59.073	**7.2**	60.371	**7.2**	52.883
	7.3	88.199	**7.3**	77.137	**7.3**	67.298	**7.3**	59.022	**7.3**	60.243	**7.3**	52.823
	7.4	88.068	**7.4**	77.093	**7.4**	67.165	**7.4**	58.954	**7.4**	60.102	**7.4**	52.749
	7.5	87.917	**7.5**	77.031	**7.5**	67.016	**7.5**	58.872	**7.5**	59.950	**7.5**	52.663
	7.6	87.747	**7.6**	76.953	**7.6**	66.855	**7.6**	58.777	**7.6**	59.786	**7.6**	52.566
	7.7	87.559	**7.7**	76.860	**7.7**	66.682	**7.7**	58.670	**7.7**	59.614	**7.7**	52.460
	7.8	87.355	**7.8**	76.752	**7.8**	66.497	**7.8**	58.552	**7.8**	59.433	**7.8**	52.344
	7.9	87.134	**7.9**	76.631	**7.9**	66.302	**7.9**	58.424	**7.9**	59.245	**7.9**	52.220
	8	86.898	**8**	76.497	**8**	66.097	**8**	58.286	**8**	59.050	**8**	52.088
	8.1	86.646	**8.1**	76.350	**8.1**	65.881	**8.1**	58.138	**8.1**	58.848	**8.1**	51.948
	8.2	86.380	**8.2**	76.189	**8.2**	65.656	**8.2**	57.982	**8.2**	58.639	**8.2**	51.802
MAX	6.9	88.473	7.2	77.164	6.7	67.702	7	59.121	6.7	60.734	6.9	52.966
Scelto	6.9	88.473	6.9	77.097	6.9	67.656	6.9	59.114	6.9	60.651	6.9	52.966
Diff. Max - scelto		0.000%		0.087%		0.068%		0.011%		0.137%		0.000%

REFERENCES

[1]Chang, Y.-J., and Wang, C.-C., 1997, "A Generalized Heat Transfer Correlation for Louver Fin Geometry," Int. J. Heat Mass Transfer, 40 3 , pp. 533– 544.

[2] Park and Jacobi, 2009a, "Air-Side Heat Transfer and Friction Correlations for Flat-Tube Louver-Fin Heat Exchangers".

[3] Park and Jacobi, 2009b, "The Air-Side Thermal-Hydraulic Performance of Flat Tube Heat Exchangers With Louvered, Wavy, and Plain Fins Under Dry and Wet Conditions".

[4] A.Vaisi, M.Esmaeilpour,H.Taherian, 2011, "Experimental investigation of geometry effects on the performance of a compact louvered heat exchanger"

[5] Junqi.D,Jiangping Chen, Zhijiu Chen,Wenfeng Zhang, Yimin Zhou, 2007, "Heat transfer and pressure drop correlations for the multi-louvered fin compact heat exchangers"

[6] Kijung Ryu, Kwan-Soo Lee, 2015, "Generalized heat-transfer and fluid-flow correlations for corrugated louvered fins".

[7] Davenport, C. J., 1983, "Correlations for Heat Transfer and Flow Friction Characteristics of Louvred Fin," Proceedings of the 21st National Heat Transfer Conference, AIChE Symposium Series No. 225, American Institute of Chemical Engineers, New York, pp. 19–27.

[8] Nae-Hyun Kim & Jin-Pyo Cho, 2007 "Air-side performance of louver-finned flat aluminum heat exchangers at a low velocity region".

[9] R. L. Webb and P. Trauger, "How structure in the louvered fin heat exchanger geometry," Experimental Thermal and Fluid Science, vol. 4, no. 2, pp. 205–217, 1991.

[10] A. Sahnoun and R. L. Webb, "Prediction of heat transfer and friction for the louver fin geometry," Journal of Heat Transfer, vol. 114, no. 4, pp. 893–900, 1992.

[11] V. P. Malapure, S. K. Mitra, and A. Bhattacharya, "Numerical investigation of fluid flow and heat transfer over louvered fins in compact heat exchanger," *International Journal of Thermal Sciences*, vol. 46, no. 2, pp. 199–211, 2007.

[12] Achaichia, A., and Cowell, T. A., 1988, “Heat Transfer and Pressure Drop Characteristics of Flat Tube and Louvered Plate Fin Surfaces,” Exp. Therm. Fluid Sci., 1 2 , pp. 147–157.

[13]Kim, M.-H., and Bullard, C. W., 2002, “Air-Side Thermal Hydraulic Performance of Multi-Louvered Fin Aluminum Heat Exchangers,” Int. J. Refrig., 25 3 , pp. 390–400.

[14] Sunden, B., and Svantesson, J., 1992, “Correlations of J- and F-Factors for Multilouvered Heat Transfer Surfaces,” Proceedings of the Third UK National Conference Incorporating First European Conference on Thermal Sciences, Institution of Chemical Engineers Symposium Series No. 129, Institution of Chemical Engineers, Rugby, UK, Vol. 2, pp. 805–811.

[15]Rugh, J. P., Pearson, J. T., and Ramadhyani, S., 1992, “A Study of a Very Compact Heat Exchanger Used for Passenger Compartment Heating in Automobiles,” Proceedings of the 28th National Heat Transfer Conference and Exhibition, Heat Transfer Division, ASME, New York, HTD-Vol. 201, pp. 15–24.

[16] Jacobi, A. M., Park, Y., Zhong, Y., Michna, G., and Xia, Y., 2005, “High Performance Heat Exchangers for Air-Conditioning and Refrigeration Applications _Non-Circular Tubes_,” University of Illinois, Phase II-Final Report No. ARTI-21CR/611-20021.

[17] Kim, J. H., Yun, J. H., and Lee, C. S., 2004, “Heat-Transfer and Friction Characteristics for the Louver-Fin Heat Exchanger,” J. Thermophys. Heat Transfer, 18_1_, pp. 58–64.

[18] T. Tanaka, M. Itoh, M. Kudoh and A. Tomita, Improvement of compact heat exchangers with inclined louvered fins, Bull. JSME 27, 219-226 (1984).

[19] R. L. Webb and S. H. Jung, Air-side performance of enhanced brazed aluminium heat exchangers, ASHRAE Trans. 98, Pt 2, 3!)1-401 (1992).

[20]*Lee, H.S.. Thermal Design : Heat Sinks, Thermoelectrics, Heat Pipes, Compact Heat Exchangers, and Solar Cells. Hoboken, NJ, USA: John Wiley & Sons, 2010. ProQuest ebrary. Web. 20 August 2015.*

[21] *http://me1065.wikidot.com/automotive-heat-exchangers*

[22] *http://likesu.fiat.it/resources/lectio/files/LectioMag_April2015_edit.pdf*

[23] D. K. Tafti, X. Zhang, and D. Guo. ¨Study of Multilouvered Heat Exchangers at Low Reynolds numbers."

[24] M. H. Kim and C.W. Bullard, "Air-side thermal hydraulic performanceof multi-louvered fin aluminum heat exchangers," *International Journal of Refrigeration*, vol. 25, no. 3, pp. 390– 400, 2002.

[25] W.M. Kays and A.L. London. "Compact Heat Exchangers". Krieger Pub Co; 3 Sub Edition (30 June 1998).

[26] P. Gunnasegaran, N. H. Shuaib,M. F. Abdul Jalal. 2012. "The Effect of Geometrical Parameters on Heat Transfer Characteristics of Compact Heat Exchanger with Louvered Fins".

[27] D. K. Tafti, X. Zhang. 2002,¨Flow efficiency in multi-louvered fins."